NASA/TM–20230013348
NESC-RP-20-01567

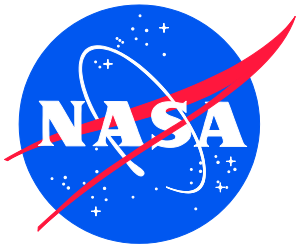

Unconservatism of Linear-Elastic Fracture Mechanics (LEFM) Analysis Post Autofrettage

Heather K. Hickman/NESC
Langley Research Center, Hampton, Virginia

David S. Dawicke
Analytical Services & Materials, Hampton, Virginia

William P. Leser
Langley Research Center, Hampton, Virginia

September 2023

NASA STI Program Report Series

Since its founding, NASA has been dedicated to the advancement of aeronautics and space science. The NASA scientific and technical information (STI) program plays a key part in helping NASA maintain this important role.

The NASA STI program operates under the auspices of the Agency Chief Information Officer. It collects, organizes, provides for archiving, and disseminates NASA's STI. The NASA STI program provides access to the NTRS Registered and its public interface, the NASA Technical Reports Server, thus providing one of the largest collections of aeronautical and space science STI in the world. Results are published in both non-NASA channels and by NASA in the NASA STI Report Series, which includes the following report types:

- TECHNICAL PUBLICATION. Reports of completed research or a major significant phase of research that present the results of NASA Programs and include extensive data or theoretical analysis. Includes compilations of significant scientific and technical data and information deemed to be of continuing reference value. NASA counterpart of peer-reviewed formal professional papers but has less stringent limitations on manuscript length and extent of graphic presentations.

- TECHNICAL MEMORANDUM. Scientific and technical findings that are preliminary or of specialized interest, e.g., quick release reports, working papers, and bibliographies that contain minimal annotation. Does not contain extensive analysis.

- CONTRACTOR REPORT. Scientific and technical findings by NASA-sponsored contractors and grantees.

- CONFERENCE PUBLICATION. Collected papers from scientific and technical conferences, symposia, seminars, or other meetings sponsored or co-sponsored by NASA.

- SPECIAL PUBLICATION. Scientific, technical, or historical information from NASA programs, projects, and missions, often concerned with subjects having substantial public interest.

- TECHNICAL TRANSLATION. English-language translations of foreign scientific and technical material pertinent to NASA's mission.

Specialized services also include organizing and publishing research results, distributing specialized research announcements and feeds, providing information desk and personal search support, and enabling data exchange services.

For more information about the NASA STI program, see the following:

- Access the NASA STI program home page at http://www.sti.nasa.gov

- Help desk contact information:

https://www.sti.nasa.gov/sti-contact-form/
and select the "General" help request type.

NASA/TM–20230013348
NESC-RP-20-01567

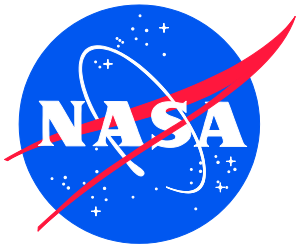

Unconservatism of Linear-Elastic Fracture Mechanics (LEFM) Analysis Post Autofrettage

Heather K. Hickman/NESC
Langley Research Center, Hampton, Virginia

David S. Dawicke
Analytical Services & Materials, Hampton, Virginia

William P. Leser
Langley Research Center, Hampton, Virginia

National Aeronautics and
Space Administration

Langley Research Center
Hampton, Virginia 23681-2199

September 2023

Acknowledgments

The NESC assessment team thanks the NASA Structures Technical Discipline Team, the Composite Pressure Vessels Working Group, the NASA JSC WSTF fabrication shop, and our peer reviewers: Phillip Allen, Bryan McEnerney, Deneen Taylor, Doug Wells, Don Parker, Andrew Chaloupka, Elliott Cramer, Jon Holladay, Steve Gentz, and Joachim Beek.

Available from:

NASA STI Program / Mail Stop 148
NASA Langley Research Center
Hampton, VA 23681-2199
Fax: 757-864-6500

NASA Engineering and Safety Center
Technical Assessment Report

Unconservatism of Linear-Elastic Fracture Mechanics (LEFM) Analysis Post Autofrettage

TI-20-01567

NESC Lead: Heather Hickman

Technical Lead: Dave Dawicke

August 24, 2023

Report Approval and Revision History

NOTE: This document was approved at the August 24, 2023, NRB.

Approved: *Original signature on file.* _____

NESC Director

Version	Description of Revision	Office of Primary Responsibility	Effective Date
1.0	Initial Release	Ms. Heather K. Hickman, Associate Principal Engineer's Office, GRC	8/24/2023

Table of Contents

List of Figures

Technical Assessment Report

1.0 Notification and Authorization

This assessment evaluated the influence of an initial elastic-plastic cycle, called the autofrettage cycle, on subsequent elastic cycles and data were generated to support the damage tolerance life analysis verification approach. Heather Hickman, NASA Engineering and Safety Center (NESC) Associate Principal Engineer at Glenn Research Center, was selected to lead this assessment.

The current assessment was broken into two phases. Phase 1 compared, measured, and analyzed crack growth that occurs during elastic cycles post autofrettage to understand if further evaluation of influence of underload was needed. Phase 2 test and analysis focused on wall thickness, crack sizes, and stresses representative of COPV liner conditions.

The key stakeholders were NASA programs/projects/organizations that use analysis for damage tolerance life verification; Wayne Gregg, Bence Bartha, and Joachim Beek, Fracture Control Methodology Panel; and Lorie Grimes-Ledesma, Composite Pressure Vessel Working Group Lead.

2.0 Signatures

Submitted by: NESC Lead

Original signatures on file.

Ms. Heather K. Hickman Date

Significant Contributors:

Dr. David S. Dawicke Date

Dr. William P. Leser Date

Signatories declare the findings, observations, and NESC recommendations compiled in the report are factually based from data extracted from program/project documents, contractor reports, and open literature, and/or generated from independently conducted tests, analyses, and inspections.

3.0 Team Members

Name	Discipline	Organization
Core Team		
Heather Hickman	NESC Lead	GRC
Dave Dawicke	Technical Lead	LaRC/AS&M
Paul Leser	Analysis Lead	LaRC
Greg Shanks	Senior Engineering Technician	LaRC
Will Johnston	Test Support	LaRC
Jim Baughman	Imaging	LaRC
Harold Claytor	Imaging and Test Support	LaRC/AMA
Jack Cervoni (ret.)	Machining	JSC/WSTF / Jacobs
John Savage	Machining	LaRC
Consultants		
Patrick Leser	Modeling and Analysis	LaRC
Kauser Imtiaz (ret.)	Technical Fellow for Structures	JSC
Rick Russell (ret.)	Technical Fellow for Materials	KSC
Lorie Grimes-Ledesma	Composite Pressure Vessels Working Group Lead	JPL
Business Management		
Linda Moore	Program Analyst	LaRC/MTSO
Assessment Support		
Kylene Kramer	Project Coordinator	LaRC/AMA
Linda Burgess	Planning and Control Analyst	LaRC/AMA
Erin Moran	Technical Editor	LaRC/AMA

3.1 Acknowledgements

The NESC assessment team thanks the NASA Structures Technical Discipline Team, the Composite Pressure Vessels Working Group, the NASA JSC WSTF fabrication shop, and our peer reviewers: Phillip Allen, Bryan McEnerney, Deneen Taylor, Doug Wells, Don Parker, Andrew Chaloupka, Elliott Cramer, Jon Holladay, Steve Gentz, and Joachim Beek.

4.0 Executive Summary

Composite Overwrapped Pressure Vessel (COPV) metallic liners have a unique loading history for damage tolerant structures. Typically, the liner plastically deforms during an initial peak pressure cycle (i.e., the autofrettage cycle), then the liner goes into compression upon depressurization. The subsequent cycles are generally at negative stress ratios ($R = S_{min}/S_{max} < 0$, where S_{max} and S_{min} are the maximum and minimum stresses of the elastic cycle, respectively). The post-autofrettage pressure cycles result in no further plastic deformation in an elastically responding COPV liner and the fracture control requirements allow for the damage tolerance life to be demonstrated by analysis.

The state of practice for analyzing damage tolerance life in elastically responding COPV liners is to independently address the crack growth due to the autofrettage cycle and the subsequent elastic cycles, as is allowed by the American National Standards Institute (ANSI)/American Institute of Aeronautics and Astronautics (AIAA) S-081B standard requirements for damage tolerance life verification [ref. 1]. AIAA S-081B Section 7.5.1 also identifies potential beneficial retardation effects on crack growth rates of the elastic cycles that follow the autofrettage cycle. Linear-Elastic Fracture Mechanics (LEFM) tools (e.g., NASGRO) [ref. 2] are used to predict crack growth in the liner during elastic cycles. Limited data from the COPV Life Test Assessment [ref. 3] introduced a concern that ignoring the influence of the autofrettage cycle in damage tolerance life analysis could result in unconservative COPV damage tolerance life predictions using LEFM tools.

The scope of this assessment was to evaluate the influence of the elastic-plastic autofrettage cycle on elastic cycles post autofrettage and generate data to support damage tolerance life analysis verification approach. This assessment does not address whether autofrettage cycles should or should not be applied. The decision to include an elastic-plastic autofrettage cycle is informed by other factors beyond damage tolerance, including manufacturing and fatigue crack initiation. Tests on aluminum (Al) 6061-T6, finite element analysis (FEA) validated by test data, and NASGRO simulations were used to study crack growth in elastic cycles with and without the autofrettage cycle. Simulated autofrettage strain of 1.5% was selected to remain below the threshold for stable tearing for the material thickness and crack size, and elastic cycles ranging from R=0.5 to -1.3 were tested and analyzed to envelope typical COPV stress ratios.

The results of this assessment are applicable to COPVs with Al 6061-T6 liners. A previous assessment [ref. 3] that examined titanium and Nickel Alloy 718, both ductile COPV liner materials, showed those materials experienced crack blunting similar to that measured in the Al material during simulated autofrettage loading. These, and other ductile COPV liner materials, are expected to be influenced by an autofrettage cycle similar to what was measured in the Al alloy, but tests and analyses have not been conducted to conclusively demonstrate the behavior in ductile COPV liner materials beyond Al 6061-T6.

The test measurements and FEA simulations suggest that the autofrettage cycle can produce beneficial and detrimental influences on the crack growth of subsequent LEFM cycles. The beneficial influence occurs for cycles with positive stress ratios. The detrimental influence occurs for cycles with negative stress ratios that are typical of the conditions in COPV liners. The ANSI/AIAA S-081B standard provides baseline requirements for COPV damage tolerance analyses (DTA) that acknowledge a potential benefit of autofrettage, rather than both potential beneficial and detrimental effects, on crack growth rates of the elastic cycles that follow the

autofrettage cycle. Not accounting for the detrimental influence of the autofrettage cycle could result in damage tolerance life predictions that are unconservative. Specifically, test and FEA results showed that cracks remained open during compressive cycles after autofrettage, allowing for a larger stress range to contribute to crack growth in each elastic cycle. It was also shown that the crack growth rate (da/dN) during elastic cycles after autofrettage did not retard in representative COPV loading conditions and was higher than the crack growth rate of identical elastic cycles that did not experience the autofrettage cycle. Finally, the NASGRO database Al 6061-T6 material model that most closely aligns with a COPV design (i.e., thin sheet) is extrapolated to conditions beyond its supporting data when used in COPV representative analysis. Corrections were introduced into NASGRO analysis to account for the detrimental influence of the autofrettage on the fatigue crack growth predictions.

The NESC recommends NASA programs/projects/organizations using COPVs that are required to comply with damage tolerance life requirements by analysis should ensure that damage tolerance life analyses account for the crack growth rate acceleration that follows the post-autofrettage compressive stresses for cycles with $R < -0.1$. These programs/projects/ organizations should also require relevant crack growth data when autofrettage cycle retardation is identified as part of conservatism rationale for cycles with $R < -0.1$. Finally, the NESC recommends the AIAA Aerospace Pressure Vessel Committee on standards should update ANSI/AIAA S-081B Section 7.5.1 to address COPV liners with compressive stresses following autofrettage depressurization for COPVs that comply with damage tolerance life requirements by analysis.

5.0 Assessment Plan

The NESC initiated an assessment to evaluate the influence of the COPV autofrettage cycle on the subsequent elastic cycles in the COPV operational life and generate data to support the damage tolerance life analysis verification approach. This assessment was initiated because limited tests from the NESC COPV Life Test Assessment [ref. 3] indicated that the autofrettage cycle may cause higher crack growth rates in subsequent elastic cycles than what would be predicted by LEFM. The scope of this assessment was to evaluate the influence of the elastic-plastic autofrettage cycle on elastic cycles post autofrettage and generate data to support damage tolerance life analysis verification approach. This assessment does not address whether autofrettage cycles should or should not be applied. The decision to include an elastic-plastic autofrettage cycle is informed by other factors beyond damage tolerance, including manufacturing and fatigue crack initiation.

The current assessment was broken into two phases. Phase 1 compared measured and simulated crack growth that occurs during elastic cycles post autofrettage to understand if further evaluation of influence of the autofrettage cycle was needed. The Phase 1 test samples were 0.25-inch thick Al 6061-T6. These were thicker than typical COPV liner wall thickness (e.g., 0.03 to 0.1 inch), but allowed for testing without the use of anti-buckling guide plates in the compressive cycles. Phase 1 testing confirmed that additional characterization of the autofrettage cycle on damage tolerance life predictions was warranted.

Phase 2 tests and analyses focused on wall thickness, crack sizes, and stresses representative of COPV liner conditions. Al 6061T-T6 was selected again for Phase 2 because it is a common COPV liner material, its material behavior allowed for testing to desired to compressive strains without excessively complicated guide plate design, and the fracture surfaces have been demonstrated to be readily interpretable after both tension and compressive loading. Phase 2 tests interrogated crack growth behavior for elastic cycles with and without an autofrettage cycle.

A pair of tests were conducted for each condition, one with an autofrettage followed by elastic cycles (AF+LEFM) and the other test with only the identical elastic cycles (LEFM-only). Each pair of tests had the same maximum stress, but different minimum stresses. This resulted in pairs of tests with different stress ranges from R = 0.5 to -1.3. The tests with negative stress ratios were representative of elastically responding COPV liners. All tests were performed at room temperature.

In Phase 2, FEAs were also conducted to enhance the understanding of the behavior of the cracks in the uniaxial coupons and to evaluate the influence of the biaxial loading present in COPV liners. The FEA used a material model developed from tensile hysteresis test data and were validated with physical measurements made during the crack growth tests. Finally, crack growth simulations of the LEFM cycles were performed using the NASGRO [ref. 2] linear elastic crack growth analysis software, and an approach was identified to adjust NASGRO predictions to more closely align with test results for negative stress ratios.

The results of this assessment are applicable to COPVs with Al 6061-T6 liners. A previous assessment [ref. 3] that examined titanium and Inconel, both ductile COPV liner materials, showed these materials experienced crack blunting similar to that measured in the Al material during simulated autofrettage loading. These, and other ductile COPV liner materials, are expected to be influenced by an autofrettage cycle similar to what was measured in the Al alloy,

but tests and analyses have not been conducted to conclusively demonstrate the behavior in ductile COPV liner materials beyond Al 6061-T6.

6.0 Problem Description and Background

COPVs have a unique loading history for damage tolerant structures. The initial autofrettage cycle has a peak pressure that plastically deforms the metallic liner and is intended to make the unflawed liner less susceptible to subsequent operational stresses[1]. The composite overwrap remains elastic and, upon depressurization, puts the metallic liner into compression that, depending on the design, can put part or all of the liner into compressive yield. The subsequent elastic cycles are generally at negative stress ratios ($R = S_{min}/S_{max} < 0$, where S_{max} and S_{min} are the maximum and minimum stresses of the elastic cycle, respectively). COPV liner materials are generally ductile, so the elastic-plastic autofrettage cycle will initially either blunt the crack tip or if the liner strains at the peak autofrettage pressure are high enough, will blunt then advance the crack under stable tearing. Blunting will generally result in minimal crack extension (<0.001 inch), but stable tearing rapidly advances the crack and is a condition that should be avoided in COPV design [ref. 3]. Some COPV designs omit the autofrettage cycle but have an elastic-plastic proof cycle. For the purposes of this report, the initial elastic-plastic cycle, either autofrettage or proof will be referred to as the autofrettage cycle.

Typically, crack growth under negative stress ratios will result in the crack being held shut during most of the compressive loading. So, a portion of the loading cycle must be spent on opening the crack before any significant damage progression can occur. However, a crack that has been first blunted due to an elastic-plastic load and unloaded to a compressive stress can be completely open at the minimum stress of the elastic cycle. Thus, the entire loading cycle will contribute to damage progression, as illustrated in Figure 1.

The NESC COPV Life Assessment [ref. 3] included fatigue crack growth tests that simulated the growth of part-through cracks (i.e., surface cracks) in COPV liners. Two tests that were conducted to examine the difference between the NASGRO prediction and measurements suggested that autofrettage, including the compressive stresses, had an accelerating influence on the subsequent crack growth, as shown in Figure 2. One test was conducted with a simulated elastic-plastic autofrettage cycle followed by constant amplitude loading that simulated the elastic operational cycles. The second test was identical, except the autofrettage cycle was omitted and only contained the elastic operational cycles. The test with the autofrettage cycle had a crack growth rate that was 1.7x faster than the identical test without the autofrettage cycle. The ANSI/AIAA S-081B requirements for the calculation of damage tolerance life analysis of COPV liners allows separate evaluation of the crack growth during the elastic-plastic autofrettage cycle and the subsequent elastic operational cycles. This suggests that the elastic analyses that comply with ANSI/AIAA S-081B, but ignore the detrimental influence of the autofrettage cycle, may provide unconservative damage tolerance life predictions for elastically responding COPVs.

[1] : https://www.nasa.gov/feature/deceptively-complex-composite-overwrapped-pressure-vessels-copv-remain-a-challenge-for

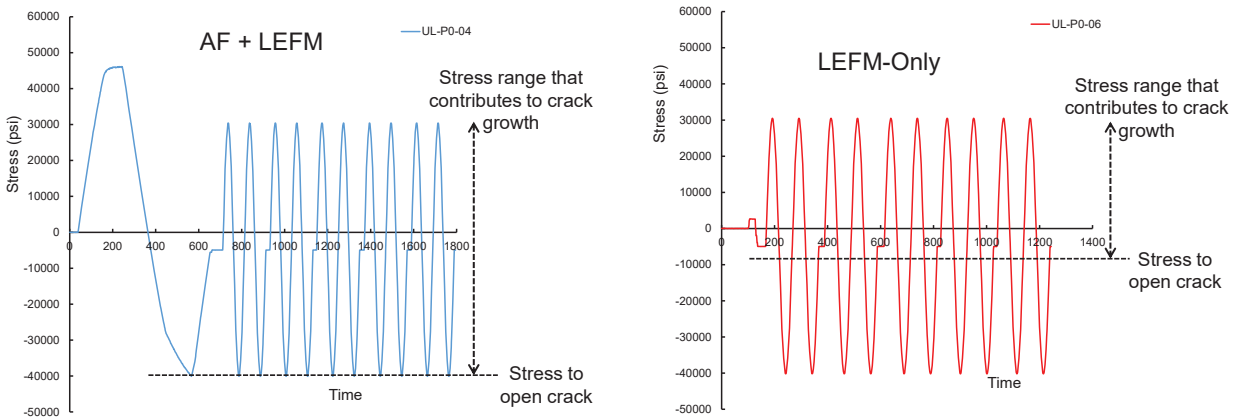

Figure 1. Illustration of the stress range that contributes to crack growth damage for elastic cycles with and without an elastic-plastic overload simulating the autofrettage cycle.

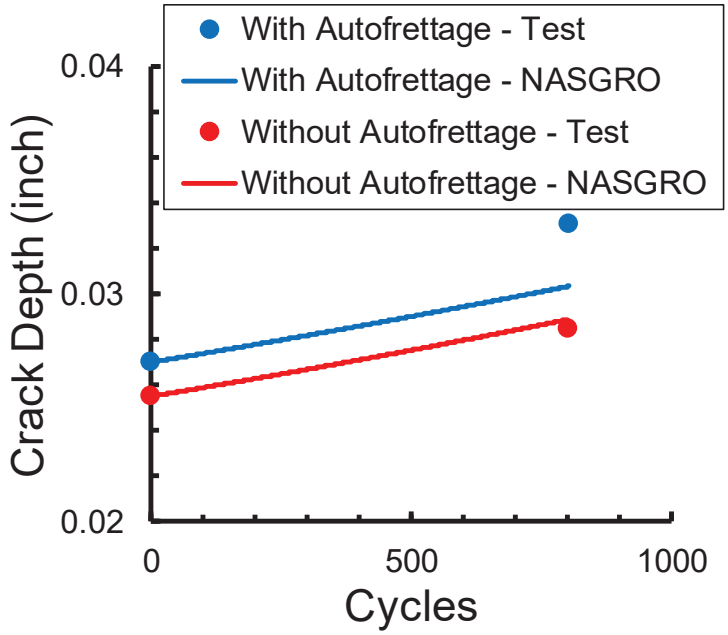

Figure 2. Crack growth as a function of cycles for two tests that were nearly identical, but one had an additional autofrettage cycle at the start of cycling.

Current Damage Tolerance Analysis Approach (ANSI/AIAA S-081B)

ANSI/AIAA S-081B standard Section 7.5.1 for pressure vessels [ref. 1] contains four requirements for DTA of pressure vessels:

1. Specifies the initial crack size as "the initial flaw (crack) size for assessment shall be greater than or equal to the minimum nondestructive testing (NDT) capability associated with the inspection technique."
2. Specifies that the autofrettage cycle can "be assessed using elastic-plastic fracture mechanics (EPFM)."
3. Specifies that for elastic service life cycles "the analysis shall use nominal or conservative values of fracture properties."
4. Finally, the standard states that "beneficial retardation effects on crack growth rates from variable amplitude loading shall not be used in the analysis."

These requirements allow the DTA to consider the influence of the autofrettage separately from that for the remaining elastic cycles. A typical DTA will start with the crack size (a_{NDT}) that represents the minimum NDT crack size associated with the inspection technique used on the COPV. The amount of crack growth (Δa_{AF}) due to the autofrettage cycle can be determined from tests or elastic-plastic analyses. The LEFM analysis for the operational cycles starts with a crack size that is the sum of the NDT crack size and the crack growth during autofrettage. The ANSI/AIAA S-081B requires that the LEFM analysis not consider "beneficial" influences (e.g., retardation) of the proceeding autofrettage cycle but does not consider the possibility of detrimental influences. The final DTA crack size (a_f) includes the amount of crack growth that the LEFM analysis predicts from the elastic cycles (Δa_{LEFM}).

$$a_f = a_{NDT} + \Delta a_{AF} + \Delta a_{LEFM} \quad (1)$$

The a_{NDT} for the analyses in this assessment was assumed to be a semi-circular with a depth of a = 0.025 inch. The amount of crack growth during autofrettage was obtained from measurements made on the post-test fracture surface and was generally less than 0.001 inch. The amount of crack growth due to the elastic cycles was measured from the post-test fracture surfaces and predicted using the NASGRO [ref. 2] LEFM crack growth analysis software.

7.0 Test and Analysis

The test measurements and FEA simulations suggest that the autofrettage cycle can produce beneficial and detrimental influences on the crack growth of subsequent LEFM cycles. The detrimental influence occurs at negative stress ratios that are typical of the conditions in COPV liners. The ANSI/AIAA S-081B standard provides baseline requirements for COPV DTAs that does not consider the possibility of detrimental influences of the autofrettage cycle. This could result in damage tolerance life predictions that are unconservative.

7.1 Phase 1 – Demonstration of the Influence of Underload Without Guide Plates

Several tests were conducted to develop additional data to support a larger investigation into the influence of an elastic-plastic autofrettage cycle on subsequent elastic cycles. The tests were conducted on 0.25-inch thick Al 6061-T6 to allow compressive loads to be applied without the need for guide plates to resist buckling. This eliminated the possibility that the guide plates could influence the measured crack growth behavior. More representative characteristics of COPV liners (e.g., wall thickness, uniaxial vs. biaxial stress state, and stress levels) are addressed in Phase 2 tests and analyses.

All of the tests were conducted with cracks that were nucleated from small laser notches. The notches were half the size (both the length and depth) of the target crack size. A single notch was placed in the center of the coupon. The coupons were fatigue cycled (precracked) with a peak stress of 20,000 psi and a stress ratio of R = 0.1. The surface crack length was periodically monitored optically during the precracking and the interval between optical measurements was decreased as the measured surface crack length approached the target length. Any test with a final surface crack length that exceeded the target length by more than 0.002 inch was not used for the Phase 1 and Phase 2 tests.

7.1.1 Phase 1 Test Approach

Eight test coupons were notched and fatigue precracked using identical conditions. The target crack size was a semi-circular surface cracks with a surface length of 2c = 0.10 inch and a depth of a = 0.05 inch (a/c = 1). These tests were nonstandard, but followed the concepts and configurations defined in ASTM STP E647 and E2899 [refs. 4, 5]. Half of the tests were conducted with a 1.25% autofrettage cycle followed by 400 LEFM cycles and the other half with only the identical 400 LEFM cycles, as summarized in Table 1. The loading of the autofrettage cycle was performed under displacement control with the global strain determined from digital image correlation (DIC) [refs. 6, 7] and virtual extensometers with a gage length of L= 1 inch, as shown in Figure 3. The autofrettage strain was the average of extensometers at the left and right coupon edges on the front and back. The displacement control ramp rate was 0.02 inch/minute and the load was decreased to the minimum stress after reaching the autofrettage strain. The subsequent elastic cycles were performed under load control with a 10-Hz sine wave. The frequency was periodically decreased to 0.01 Hz to allow the crack mouth opening displacement (CMOD) to be measured with a virtual extensometer (L = 0.02 inch) that was centered on the crack, as shown in Figure 3. The tests without an autofrettage cycle were conducted under load control with a sine wave that was identical to the cycles that followed the autofrettage cycle.

Table 1. Summary of Phase 1 Tests

	Type	Min LEFM Stress (ksi)	Max LEFM Stress (ksi)	Delta-CMOD (inch)	Delta-a LEFM (inch)	Delata NASGRO (inch)	Delta-a Autofrettage (inch)	Cycles	da/dN (in/cycle)	Striation da/dN (in/cycle)
UL-P0-02	LEFM	-30	30	0.0007	0.004	0.0018	N/A	400	1.00E-05	1.30E-05
UL-P0-03	AF & LEFM	-30	30	0.00123	0.007	0.0018	< 0.0005	400	1.75E-05	2.80E-05
UL-P0-04	AF & LEFM	-40	30	0.00139	0.012	0.002	< 0.0005	400	3.00E-05	7.70E-05
UL-P0-06	LEFM	-40	30	0.00083	0.005	0.002	N/A	400	1.36E-05	1.50E-05
UL-P0-07	AF & LEFM	-40	25	0.00124	0.007	0.0013	< 0.0005	400	1.80E-05	1.50E-05
UL-P0-08	LEFM	-40	25	0.0007	0.002	0.0013	N/A	400	4.38E-06	--
UL-P0-09	AF & LEFM	-40	20	0.00115	0.005	0.0008	< 0.0005	400	1.40E-05	--
UL-P0-10	LEFM	-40	20	0.000588	0.001	0.0008	N/A	400	2.50E-06	--

Note: UL-PO-01 is not included due test control failure not allowing it to complete the target stress/strain and number of a cycles. UL-PO-05 is not included because the initial crack exceeded the target size.

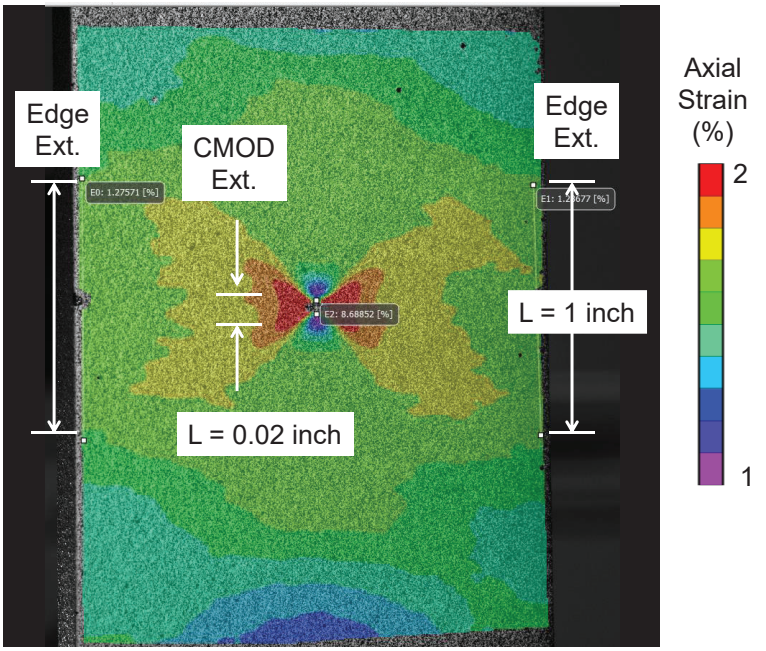

Figure 3. DIC strain field with virtual extensometer measurement of the edge strain and CMOD.

7.1.2 Test Results

The fatigue tests were conducted using loading spectrum similar to that shown in Figure 2. Half of the tests started with an autofrettage cycle followed by the LEFM cycles (AF+LEFM) and the other half of the tests omitted the autofrettage cycle (LEFM-only). The initial cycle of the AF+LEFM tests was above the material yield stress, as seen by the large increase in the global strain of the blue curve shown in Figure 4. The unloading following the autofrettage cycle had evidence of yielding as the stress approached -30,000 pounds per square inch (psi). The subsequent LEFM cycles had a linear relationship between the global strain and the stress. The LEFM-only test, shown as the red curve of Figure 4, also had a linear relationship between the global strain and the stress. The cyclic global strain range ($\Delta\varepsilon$) of the LEFM cycles for the two tests were nearly identical.

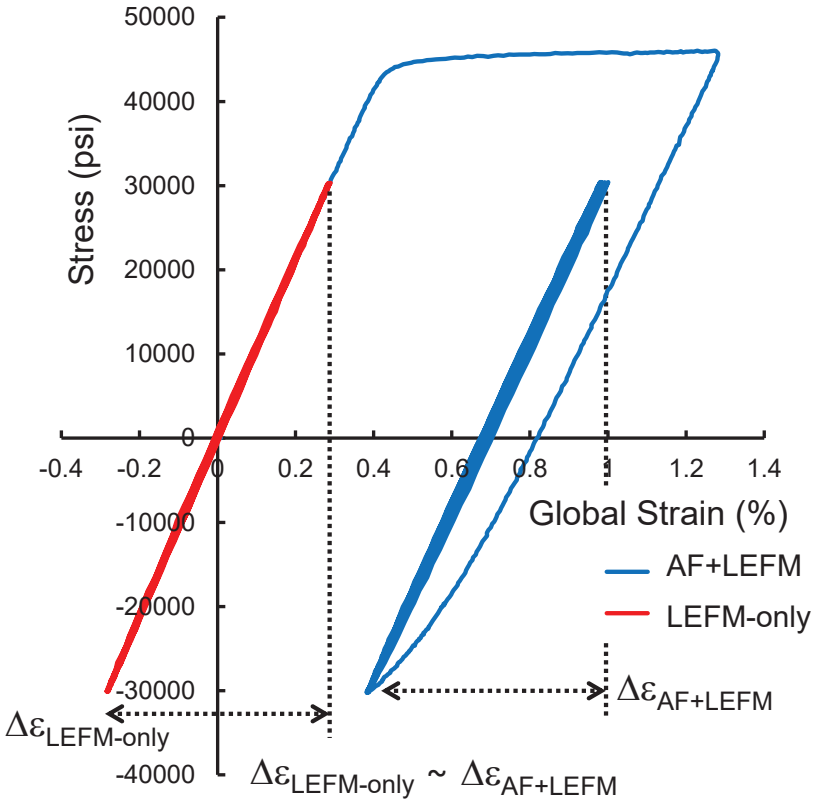

Figure 4. Representative stress versus global strain for a test with and without an autofrettage cycle.

The noise floor in the CMOD data was evaluated by examining the CMOD measurements for the first 50 image pairs that were acquired prior to the loading, as shown in Figure 5. The measured CMOD data exhibited a slight increase during the 50 seconds of unloaded data and the measurements ranged from -0.000005 inch to 0.00002 inch. This was more than an order of magnitude less than the peak displacements.

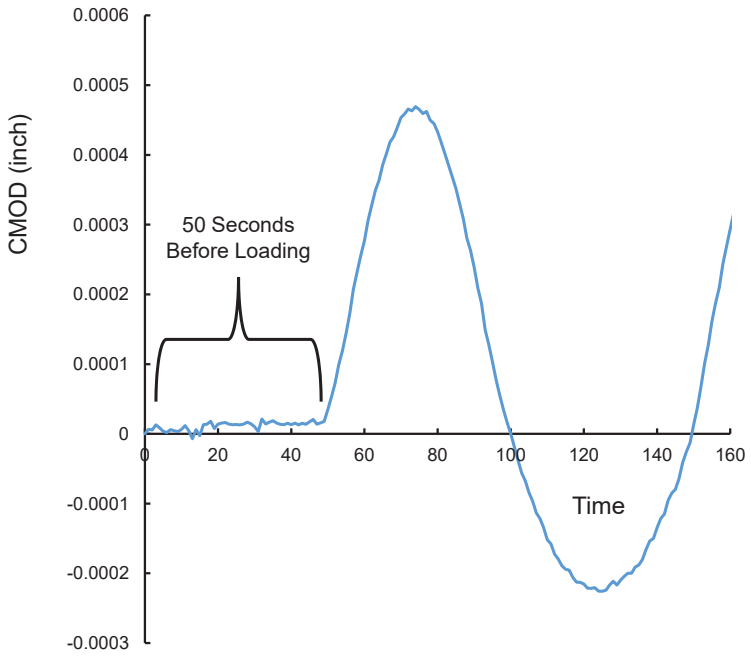

Figure 5. Noise level in the CMOD measurements.

The data from the tests shown in Figure 4 were extracted from the DIC measurements and plotted as global strain as a function of CMOD, as shown in Figure 6. The yielding of the autofrettage cycle was evidenced by the change in slope at a global strain of about 0.4% of the blue curve shown in Figure 6. The subsequent unloading exhibited yielding as the minimum unloading strain was reached. The CMOD was a linear function of the global strain for the subsequent LEFM cycles and always positive. This suggests that the crack surfaces were open, even when the global strains (and stresses) were negative.

The relationship between the CMOD and the global strain for the LEFM-only tests had two linear sections, as shown by the red curve of Figure 6. The linear section slope for positive global strains was about the same as that of the LEFM portion of the AF+LEFM test. The slope was higher for the section of the LEFM-only test for the negative global strains. This resulted in a larger cyclic CMOD range (ΔCMOD) for the LEFM cycles of the AF+LEFM test than for the same LEFM cycles in the LEFM-only test. The negative CMOD measurements observed in the LEFM-only test suggest that the crack surfaces were in contact for the negative global strains. The DIC measurement location for the CMOD was 0.01 inch above and below the edge of the crack. The negative CMOD was likely a result of material deformation between the crack edges and the measurement location as the crack surfaces come into contact. The measurement of CMOD directly at the edge of a crack with the surfaces in contact would be zero (i.e., a vertical line as a function of global strain).

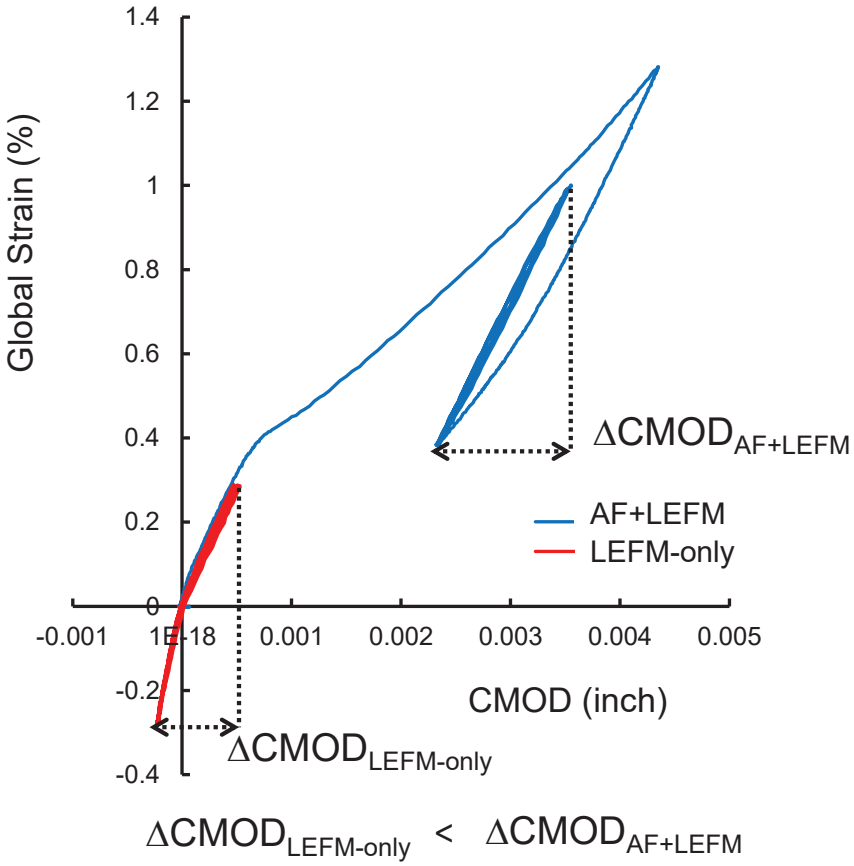

Figure 6. Representative global strain versus CMOD for a test with and without an autofrettage cycle.

The DIC strain fields were extracted for the peak and minimum stresses for the first two cycles of an AF+LEFM test with R = -1, as shown in Figure 7. The crack tip strains exceed 2% at the autofrettage cycle peak. The strains are reduced at the minimum strain of the autofrettage cycle but are still tensile, suggesting that the crack is open at a compressive stress of -30,000 psi. Similar DIC strain fields were extracted for the first LEFM cycle of a LEFM-only test with R = -1, as shown in Figure 8. The peak stress for the first LEFM-only cycle had a significantly lower crack tip strain than that of the AF+LEFM test, as shown by comparing the strain fields of Figures 7 and 8. Note that the scale in Figure 7 had been reduced to highlight the lower strains. The crack tip strains at the minimum stress of the first LEFM cycle were compressive, suggesting that the crack was closed. The stresses remained compressive until the stress became positive on the subsequent loading cycle.

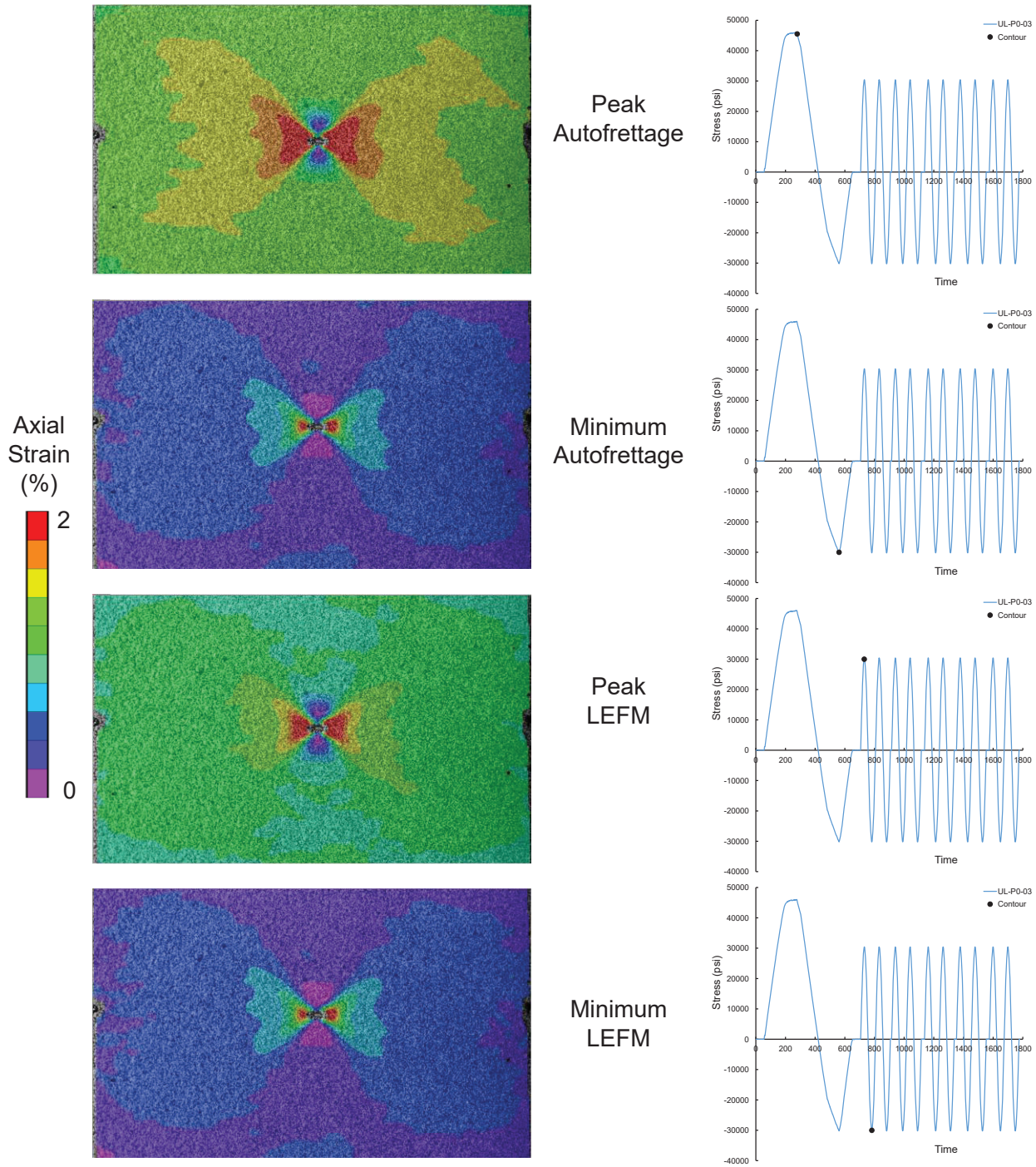

Figure 7. DIC strain fields for the peak and minimum stresses for the first two cycles of an AF+LEFM R = -1 test.

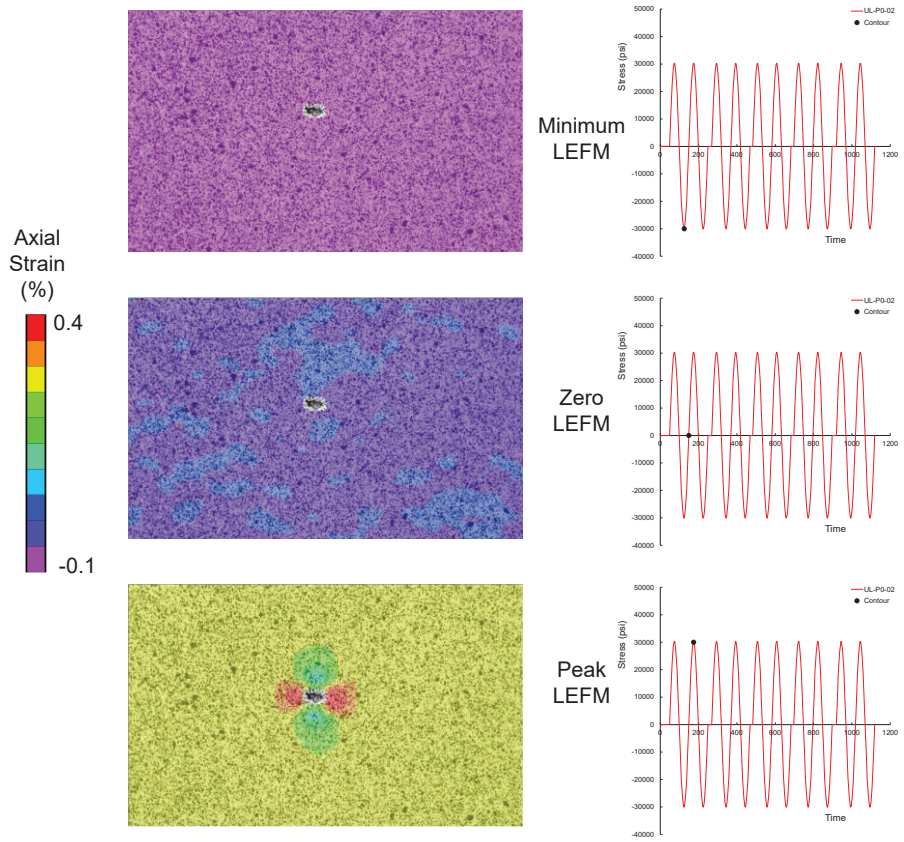

Figure 8. DIC strain fields for the peak and minimum stresses for the first cycle of an LEFM-only R = -1 test.

The DIC measurements were used to characterize the cyclic strain by defining the image pair captured at the minimum stress of the first LEFM cycle as the "undeformed" condition. The strain at the subsequent peak stress would be the cyclic strain due to the loading. The cyclic strains were extracted for AF+LEFM and LEFM-only tests with a stress ratio of R = -1.33, as shown in Figure 9. The cyclic strains for the AF+LEFM test were significantly higher than measured in the LEFM-only test.

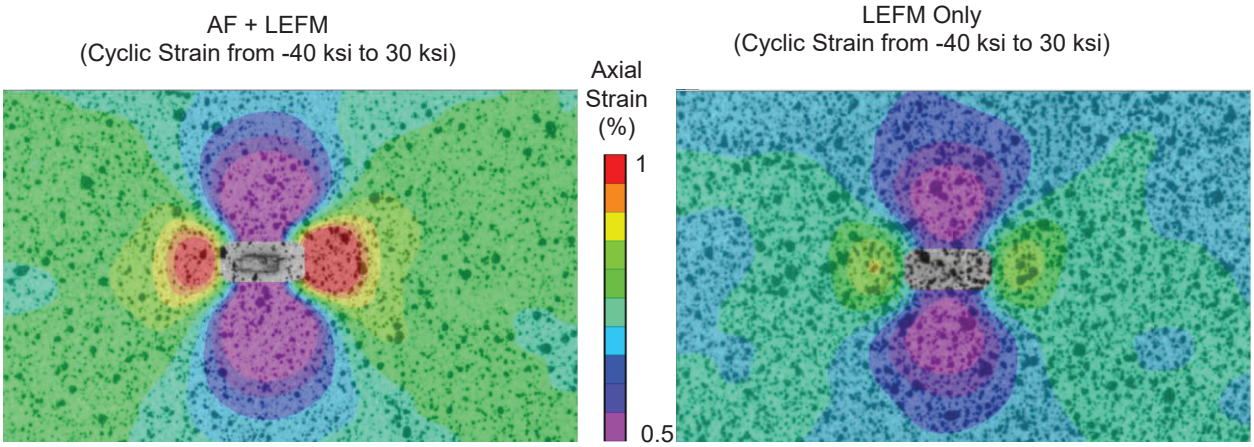

Figure 9. Cyclic strains for AF+LEFM and LEFM-only tests conducted at a stress ratio of R = -1.33.

The crack growth was measured from the post-test fracture surface. The coupons were notched from the edges to within 0.05 inch of the visible surface crack tip, then loaded monotonically to failure after the completion of the LEFM cycles. The notching reduced the plasticity at failure and minimized distortions to the fracture surface. Post-test examination of the fracture surface revealed several different regions that were a result of the loading: (1) laser notch, (2) elastic precrack, (3) autofrettage cycle, (4) LEFM cycles, and (5) ductile tearing, as shown in Figure 10.

The crack growth during the LEFM cycles can be directly measured from the fracture surfaces. The autofrettage cycle produced a distinct line that marked the boundary between the crack growth produced by the elastic precracking and the LEFM cycles, as shown in Figure 10. The ductile fracture that resulted from the monotonic loading to failure also produced a distinct interface that defined the end of the LEFM cycles. The crack growth was measured as the distance between the autofrettage mark and the start of ductile fracture. The average crack growth rate for the LEFM cycles was determined by dividing by the number of LEFM cycles applied.

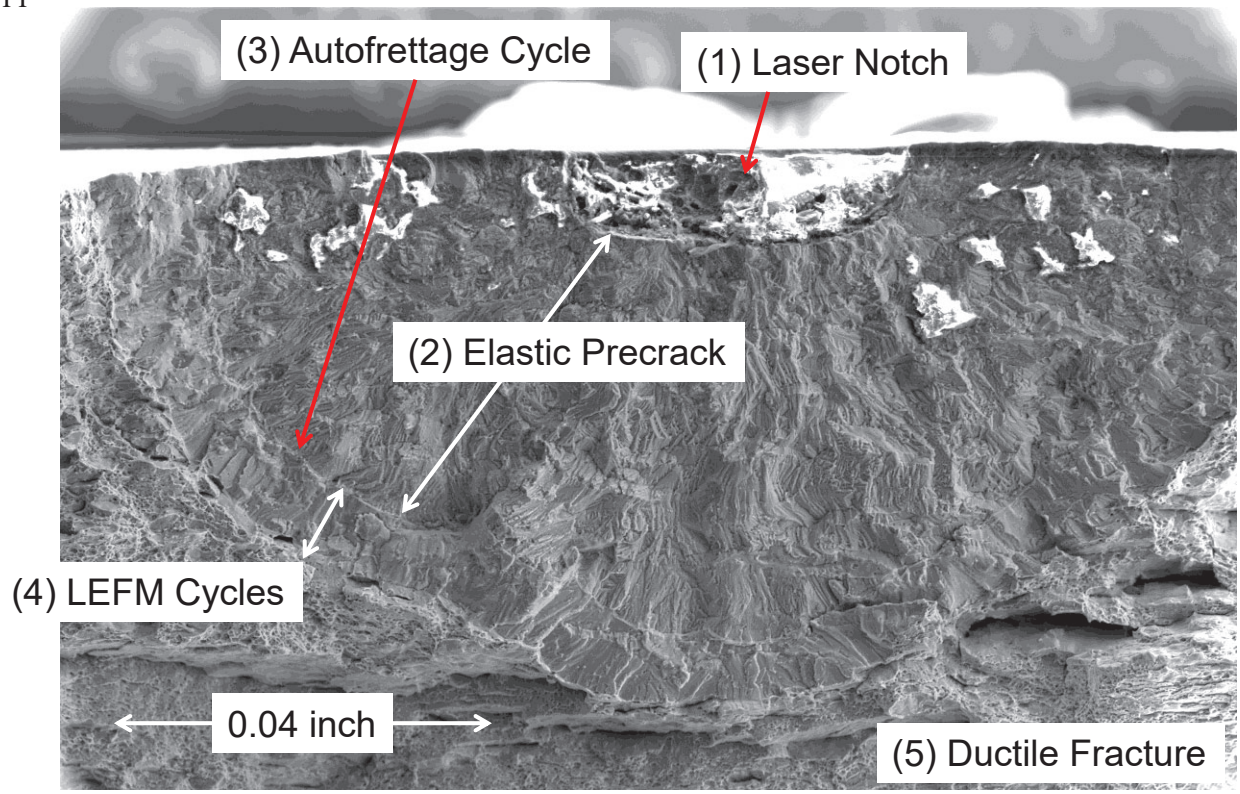

Figure 10. Typical fracture surface from an AF+LEFM test with the different regions of the fracture surface identified.

The fracture surfaces from two tests that were conducted with the same 400 LEFM cycles, one with and one without an autofrettage cycle, is shown in Figure 11. The crack growth of the AF+LEFM test had significantly more crack growth than measured in the LEFM-only test with the same number of LEFM cycles. The average crack growth rate was obtained by dividing the measured crack growth by the number of applied cycles. The average crack growth rate of the AF+LEFM test was about 9 times faster than that of the LEFM-only test. The Phase 1 tests were conducted with identical autofrettage peak strains and the subsequent minimum stress either -30,000 psi or -40,000 psi, as shown previously in Table 1. Three different values of peak LEFM

stress (20,000 psi, 25,000 psi, and 30,000 psi) were applied to the different tests. The resulting measurements indicated that the crack growth rate was faster in each AF+LEFM test than in the corresponding LEFM-only test, as shown in Figure 12 where the average crack growth rate (da/dN) is plotted as a function of the average stress intensity factor at maximum stress (K_{max}). The Phase 1 fracture surfaces for each test are provided in Appendix B.

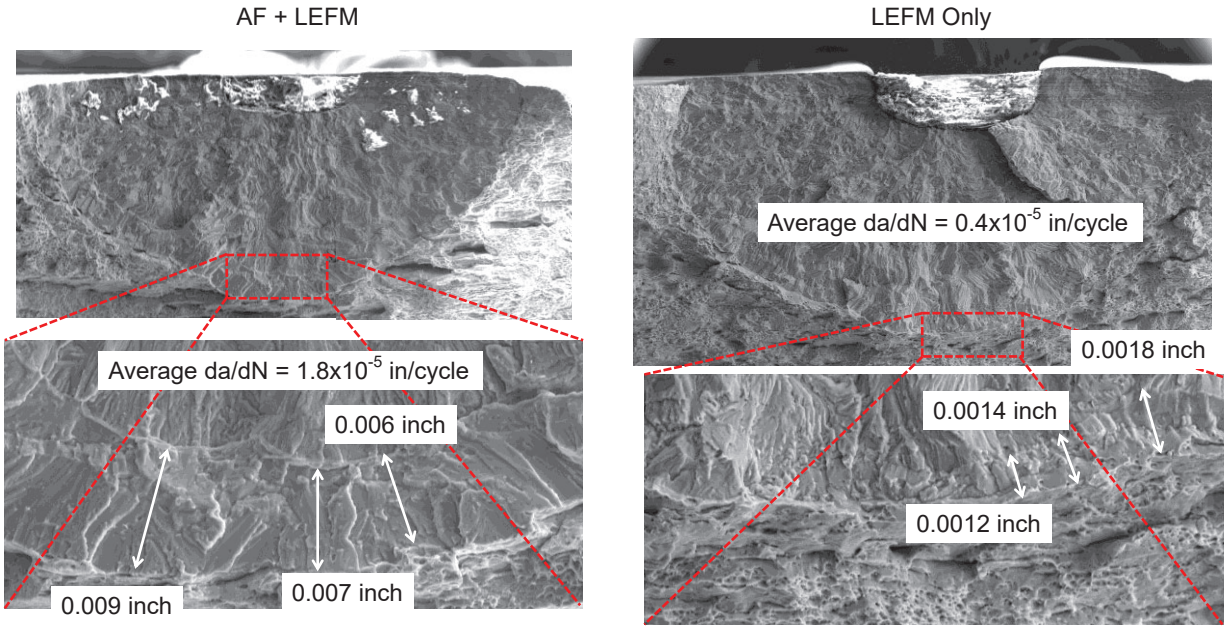

Figure 11. Fracture surfaces of AF+LEFM and LEFM-only tests that were conducted with a stress ratio of R = -1.6.

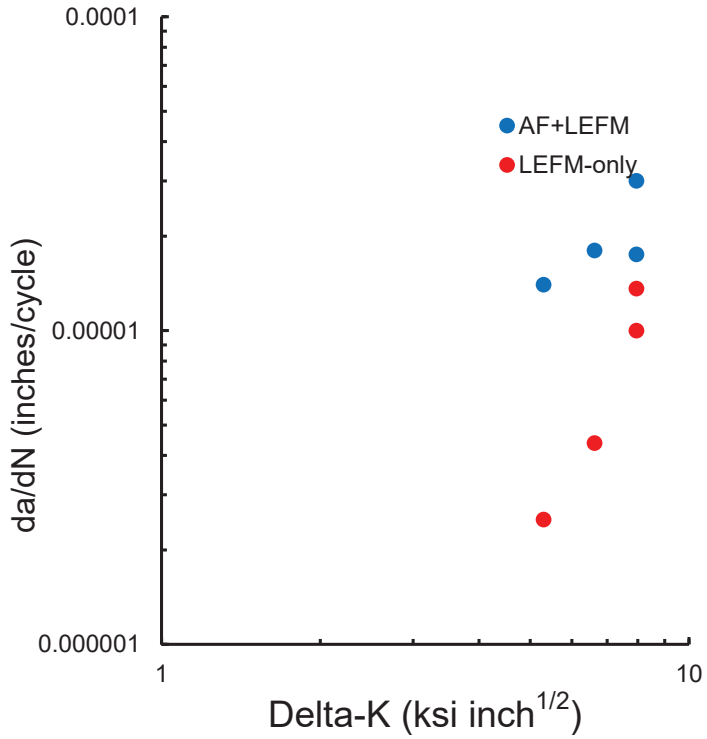

Figure 12. Crack growth rate from the Phase 1 tests.

7.1.3 Phase 1 Summary

The test techniques used in the Phase 1 study provided an approach that could be used to evaluate the influence of the elastic-plastic autofrettage cycle on the subsequent elastic cycles. The fracture surface measurements provided direct evidence of faster crack growth following the autofrettage cycle. The DIC data provided several measurements that provide evidence for the sources of the accelerated crack growth that were explored in Phase 2. This evidence includes:

1. The CMOD remained completely open for the LEFM cycles that followed the autofrettage cycle, while the CMOD was closed for the negative portion of the LEFM-only cycles. A closed crack requires a portion of the cyclic stress range to open the crack before damage can occur at the crack tip [refs. 8, 9, 10].
2. The ΔCMOD for the LEFM cycles that followed an autofrettage was greater than the ΔCMOD for LEFM-only cycles. Supporting the previous concept that smaller portion of the cyclic stress range is available to cause damage at the crack tip for a closed crack.
3. The cycle strain at the crack tip was greater for the LEFM cycles that followed the autofrettage cycle than for LEFM-only cycles. Crack growth has been suggested to be influenced by the cyclic strain range [refs. 11, 12].

7.2 Phase 2 – COPV Liner Representative Tests, Analyses, and Simulations

The Phase 2 effort was a combined experimental, finite element modeling (FEM), and numerical crack growth simulation task. The Phase 2 tests were conducted under conditions that were representative of COPV liners.

- A common COPV liner material (Al 6061-T6) was selected
- A thickness (0.060 inch) was selected to be within the range of typical COPV liners (0.03 inch to 0.1 inch)
- An NDT crack size (a = 0.025 inch and a/c = 1) was selected to be representative of the detectable size for dye penetrant and eddy current
- A global autofrettage strain (1.5%) was selected to be below the threshold for stable tearing at the selected crack size [ref. 3]
- The peak stress (30,000 psi) for the LEFM cycles was selected to be about 70% of the Al 6061-T6 yield

Pairs of tests were conducted with (AF+LEFM) and without (LEFM-only) an autofrettage cycle and identical LEFM cycles. The minimum stress of the LEFM cycles was different for each pair of tests and selected to provide different LEFM stress ranges from $-1.3 < R < 0.5$. The negative stress ranges enveloped most stress ranges for elastically responding COPV liners. Tensile hysteresis tests were also conducted to support the validation of the elastic-plastic FEA.

FEAs were conducted to enhance the understanding of the behavior of the cracks in the uniaxial coupons and to evaluate the influence of biaxial loading. The FEAs were validated with physical measurements made during the AF+LEFM and LEFM-only tests. The validated FEA characterized near crack tip conditions away from the crack surface where DIC measurements were recorded. COPV liners are loaded biaxially while damage tolerance tests are loaded uniaxially. A validated FEA examined the difference between the response in uniaxial coupons and biaxial COPV liners. Finally, crack growth simulations of the LEFM cycles were performed using the NASGRO [ref. 2] linear elastic crack growth analysis software. The crack growth

parameters for the Al 6061-T6 were obtained from the NASGRO material database. The simulations were compared to crack growth measurements made on tests with and without the autofrettage cycle.

7.2.1 Phase 2 Test Approach

Fatigue crack growth tests were conducted on 0.06-inch thick Al 6061-T6 sheet material using procedures similar to that used in Phase 1. The coupons were 2-inch wide in the gage section with a small laser notch in the coupon's center, as shown in Figure 13. The laser notch had a target length and depth of 0.02 inch and 0.01 inch, respectively. This notch size was selected to be less than half of the target crack length after precracking. The laser notching process created a nearly rectangular notch with a width of about 0.01 inch.

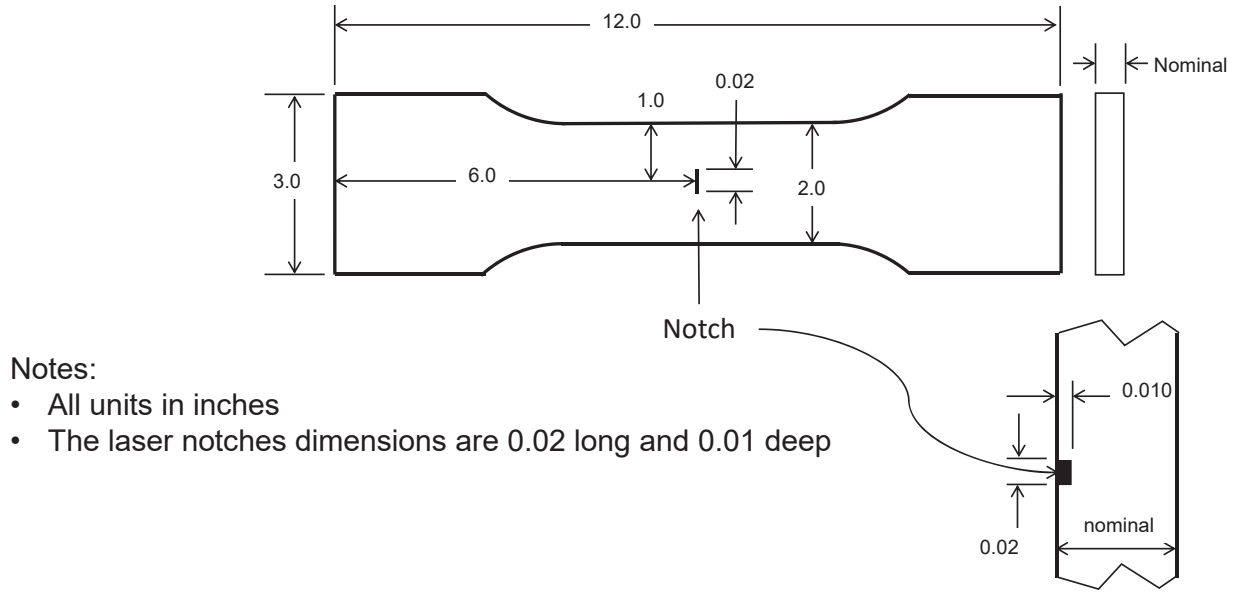

Figure 13. Schematic of the coupon used for the surface crack fatigue tests.

The target crack size was a semi-circular surface crack (a/c = 1) with a depth of a = 0.025 inch and a surface crack length of 2c = 0.05 inch. The surface around the notch was polished prior to fatigue cracking to allow optical crack length measurements. The coupons were fatigue cycled under load control at a frequency of 10 Hz. The maximum stress (S_{max} = 20,000 psi) was selected to less than half of the material yield stress and below the stress level of the LEFM cycles. The minimum stress (S_{min} = 2,000 psi) was selected to be a small tensile value to eliminate the risk of buckling the coupon. The resultant stress ratio was $R = S_{min}/S_{max} = 0.1$. The selected stress conditions resulted in cracks nucleating from the laser notch and propagating to the target surface crack length (2c=0.050 inch) in about 200,000 cycles.

The experimental investigation of the influence of the autofrettage was performed similarly as was done in Phase 1. The most significant differences were the use of guide plates to restrict the buckling of the coupon under compressive loads and the use of physical extensometers to measure the autofrettage strain. The guide plates consisted of two Al plates that were about 0.5-inch thick. The guide plates "sandwiched" the coupon and were held in place with finger tightened bolts, as shown in Figure 14. Teflon™ tape was placed on the inside surfaces of the guide plates to reduce the friction between the plates and coupon, thus minimizing the load transfer through the guide plates. The width of the guide plates (w = 1.950 inches) was 0.05 inch

narrower than the coupon's gage section to allow edge extensometers to contact the coupon's edge. The average of the strain measured by the two edge extensometers was used to control the loading to the target autofrettage strain. Tapered holes with an inside diameter of 0.5 inch and an outside diameter of 1 inch were drilled into both sides of the guide plates to allow an optical path for DIC measurements around the crack and the back surface opposite the crack.

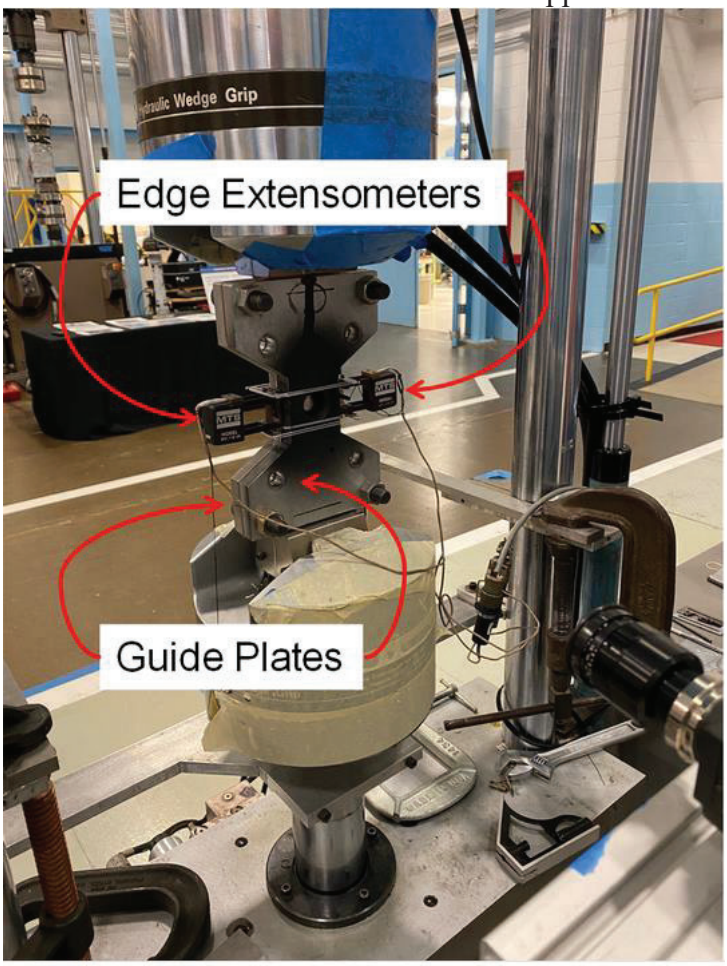

Figure 14. Guide plates used in the fatigue testing of the Phase 2 coupons.

The loading spectrum for the tests with an autofrettage cycle (AF+LEFM) was performed with a combination of displacement control (for the AF cycle to 1.5% strain) and load control (for the LEFM cycles), as illustrated in Figure 15. The displacement controlled loading had a rate of 0.02 inch/minute. The first two LEFM cycles were performed with a frequency of 0.01 Hz and DIC images were captured. The frequency was increased to 10 Hz and additional cycles were applied. The frequency was periodically decreased to 0.01 Hz for blocks of two cycles to allow the capture of DIC images. The loading spectrum for the LEFM-only tests consisted of sine waves under load control, as illustrated in Figure 15. The loading frequency and DIC image acquisition were performed identically to the AF+LEFM tests.

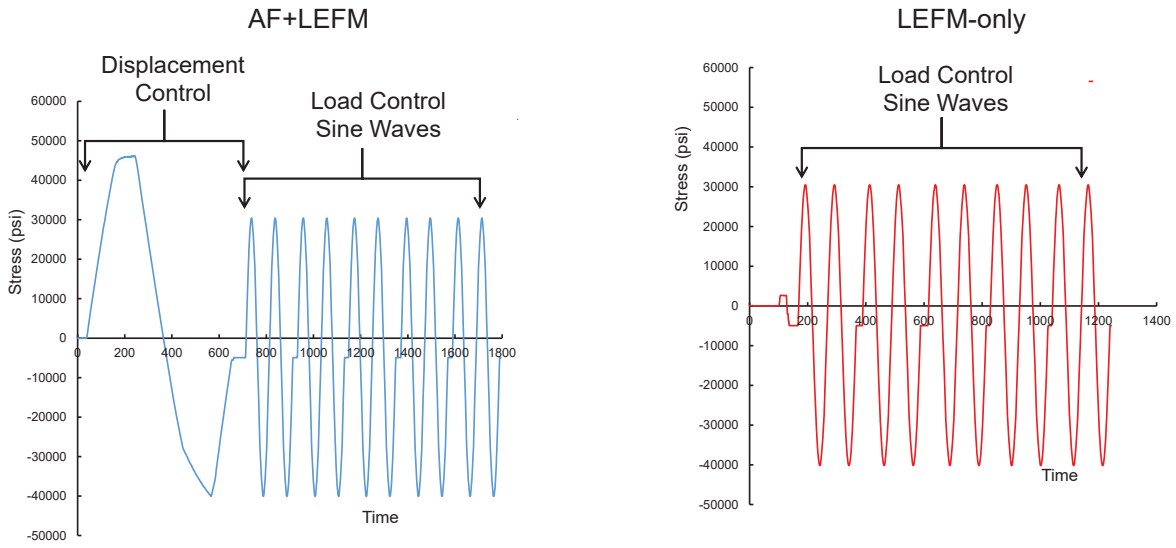

Figure 15. Schematic of the methods used to apply the autofrettage and LEFM cycles.

The autofrettage strain level and the maximum LEFM stress for the Phase 2 AF+LEFM tests were 1.5% and 30,000 psi, respectively. The minimum LEFM stress varied with each test to produce stress ratios between R = -1.3 (highly compressive at minimum stress) and R = 0.5 (tensile minimum stress). Each AF+LEFM test had a corresponding LEFM-only test with identical maximum and minimum stresses for the LEFM cycles.

7.2.2 Phase 2 Test Results

The CMODs were extracted from the DIC data using a virtual extensometer with a gage length of L= 0.02 inch, The virtual extensometer was centered on the crack, as shown in Figure 16, for a test with LEFM cycles that had a stress ratio of R = -1.3. The crack tip tensile yielding is evident by the large increase in CMOD for the initial autofrettage cycle. The stress versus CMOD behavior was initially linear during the unloading that followed the peak autofrettage strain but became nonlinear around -25,000 psi as global yielding of the coupon occurred. The stress versus CMOD behavior was linear during the loading of the first LEFM cycle until about 25,000 psi when a small deviation from linearity was observed.

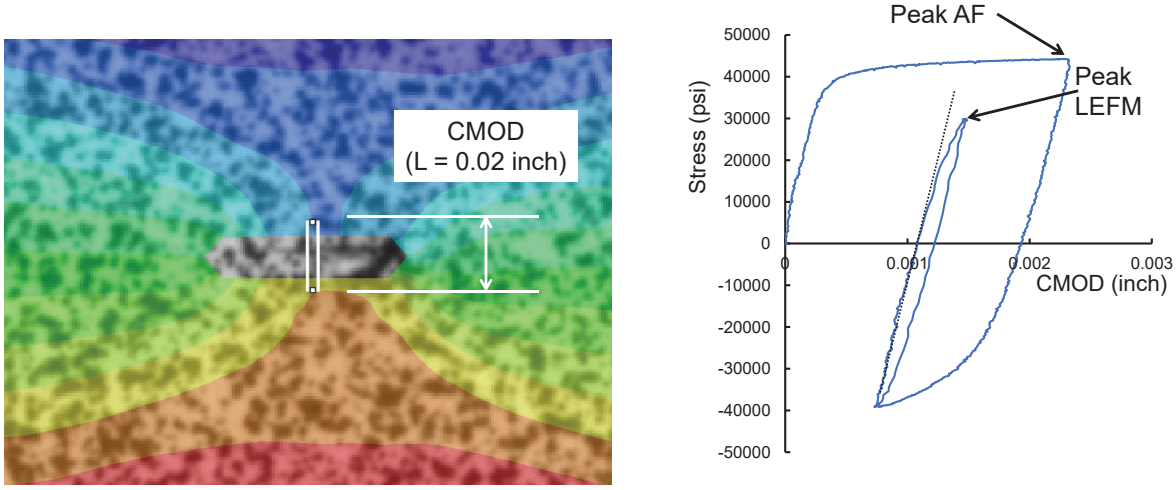

Figure 16. CMOD measurements for a Phase 2 AF+LEFM test at R = -1.3.

The crack growth during autofrettage and the LEFM cycles was obtained from measurements taken from the fracture surfaces that were broken open after each test. The notch, elastic precrack region, autofrettage cycle, LEFM cycles, and the ductile tearing regions are visible, as previously described in Figure 10. The fracture surfaces from two tests, one with an initial autofrettage (19B, AF+LEFM) and one without an initial autofrettage cycle (20B, LEFM-only) are shown in Figure 17. The autofrettage cycle left a clear indication of the crack front on the left-hand fracture surfaces (19B). The distance between the mark left by the autofrettage cycle and the ductile fracture region was the amount of crack growth (Δa=0.0077 inch) due to the LEFM cycles. The difference between the elastic precrack region and the LEFM crack growth region was less well defined in the LEFM-only test (20B), but a faint change in the fracture surface can be identified in the higher magnification image shown in the lower right of Figure 17. The amount of crack growth due to the LEFM cycles in the LEFM-only test was Δa=0.0022 inch, more than 3x slower than that in the identical AF+LEFM test. The Phase 2 fracture surfaces for each test are provided in Appendix C.

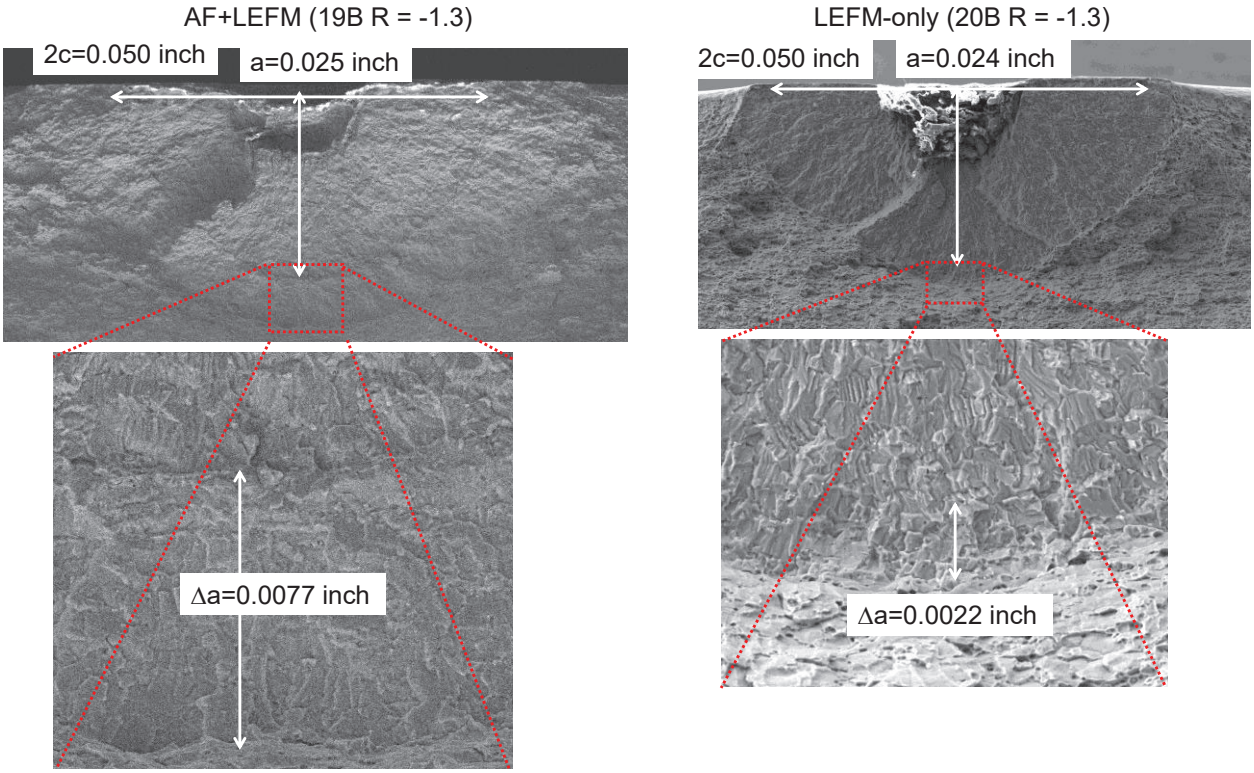

Figure 17. Fracture surfaces for two tests at R = -1.3, one with (AF+LEFM) and one without (LEFM-only) an initial autofrettage cycle.

The crack growth rate (da/dN) during the LEFM cycles was measured for tests with stress ratios of $-1.3 < R < 0.5$, as shown in Figure 18. The LEFM-only tests were representative of a typical damage tolerance test approach. ANSI/AIAA S-081B requirements allow the damage tolerance life of the LEFM cycles following the autofrettage cycle to be determined without regard to the influence of the autofrettage cycle. The AF+LEFM tests represent the actual conditions of an elastically responding COPV liner. The crack growth in the AF+LEFM tests was faster (unconservative) relative to the LEFM-only tests for the loading conditions that bound the behavior of COPV liners ($R < 0$), as shown in Figure 19. The crack growth rates in the

AF+LEFM tests were slower (conservative) relative to the LEFM-only tests for positive stress ratios. The cyclic CMOD (ΔCMOD) DIC measurements were extracted from the AF+LEFM and LEFM-only tests, as shown in Figure 20. The ΔCMOD of the AF+LEFM tests was greater than the corresponding LEFM-only tests for the negative stress ratios. This suggests that the AF+LEFM tests have more energy available for crack growth than the LEFM-only tests, corroborating the faster crack growth rate observed in the AF+LEFM tests. The ΔCMOD measurements for the positive stress ratios were nearly identical for the AF+LEFM and LEFM-only tests, suggesting that a mechanism other than cyclic energy was contributing to the slower crack growth in the AF+LEFM tests. The FEAs described in the next section investigated the crack tip behavior in greater detail.

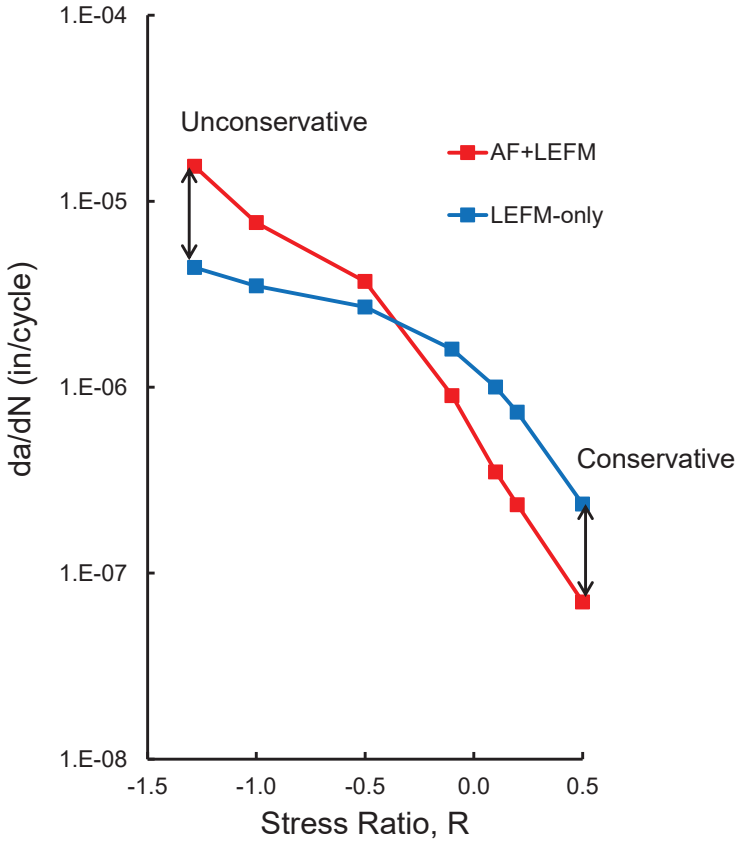

Figure 18. Crack growth rate for the LEFM cycles in the AF+LEFM and LEFM-only tests.

ID	LEFM Cycles	da (inch)	da/dN (in/cycle)	AF (% Strain)	Max Stress (psi)	Min Stress (psi)	R
19B	500	0.0077	1.5E-05	1.5	30000	-38500	-1.3
20B	500	0.0022	4.4E-06	None	30000	-38500	-1.3
04T	600	0.0046	7.7E-06	1.5	30000	-30000	-1.0
07T	600	0.0021	3.5E-06	None	30000	-30000	-1.0
02T	1000	0.0037	3.7E-06	1.5	30000	-15000	-0.5
03T	1000	0.0027	2.7E-06	None	30000	-15000	-0.5
12T	2000	0.0018	9.0E-07	1.5	30000	-3000	-0.1
10T	2000	0.0032	1.6E-06	None	30000	-3000	-0.1
06T	4000	0.0014	3.5E-07	1.5	30000	3000	0.1
01T	4000	0.0040	1.0E-06	None	30000	3000	0.1
09T	6000	0.0014	2.3E-07	1.5	30000	6000	0.2
08T	6000	0.0044	7.3E-07	None	30000	6000	0.2
14T	10000	0.0014	1.4E-07	1.5	30000	15000	0.5
13T	10000	0.0047	4.7E-07	None	30000	15000	0.5

Typical of COPV Liner Conditions

Indicates AF + LEFM has a higher crack growth rate

Indicates LEFM-only has a higher crack growth rate

Figure 19. Summary of the Phase 2 AF+LEFM and LEFM-only tests.

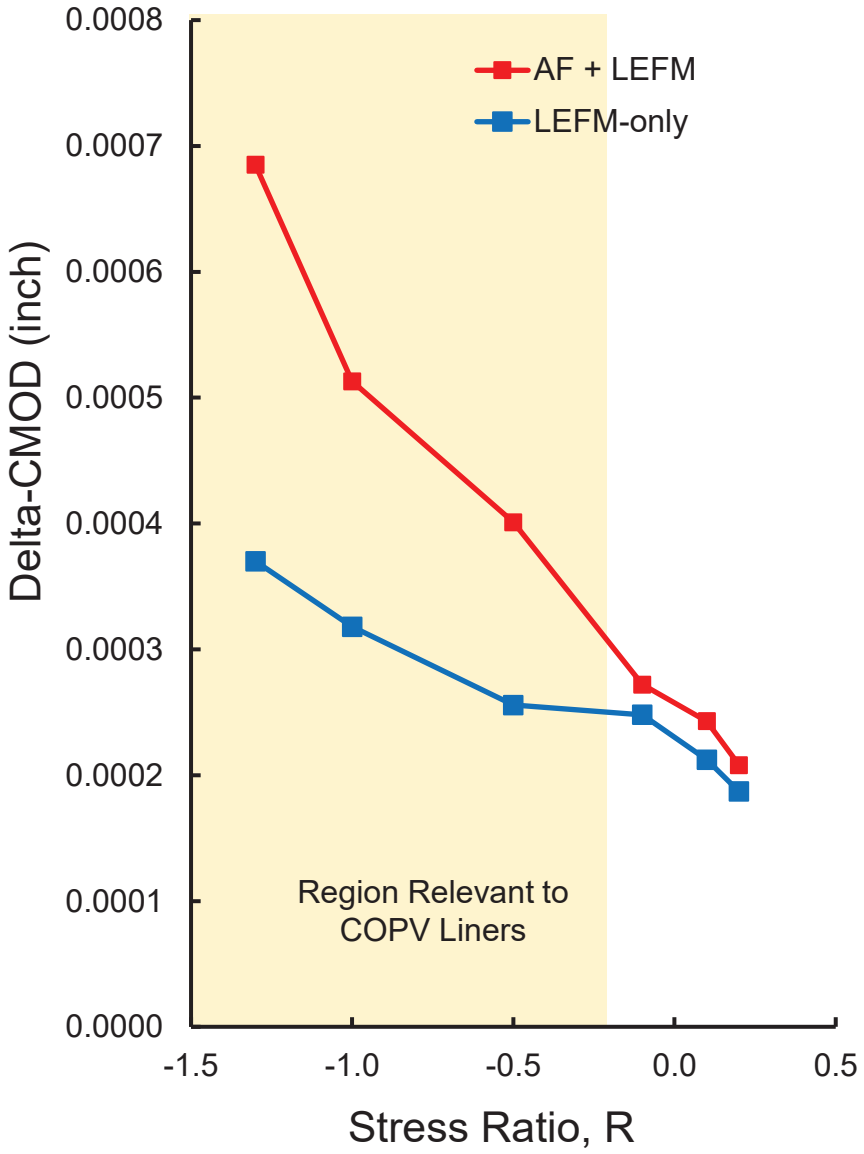

Figure 20. Cyclic crack opening displacement for the Phase 2 AF+LEFM and LEFM-only tests.

7.2.3 Phase 2 FEM Validation

FEA was performed using Abaqus [ref. 13]. The elastic-plastic material behavior was derived from cyclic tensile tests conducted on material extracted from the same Al 6061-T6 sheet as was used for the Phase 2 fatigue crack growth tests. Details of the FEM are provided in Appendix A. FEA validation was done through comparison with DIC measurements taken during mechanical tests. A comparison between simulated cyclic tensile response and the measured response is shown in Figure 21. The FEA is in agreement with the observed cyclic tensile response.

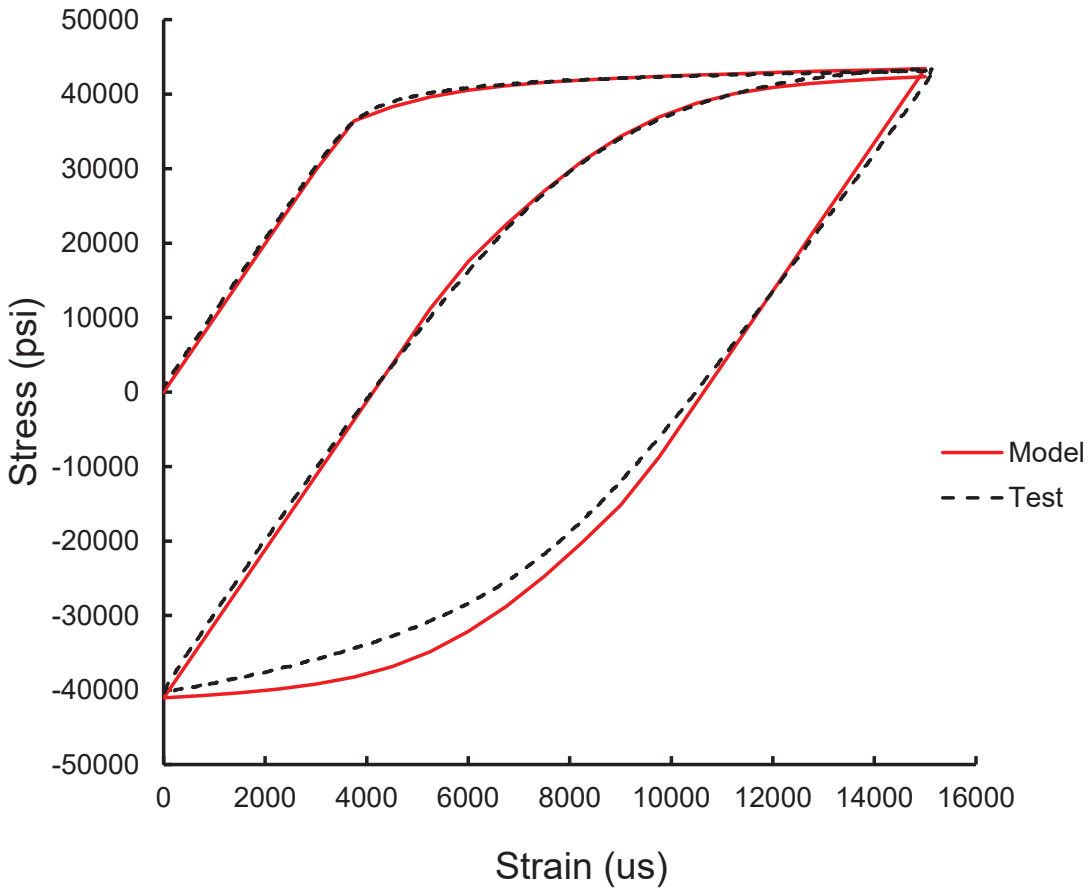

Figure 21. Test measurements and FEA simulation of the cyclic tensile test.

The steps in the surface crack FEA validation included comparison of test measurements and FEA simulations of: (1) crack tip surface strains, (2) CMOD at the autofrettage strain of 1.5%, (3) CMOD at the peak LEFM stress as a function of stress ratio, and (4) crack tip opening displacements (CTOD) near the surface at the autofrettage strain of 1.5%.

The surface strain field in the direction of loading was obtained from the DIC measurements for the 1.5% autofrettage stain conditions. This strain field contour was compared qualitatively to the strain field from the FEA for the same 1.5% strain, as shown in Figure 22. The magnitude and extent of the peak strains at the crack tip from the FEA are in reasonable agreement with the test measurements.

A quantitative comparison of the CMOD at peak autofrettage strain was made between the DIC measurements and FEA simulation. The CMOD was extracted at points 0.01 inch above and below the center of the crack, as shown in Figure 23. The DIC measurements were made during the loading to the 1.5% strain for six tests and plotted as a function of the applied stress. The FEA model simulated the identical conditions of the test and was in good agreement with the magnitude of the CMOD during the loading, as shown by the green curve of Figure 23. The CMOD measurements were made at the same distance above and below the crack as were the DIC measurements. The CMOD for the peak stress of the first LEFM cycle was extracted from the DIC data and the FEA simulations as a function of the stress ratio of the Phase 2 tests, as shown in Figure 24. The FEA simulations of the CMOD were within 10% of the DIC

measurements from the tests for all stress ratios and the average difference for all tests and analyses was 3%.

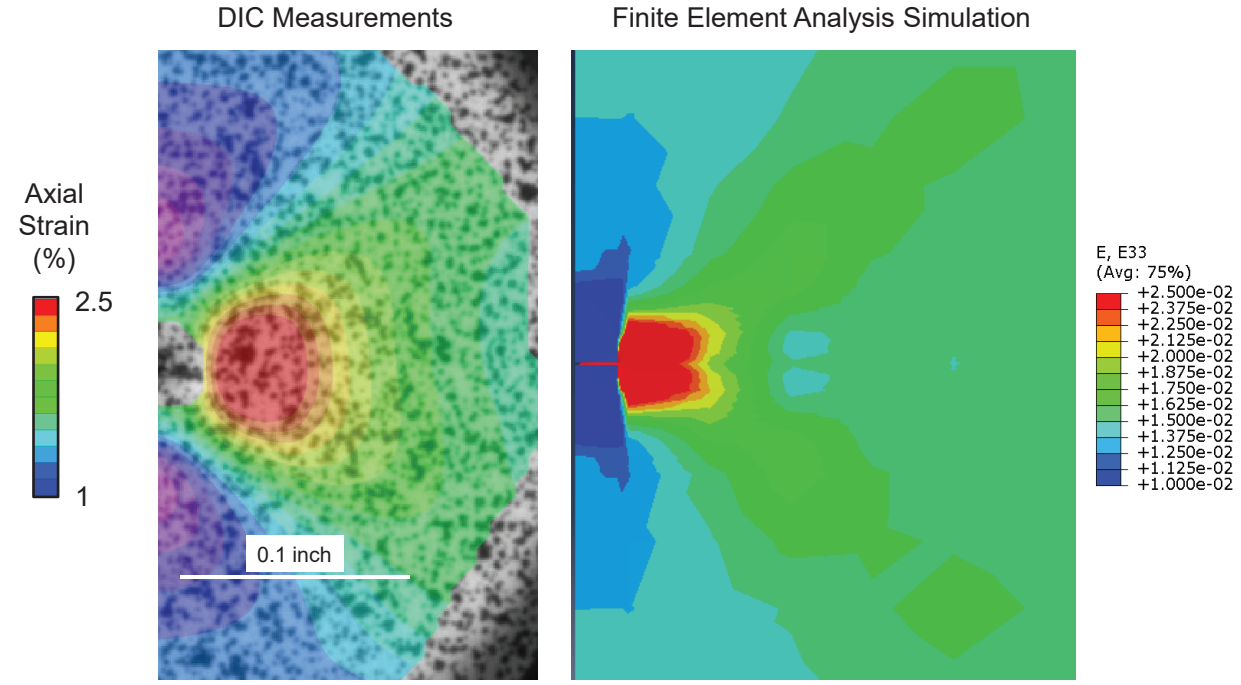

Figure 22. Crack tip stress fields at the surface from the DIC measurements and the FEA simulation for conditions at the autofrettage strain of 1.5%.

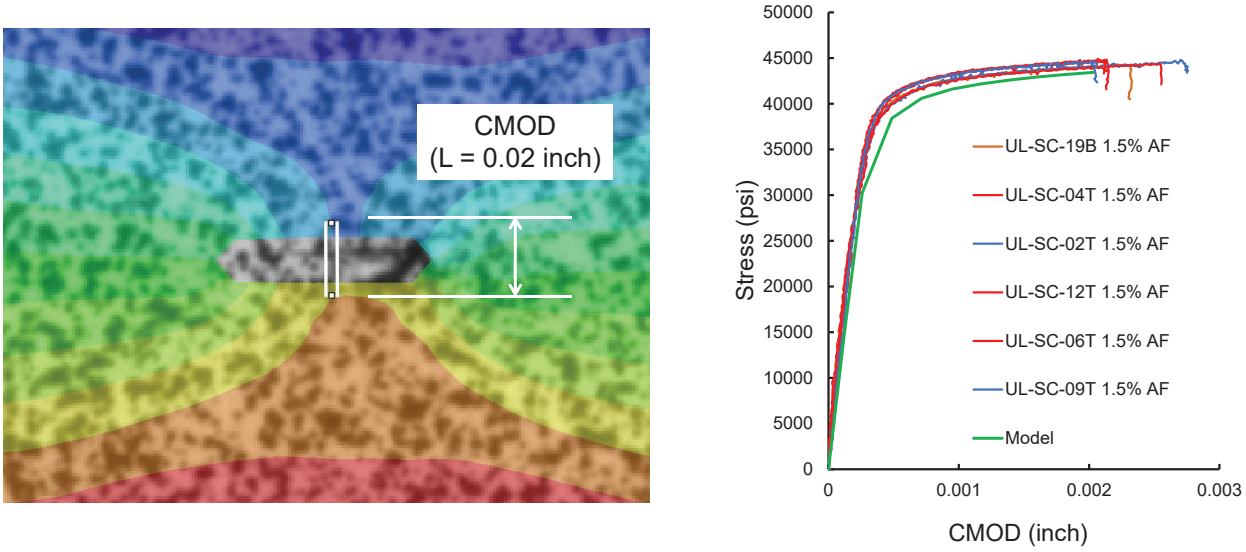

Figure 23. CMOD during the loading portion of an autofrettage cycle from DIC measurements and an FEA simulation.

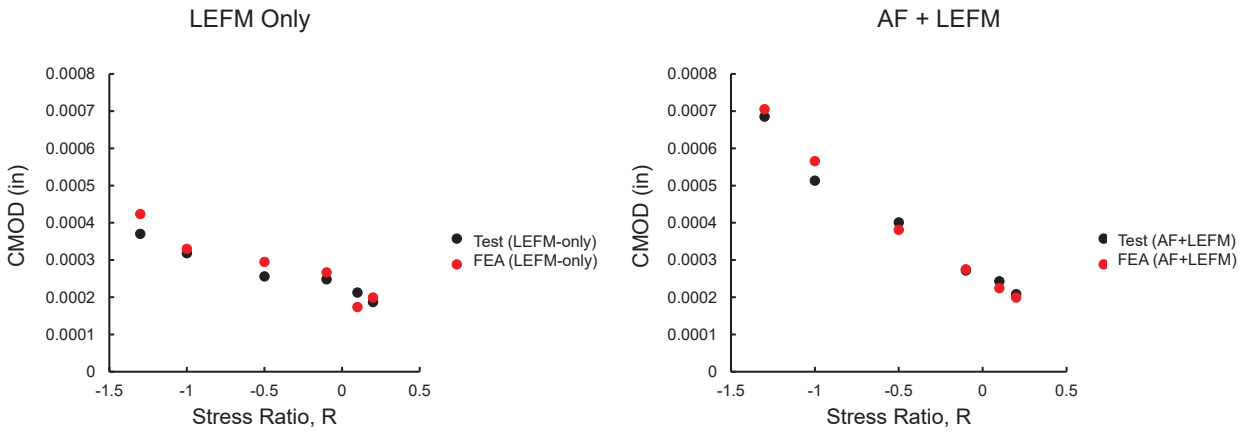

Figure 24. CMOD extracted at the peak stress of the first LEFM cycle from the DIC data and the FEA simulations.

The CTOD provides a quantification of the near crack tip behavior but is difficult to determine from the DIC data without using higher magnification images. A technique was developed to measure the CTOD near the surface using Repliset™ [ref. 14] to make a mold of the crack surfaces at the 1.5% autofrettage strain. The test coupon had a laser notch that was fatigue precracked elastically to the target crack size (2c = 0.050 inch and a = 0.025 inch). The coupon was loaded to 1.5% strain and held to keep the crack open. The Repliset ™ compound was applied to the crack surface and allowed to flow into the crack depth. The mold was allowed to set for 15 minutes to solidify, then the coupon was pulled to failure to free the mold. The schematic of the coupon, shown in Figure 25, contains an exaggerated drawing of the surface view of the rectangular notch with cracks growing from the top corners. The Repliset ™ flowed into both the notch and cracks. The extracted mold was a reverse of the notch and crack; the notch is a hole in the coupon, but a raised rectangle in the mold, as shown in the top view of Figure 25. The mold was tilted 55° to reveal the bottom crack surface and the depth (0.004 inch) that the Repliset ™ was able to flow into the crack. The blunted crack shape is visible in the tilted view of the mold. The CTOD was measured from the top surface of the mold that represents the crack front at a distance of 0.004 inch from the surface. The CTOD from the FEA simulation was in good agreement with the measurements from the mold, as shown in Figure 26.

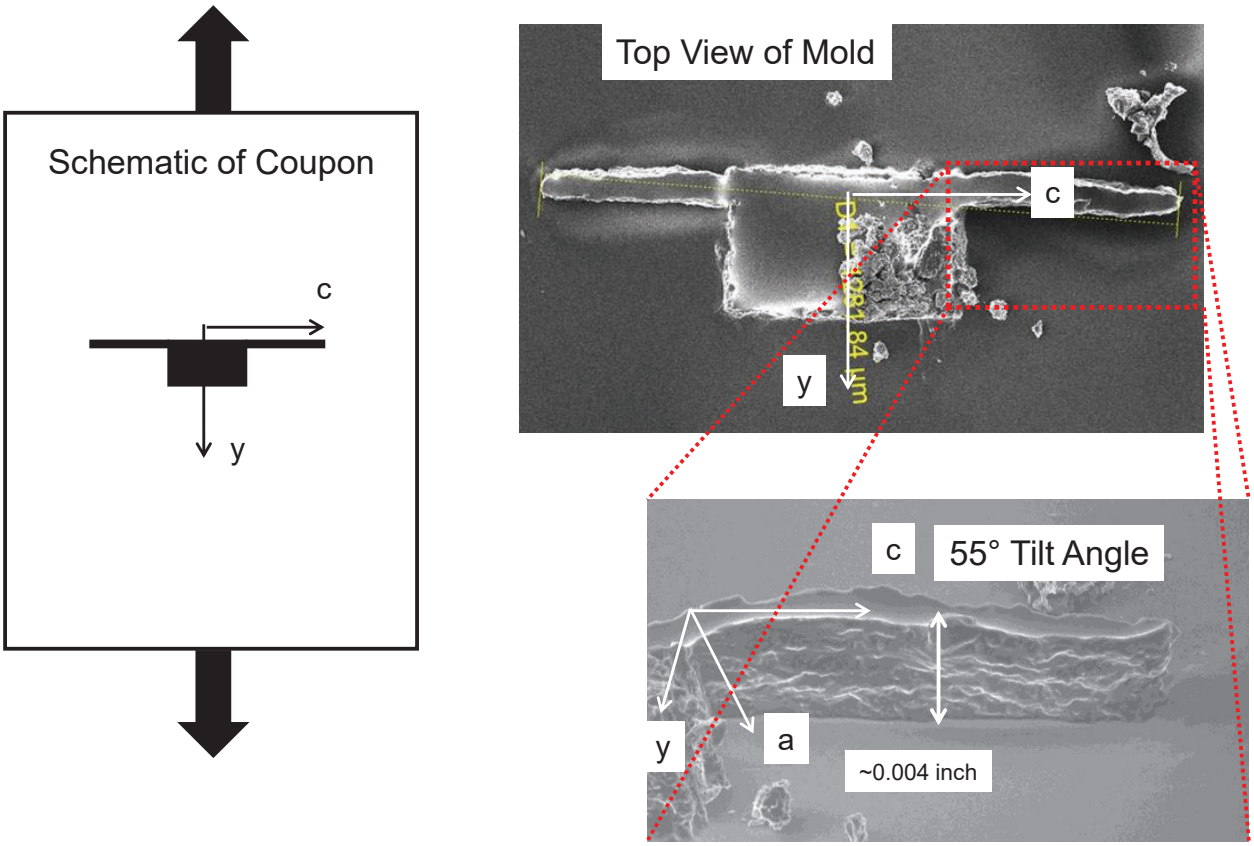

Figure 25. Repliset™ mold of a crack that is held open at a global strain of 1.5%.

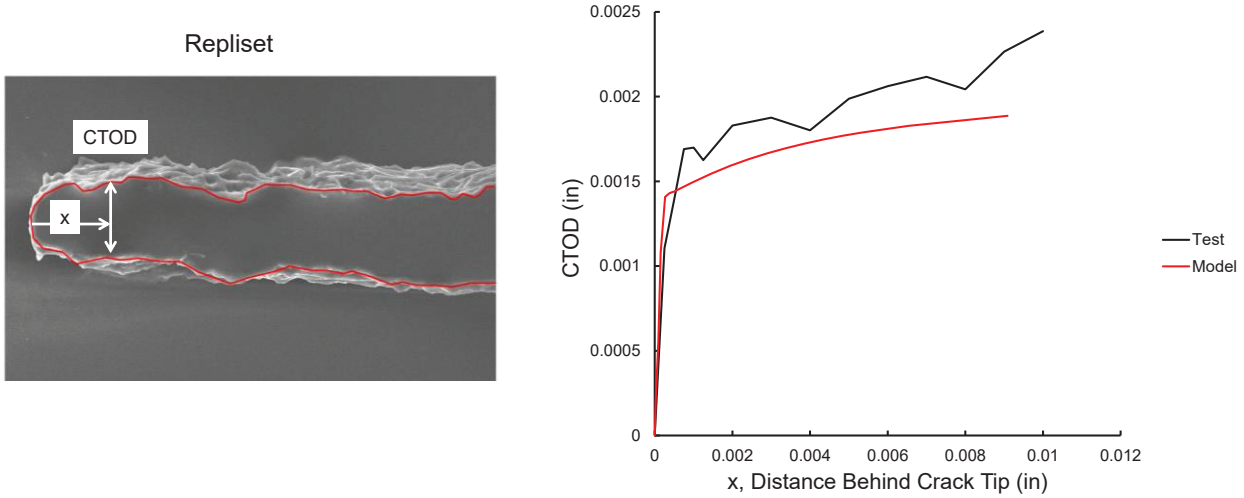

Figure 26. CTOD measured from the Repliset™ mold and the FEA simulation.

7.2.4 Phase 2 FEM Results

The FEA simulations were validated against strain fields and CMOD measurements at the surface made by DIC and from CTOD measurements that were made from a mold of a loaded crack. These validated FEA simulations were used to extract the CTOD behind the crack and the strains ahead of the crack to evaluate the influence of the autofrettage cycle on the conditions at the crack tip. The Phase 2 tests were conducted on uniaxial coupons, but a COPV liner is

subjected to biaxial loading. The validated FEA simulations were also used to evaluate if the biaxial stress state would significantly change the influence of the autofrettage on the subsequent LEFM cycles.

The test measurements indicated that the cracks remained open for the entire LEFM loading that followed an autofrettage cycle and grew faster than identical tests without an autofrettage cycle. Data were extracted from the FEA simulations to investigate these test observations. The CTOD was extracted along a line normal to the cracked surface at the maximum depth location for the maximum and minimum stresses of the first linear responding cycle after the AF for the AF+LEFM and LEFM-only FEA simulations with R = -1.3, as shown in Figure 27 and described in Appendix A. The solid lines represent the CTOD at the maximum LEFM stress and the dash lines represent the CTOD at the minimum LEFM stress. The CTOD in the AF+LEFM simulation is shown to be completely open at minimum stress, while the crack is closed in the LEFM-only simulation. The cyclic crack tip opening displacement (ΔCTOD) in the AF+LEFM simulation is more than 2 times larger than that of the LEFM-only simulation.

The strain in the direction of loading was extracted along a line normal to the surface at the maximum depth location from the FEA simulation data of R = -1.3 tests, as shown in Figure 28. The solid lines represent the strain at the maximum stress of the first LEFM cycle and the dashed lines represent the strain at the minimum stress of the first LEFM cycle. The crack tip strains in the AF+LEFM simulation are always tensile, while the minimum strain in the LEFM-only simulation is in compression. This compression strain must be relieved before the crack opens and damage can accumulate at the crack tip. The small increase in the CTOD for the LEFM-only FEA simulation is due to a small meshing perturbation about 0.0005 inch from the crack tip to enhance convergence as described in Appendix A.

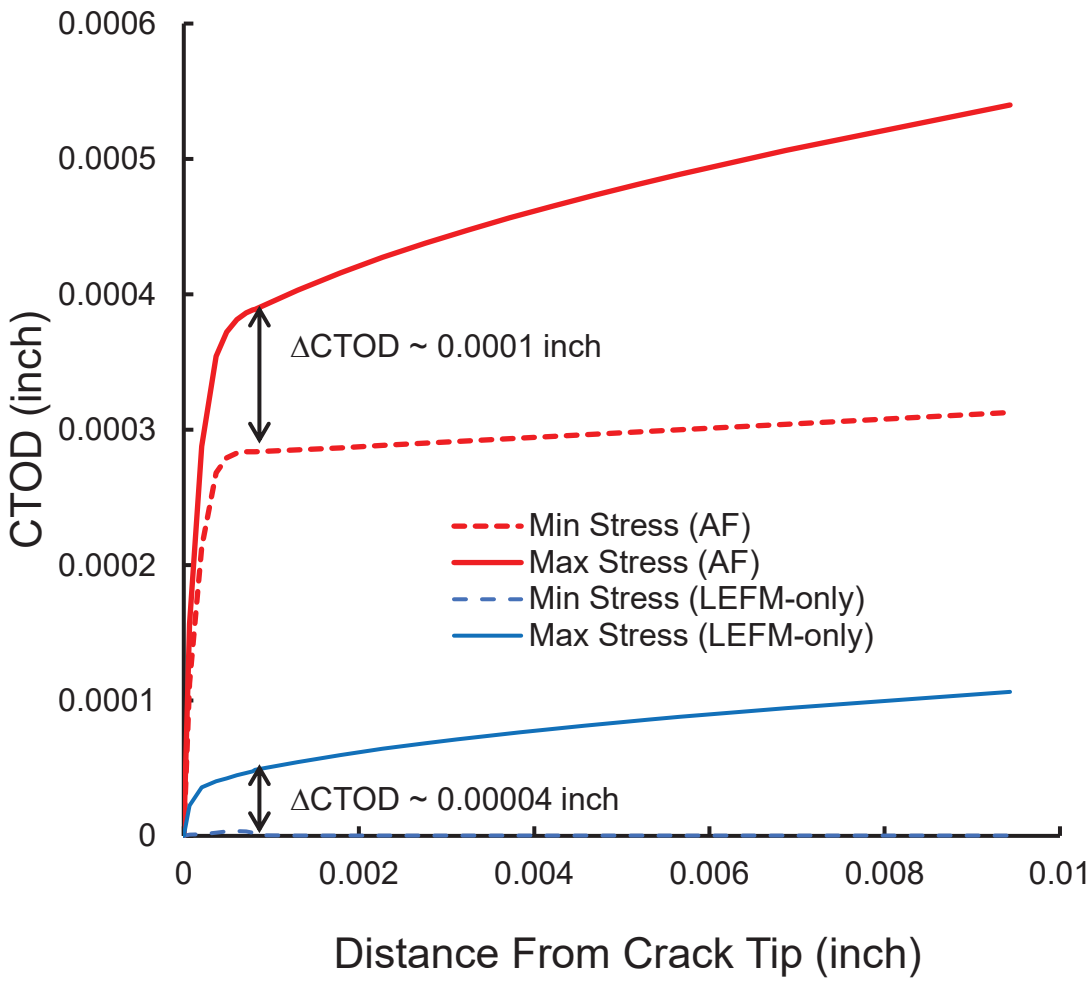

Figure 27. FEA simulations of the CTOD along a line normal to the surface at the maximum depth location at the maximum and minimum LEFM stresses.

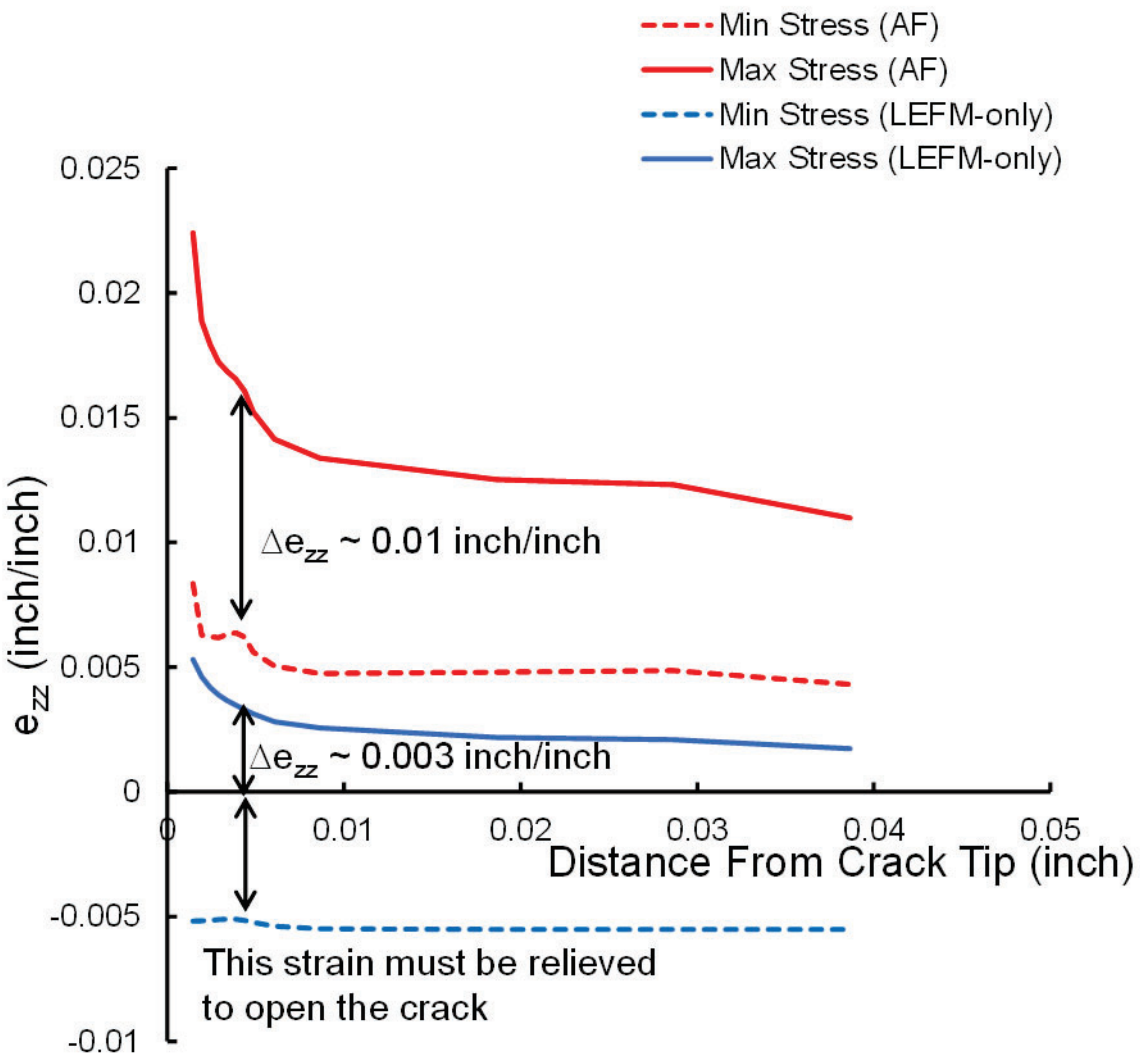

Figure 28. FEA simulations of the strains in the direction of loading along a line normal to the surface at the maximum depth location at the maximum and minimum LEFM stresses.

The crack opening visualization can be enhanced by displaying the surface crack opening behavior from the FEA. The AF+LEFM FEA simulations start with the crack surfaces closed and the crack begins to open elastically as the applied displacement is increased to a stress of 30,000 psi, as shown by Figures 29A and B. The elastic-plastic autofrettage cycle (1.5% strain) opens the crack significantly more than the elastic loading and blunts the crack tip, as shown in Figure 29C. The unloading from the peak autofrettage strain to the minimum LEFM stress (-40,000 psi) reduces the crack opening, but the entire crack surface remains open, as shown in Figure 29D. The subsequent loading back to the maximum LEFM stress (30,000 psi) opens the crack, but not as much as the autofrettage loading, as shown in Figure 29E. The cyclic crack opening is the difference between the crack opening shown in Figures 29D and E.

The LEFM-only FEA simulations also start with crack surfaces closed, as shown in Figure 30A. All of the LEFM-only cycles are elastic, so the crack opening at 30,000 psi, as shown in Figure 30B, was small relative to the post-autofrettage crack opening at 30,000 psi shown in Figure 29E. The crack surfaces are completely closed at the minimum LEFM stress (-40,000 psi), as

shown in Figure 30C. The cyclic crack opening is the difference between the crack opening shown in Figures 30B and C, and is considerably smaller than the cyclic crack opening of the AF+LEFM simulation shown in Figures 29 D and E.

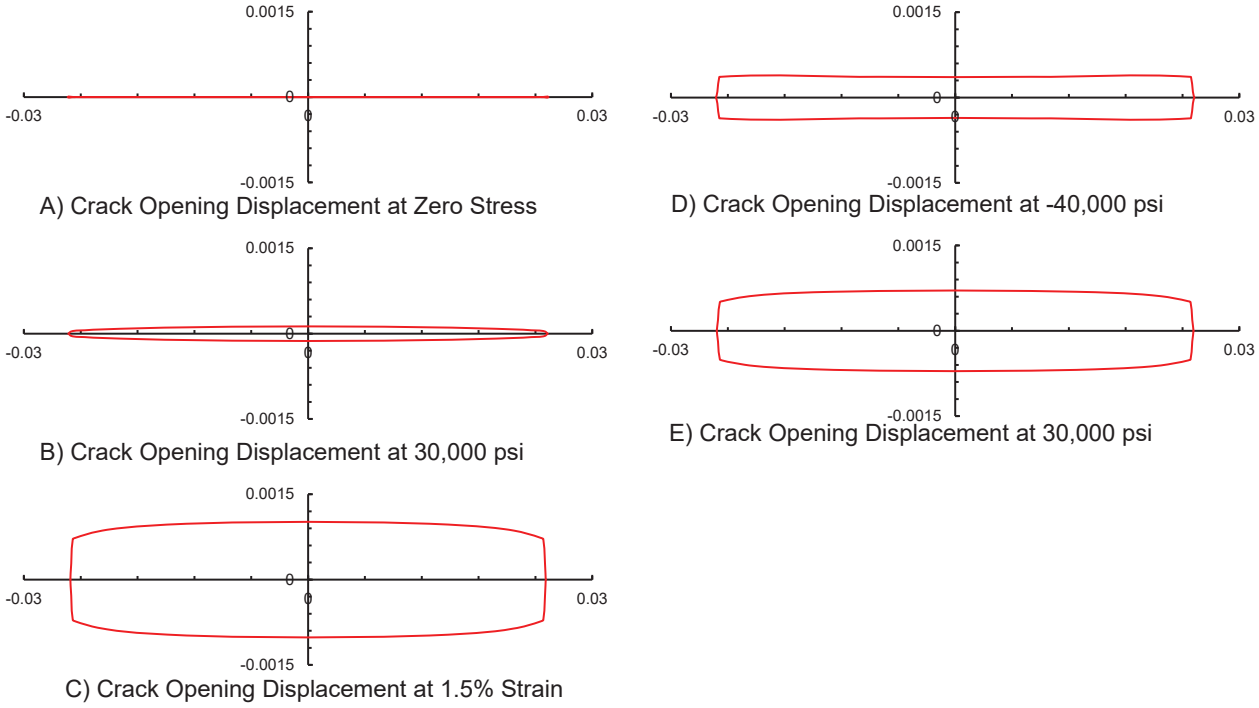

Figure 29. Surface crack opening displacement for the FEA simulation of the R = -1.3 AF+LEFM test.

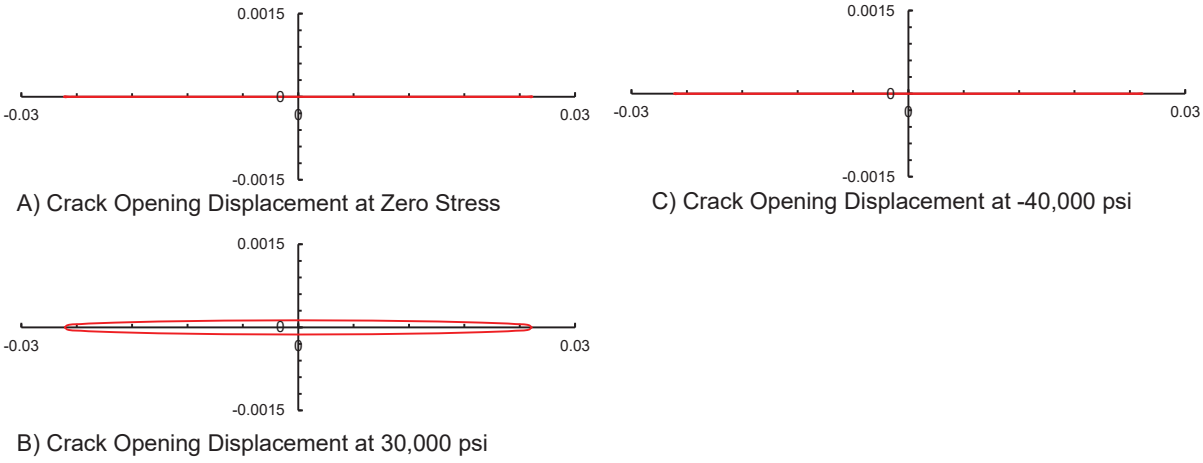

Figure 30. Surface crack opening displacement for the FEA simulation of the R = -13 LEFM-only test.

FEA simulations were conducted with 1:1 (hoop stress equal to axial stress as representative of liners of spherical COPVs) and 2:1 (hoop stress greater than the axial stress as representative of liners of cylindrical COPVs) to evaluate the influence of biaxial loading on the LEFM cycles that follow an autofrettage cycle. The FEA simulation calculated the ΔCTOD for the first LEFM cycle, with and without a preceding autofrettage cycle, as shown in Figure 31. The uniaxial results are represented with the solid lines and the biaxial results are represented with open

symbols. For the uniaxial, LEFM only case, the delta CTOD is relatively flat as the crack is being forced closed for R<0. At R=-1.3 the material is being yielded in compression, and the subsequent tensile cycle yield behavior is altered resulting in some yielding at the maximum load that results in a larger delta CTOD. This is not seen in the autofrettage case due to the hardening in the autofrettage cycle. The biaxial simulations resulted in a slightly lower ΔCTOD for both the AF+LEFM and LEFM-only conditions. However, the large difference between the ΔCTOD for the AF+LEFM and LEFM-only tests is still present in the biaxial tests. This suggests that the influence of the autofrettage cycle on the subsequent LEFM crack growth rate that was observed in the tests will be present in COPV liners that are subjected to biaxial loading. The FEA simulations under uniaxial and biaxial conditions were performed to extract the stress intensity factor range (ΔK) and the cyclic CTOD with similar results, as shown in Figure 31.

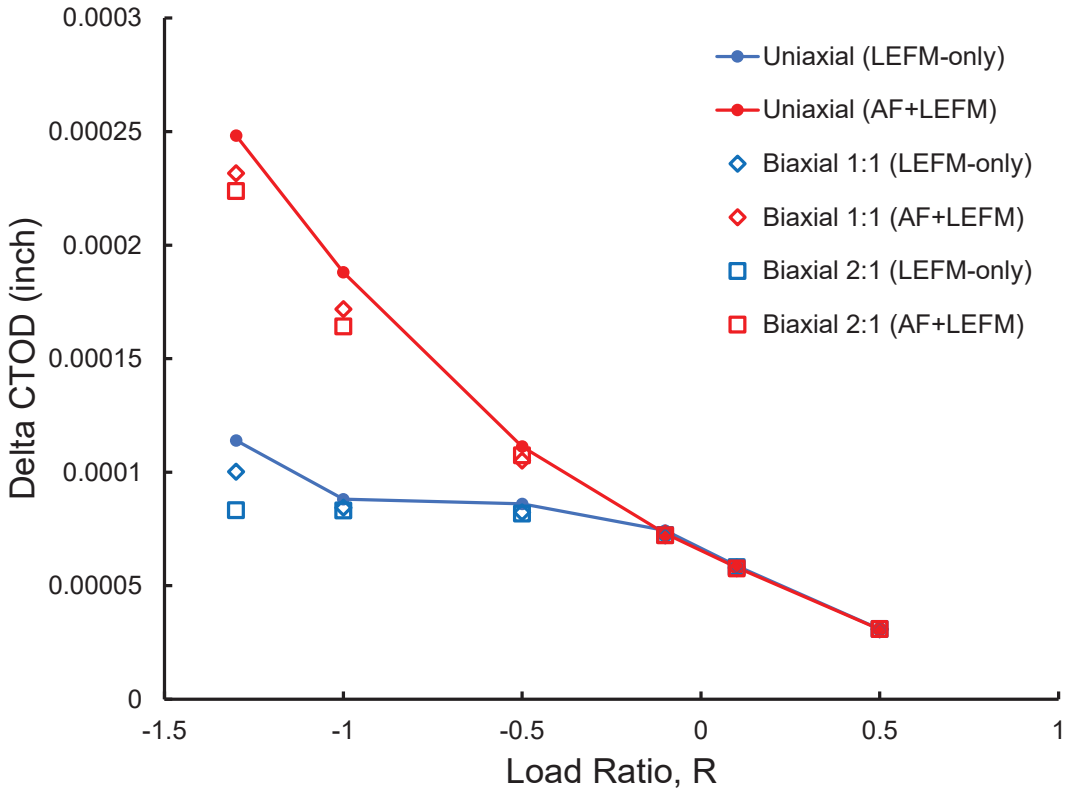

Figure 31. Cyclic crack tip opening displacements (ΔCTOD) for uniaxial and biaxial FEA simulations.

7.2.5 LEFM Crack Growth Calculations using NASGRO

The allowed ANSI/AIAA S-081B approach considers the crack growth behavior of the LEFM cycles in the AF+LEFM and LEFM-only tests to be identical. However, Figure 17 presented test data that demonstrated the LEFM cycles for the AF+LEFM tests at negative stress ratios experience faster crack growth rates than the LEFM-only tests. Thus, a crack growth analysis system like NASGRO [ref. 2] will be unable to predict the behavior of both types of tests without accounting for the detrimental influence of the autofrettage cycle. The approach taken was to demonstrate that NASGRO could predict the behavior of the LEFM-only tests, then propose a method of accounting for the detrimental influence of the autofrettage cycle on the AF+LEFM tests.

The NASGRO LEFM crack growth calculation software was used to estimate the damage tolerance life of elastically responding COPV liners using the allowed ANSI/AIAA S-081B approach. This approach has three components: (1) defining the starting crack size from NDT detection capabilities, (2) determination of the crack growth during autofrettage, and (3) calculation of the crack growth due to the LEFM cycles.

The NDT starting crack size was a semi-circular crack with a surface crack length of 2c = 0.050 inch and a crack depth of a = 0.025 inch. The 1.5% autofrettage cycle blunted the crack tip and resulted in negligible crack extension. The calculation of crack growth due to the LEFM cycles ignored any influence of the autofrettage cycle and used the NASGRO material model M6AB13AB1 (Al 6061-T6) and the surface crack stress intensity factor solution SC30. The number of cycles and the stresses were entered into the load block section and the amount of crack growth was calculated for each stress ratio tested. The average crack growth rate was calculated by dividing the crack growth by the number of applied LEFM cycles in the same manner as was done for the LEFM-only and AF+LEFM tests. The NASGRO crack growth rate predictions were unconservative for the negative stress ratios that are relevant for COPV liners and conservative for positive stress ratios, as shown in Figure 32. The inability to predict the LEFM-only tests was unacceptable from the standpoint of evaluating methods of accounting for the detrimental influence of the autofrettage cycle, so the NASGRO input parameters were evaluated to locate a source for the poor predictions of the LEFM-only behavior.

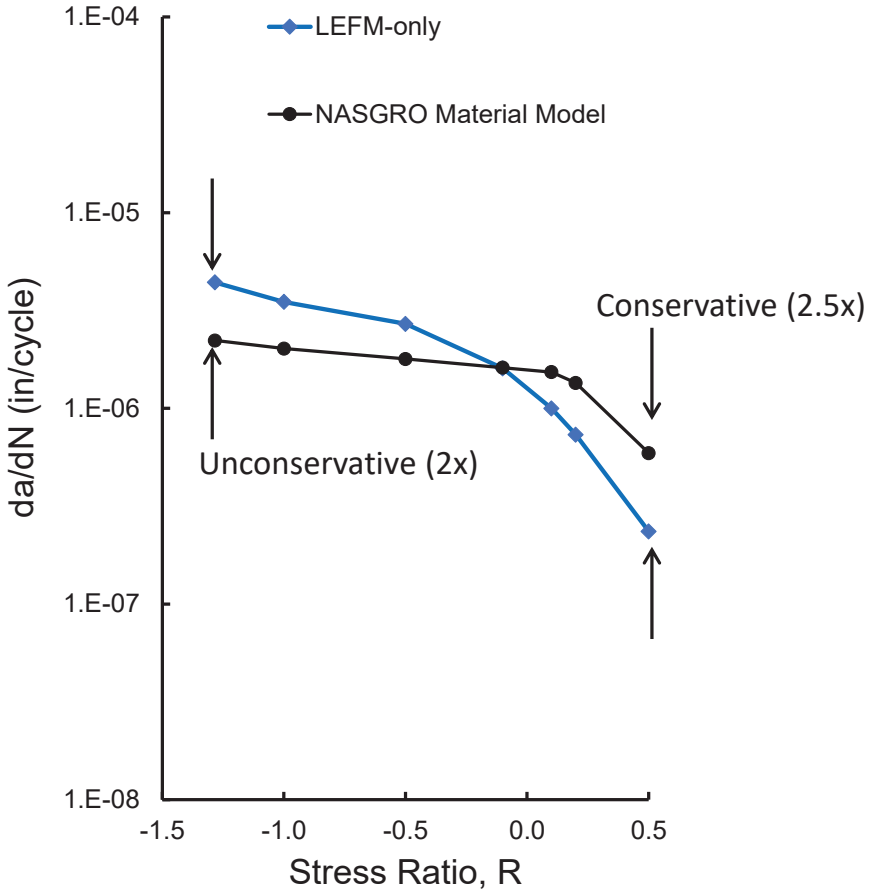

Figure 32. Crack growth rate from the LEFM-only tests and the NASGRO predictions.

Figure 33 shows the crack growth rate model from the NASGRO database compared to the average crack growth rate measured in the tests as a function of K_{max}. The data used to generate the NASGRO model were based on tests conducted at positive stress ratios and at K_{max} values above those of the LEFM-only tests. Also, the 0.25 inch material thickness used to generate the test data for the NASGRO database Al 6061-T6 material model was greater than the thickness of coupons used in the Phase 2 testing (0.062 inch). Thus, the use of this NASGRO crack growth rate model required extrapolation beyond the underlying data in terms of the stress intensity factor, stress ratio, and material thickness. This extrapolation was shown to not accurately describe the measured crack growth rate behavior of the surface crack tests. The LEFM-only test results were used to create a table of the crack growth rate behavior as a function of stress ratio that forces NASGRO to interpolate rather than extrapolate to obtain the crack growth rate. This results in the NASGRO calculation of the LEFM-only tests being a "simulation" rather than a "prediction", but accurate simulations were necessary to evaluate methods that would allow NASGRO to predict the AF+LEFM tests. The stress intensity factor for the surface cracks in the LEFM-only and AF+LEFM tests increased by about 10% as the crack grew from the initial target size to the final crack length. This required the crack growth rate model used in NASGRO to be accurate for only a limited range of stress intensity factors. The tabular crack growth rate data developed used a simple power law relationship between the stress intensity factor and the crack growth rate. The slope of the power law was obtained from the NASGRO material model M6AB13AB1 previously mentioned. The influence of stress ratio was characterized by forcing three power laws (all with the same slope) through the LEFM-only tests at R = 0.5, 0.1, and -1.3, as shown in Figure 34. The figure also shows the use of the tabular data for the material model makes the NASGRO calculation of the LEFM-only data a simulation rather than a prediction and agrees with the test measurements.

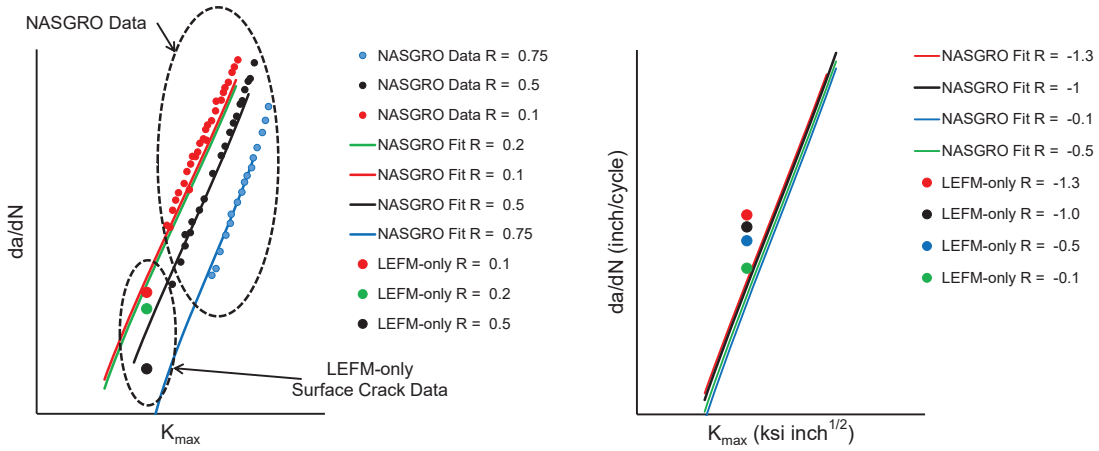

Figure 33. Comparison of the NASGRO crack growth rate models and supporting data with the LEFM-only test results.

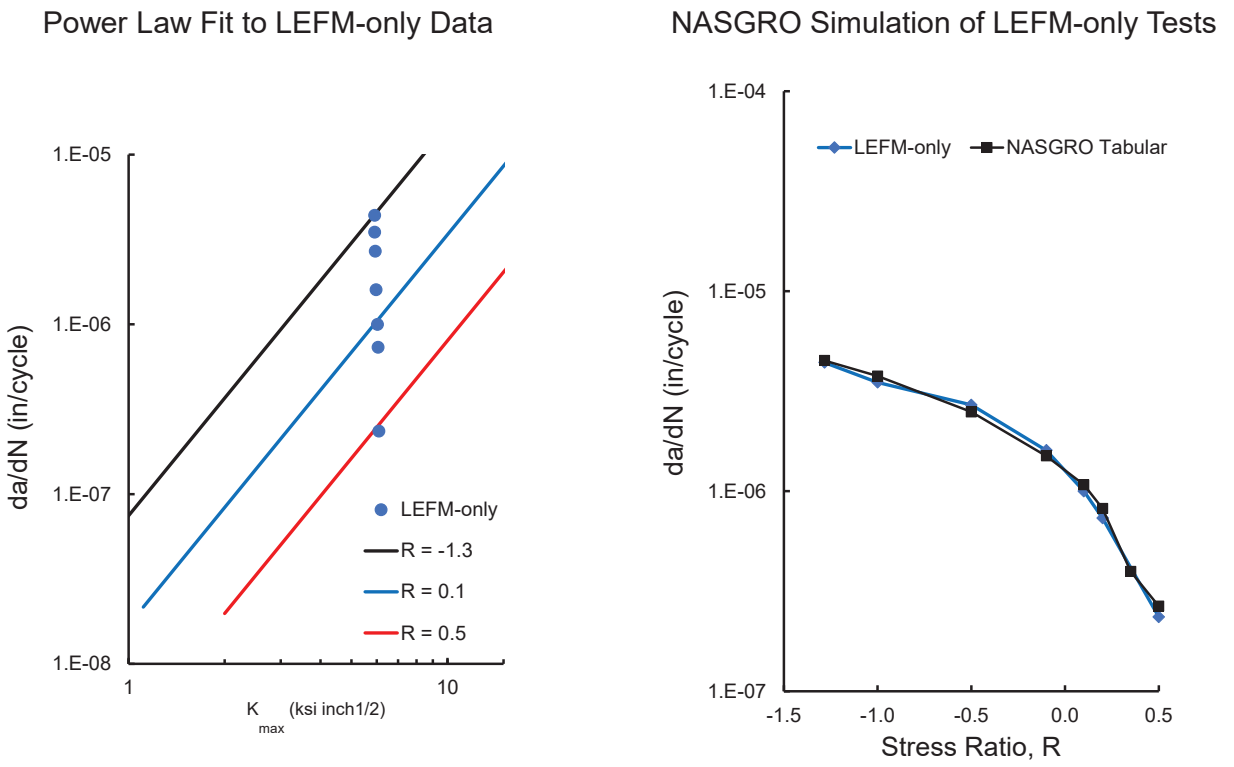

Figure 34. Tabular fit used to characterize the crack growth rate data and the NASGRO simulation of the LEFM-only tests.

The test measurements and FEA simulations of the AF+LEFM tests at negative stress ratios indicate that the crack is completely open after the application of the autofrettage cycle. Predictions from crack growth software like NASGRO inherently assume that the crack is closed during most of the negative portion of the loading cycle due to the types of tests used to generate the underling crack growth rate model. This suggests that the entire cyclic stress range contributes to damage in the AF+LEFM tests, while only a portion of the cyclic stress range contributes to damage in the LEFM-only tests, as illustrated in Figure 35. The NASGRO input data can be modified to account for the completely open crack following the autofrettage cycle by artificially increasing the mean stress to the point that the minimum stress is zero rather than negative. The cyclic stress range is kept constant. This concept is illustrated in Figure 36 for LEFM cycles with a negative stress ratio and another with a positive stress ratio. The LEFM cycles with the negative stress ratio are shifted upward to produce a stress ratio of R = 0. The LEFM cycles with positive stress ratios are not changed. The following steps can be used to create a NASGRO input file that forces the entire stress range to contribute to crack tip damage:

1. Create the NASGRO input file for the LEFM-only conditions.
2. Artificially increase material yield stress and fracture toughness to prevent the software from terminating the analysis prematurely (where the check on yield and fracture must be evaluated separately).
3. Increase the minimum cyclic stress to zero and increase the maximum cyclic stress to keep the total stress range the same.
4. Run the NASGRO analysis normally.

The NASGRO predictions with the shifted stress range is shown in Figure 37 for the AF+LEFM tests. The NASGRO predictions for the AF+LEFM tests at positive ratios are the same as the predictions for the LEFM-only tests because the loading spectrum was not shifted. These predictions are conservative because the beneficial influence of the autofrettage cycle is not accounted for in the analyses. The NASGRO predictions for the AF+LEFM tests at negative stress ratios are less unconservative and capture the trend of the crack growth rate in the tests. The difference between the test and the shifted NASGRO analysis is most unconservative for the test conducted at the lowest stress ratio (R = -1.3). The CMOD measurements shown in Figure 35 exhibited nonlinear behavior near the maximum stress of the LEFM cycles. This suggests that this extreme case is experiencing elastic-plastic behavior.

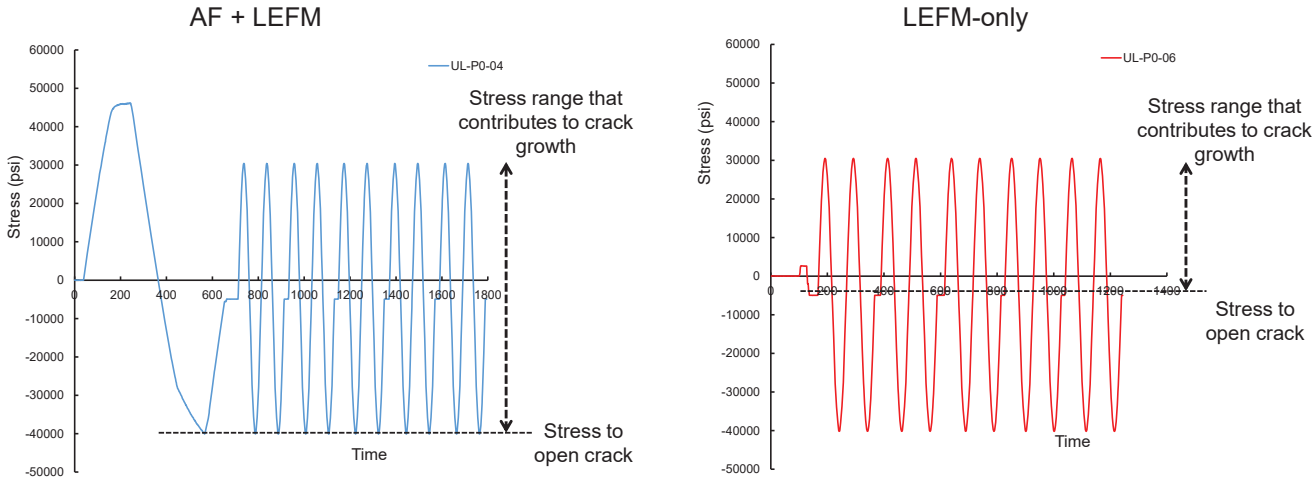

Figure 35. Illustration of the cyclic stress range that contributes to damage in the AF+LEFM and LEFM-only tests.

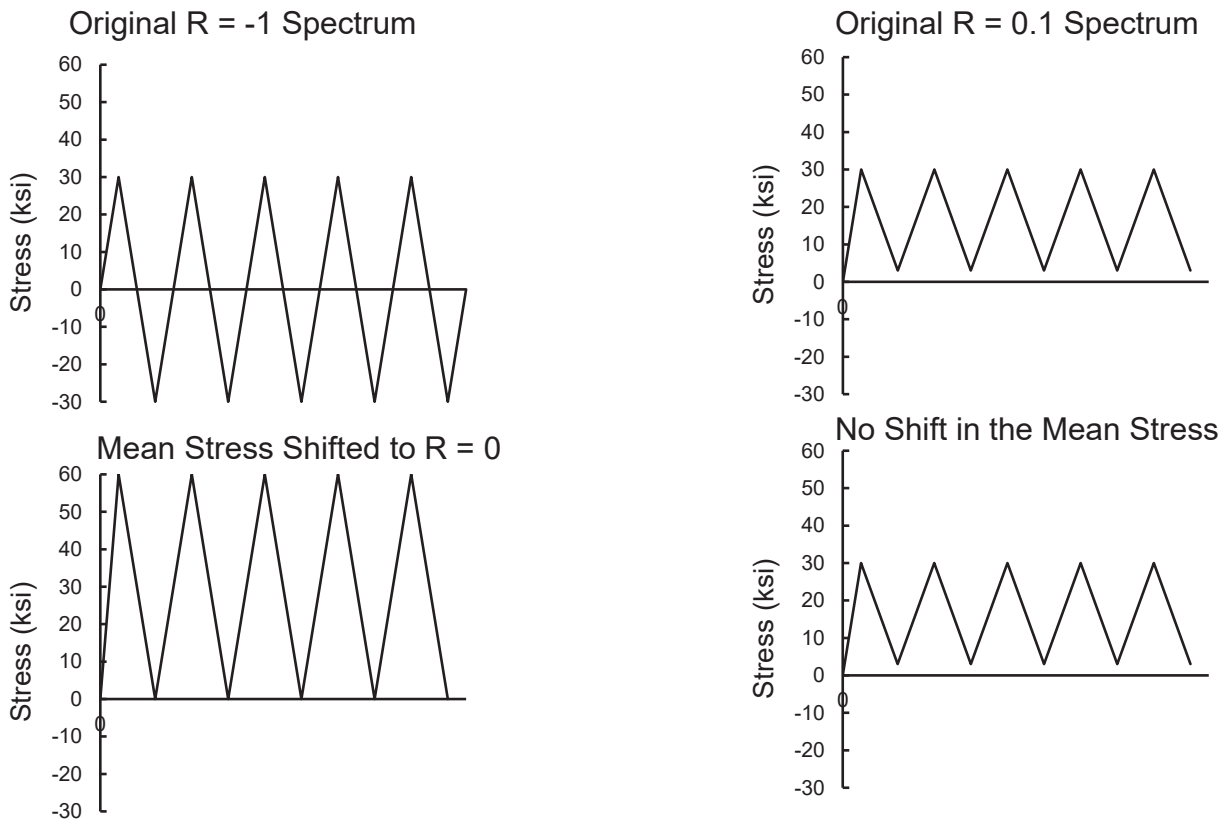

Figure 36. Illustrated of the shifting of the mean stress to account for the detrimental influence of an autofrettage cycle on the subsequent elastic cycles.

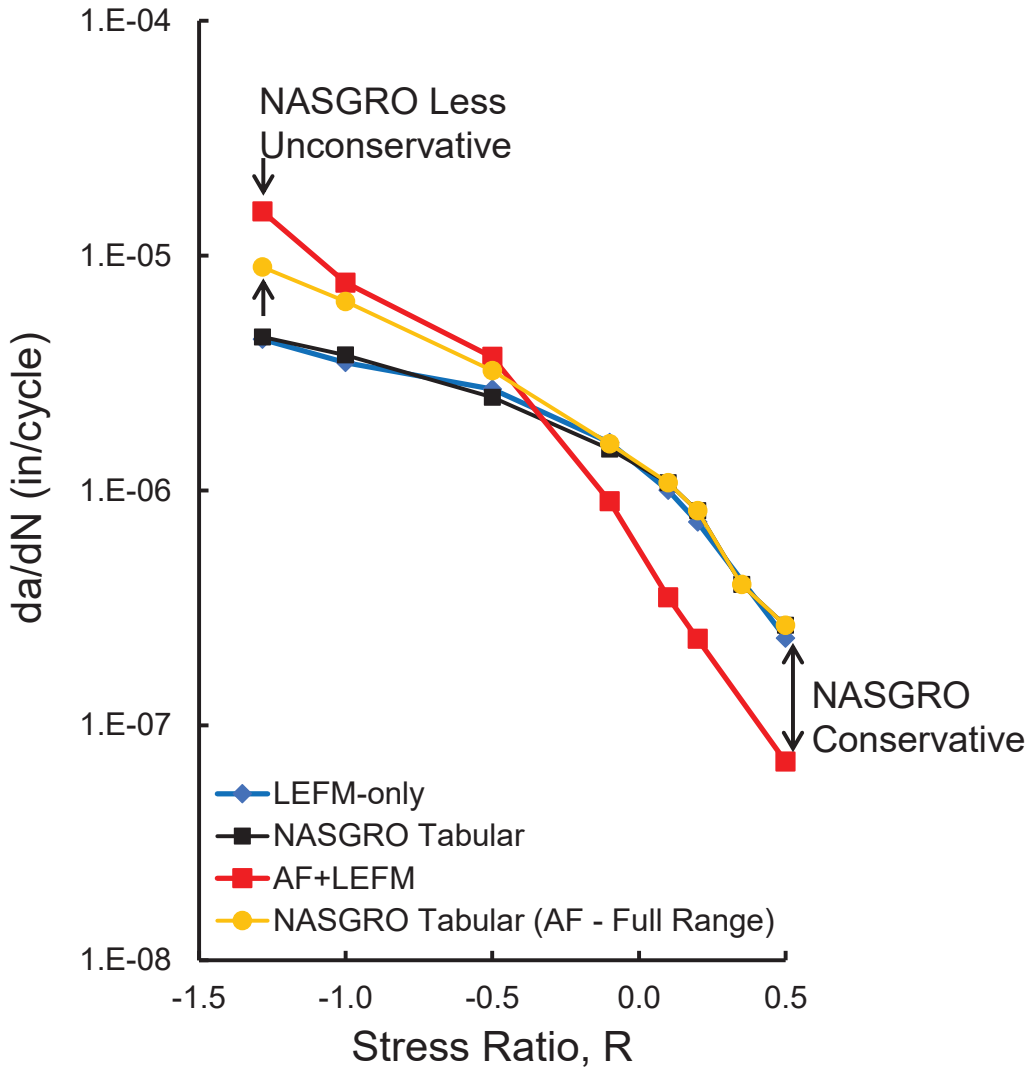

Figure 37. Predicted crack growth rate for the AF+LEFM using NASGRO with the shifted stress range.

8.0 Findings, Observations, and NESC Recommendations

8.1 Findings

F-1. The autofrettage cycle did not retard the crack growth for simulated COPV loading spectrum with stress ratios of $R < -0.1$.

F-2. Tests and analyses both indicated that the crack blunted at the peak COPV autofrettage strain and did not close under the subsequent compressive load at depressurization.

F-3. The crack growth rate during elastic cycles after autofrettage was as much as 3.5 times faster than the crack growth rate of identical elastic cycles that did not experience the autofrettage cycle.

F-4. The NASGRO crack growth simulations with a shifted stress range (i.e., same stress range magnitude, but $R = 0$) was less unconservative than the heritage approach of ignoring the influence of the autofrettage cycle on the subsequent maximum design pressure (MDP) cycles.

8.2 Observations

O-1. The NASGRO database Al 6061-T6 material model that most closely aligns with a COPV design (i.e., thin sheet) is extrapolated to conditions beyond its supporting data when used in COPV representative analysis (i.e., Phase 2 conditions)

O-2. ANSI/AIAA S-081B Section 7.5.1 identifies potential beneficial retardation effects, rather than both potential beneficial and detrimental effects, on crack growth rates due to the autofrettage cycle.

8.3 NESC Recommendations

The following NESC recommendations are directed to NASA programs/projects/organizations that use COPVs required to comply with damage tolerance life requirements:

R-1. Ensure that any damage tolerance life analyses account for crack growth rate acceleration that can follow the post-autofrettage compressive stresses for cycles with $R < -0.1$. ***(F-2, F-3, F-4, O-2)***

R-2. Require relevant crack growth data when autofrettage cycle retardation is identified as part of conservatism rationale for cycles with $R < -0.1$. ***(F-1, O-2)***

The following NESC recommendation is directed to the AIAA Aerospace Pressure Vessel Committee on standards:

R-3. Update ANSI/AIAA S-081B Section 7.5.1 to address COPV liners with compressive stresses following autofrettage depressurization for COPVs that comply with damage tolerance life requirements by analysis. ***(F-2, F-3, F-4, O-2)***

9.0 Alternate Technical Opinion(s)

No alternate technical opinions were identified during the course of this assessment by the NESC assessment team or the NESC Review Board (NRB).

10.0 Other Deliverables

No unique hardware, software, or data packages, other than those contained in this report, were disseminated to other parties outside this assessment.

11.0 Recommendations for the NASA Lessons Learned Database

No recommendations for NASA lessons learned were identified as a result of this assessment.

12.0 Recommendations for NASA Standards, Specifications, Handbooks, and Procedures

NESC recommendation R-3 addresses the AIAA Aerospace Pressure Vessel Committee to update ANSI/AIAA S-081B standard, Section 7.5.1. This update will address COPV liners with compressive stresses following autofrettage depressurization for COPVs that comply with damage tolerance life requirements by analysis.

13.0 Definition of Terms

Corrective Action	Changes to design processes, work instructions, workmanship practices, training, inspections, tests, procedures, specifications, drawings, tools, equipment, facilities, resources, or material that result in preventing, minimizing, or limiting the potential for recurrence of a problem.
Finding	A relevant factual conclusion and/or issue that is within the assessment scope and that the team has rigorously based on data from their independent analyses, tests, inspections, and/or reviews of technical documentation.
Lesson Learned	Knowledge, understanding, or conclusive insight gained by experience that may benefit other current or future NASA programs and projects. The experience may be positive, such as a successful test or mission, or negative, as in a mishap or failure.
Observation	A noteworthy fact, issue, and/or risk, which is not directly within the assessment scope, but could generate a separate issue or concern if not addressed. Alternatively, an observation can be a positive acknowledgement of a Center/Program/Project/Organization's operational structure, tools, and/or support.
Recommendation	A proposed measurable stakeholder action directly supported by specific Finding(s) and/or Observation(s) that will correct or mitigate an identified issue or risk.

14.0 Acronyms and Nomenclature List

Δa_{AF}	Crack Growth
ΔaLEFM	Analysis Predicts (from the elastic cycles)
$\Delta\varepsilon$	Cyclic Global Strain Range
a_f	DTA crack size
AIAA	American Institute of Aeronautics and Astronautics

Al	Aluminum
ANSI	American National Standards Institute
a_{NDT}	Crack Size
CMOD	Crack Mouth Opening Displacement
COPV	Composite Overwrapped Pressure Vessel
CTOD	Crack Tip Opening Displacement
DIC	Digital Image Correlation
DTA	Damage Tolerance Analysis
EDM	Electrical Discharge Machining
EPFM	Elastic-Plastic Fracture Mechanics
FEA	Finite Element Analysis
LEFM	Linear-Elastic Fracture Mechanics
MDP	Maximum Design Pressure
NDT	Nondestructive Testing

15.0 References

1. "Space Systems – Composite Overwrapped Pressure Vessels," ANSI AIAA S-081B, American Institute of Aeronautics and Astronautics, 2018.
2. NASGRO, Fracture Mechanics and Fatigue Crack Growth Analysis Software, Reference Manual, v10.0, October 2021.
3. "Composite Overwrapped Pressure Vessel (COPV) Damage Tolerance Life Analysis Methodology and Test Best Practices", NESC-RP-16-01183, July 2020.
4. ASTM E647-15, "Standard Test Method for Measurement of Fatigue Crack Growth Rates," ASTM International, West Conshohocken, PA, 2015.
5. ASTM E2899-15, "Standard Test Method for Measurement of Initiation Toughness in Surface Cracks Under Tension and Bending," ASTM International, West Conshohocken,
6. Peters, W. H. and Ransom, W. F., "Digital Imaging Techniques in Experimental Stress Analysis," Opt. Eng. **21** (3), 427-432 (1982).
7. Sutton, M. A., Orteu, J. J., and Schreier, H. W., "Image Correlation for Shape, Motion, and Deformation Measurements," Springer Science and Business Media, 2009.
8. Elber, W. "Fatigue Crack Closure Under Cyclic Tension," Engineering Fracture Mechanics, Vol. 2, pp 37-45, 1970.
9. Elber, W. "The Significance of Fatigue Crack Closure," Damage Tolerance in Aircraft Structures, pp. 230-230, 1971.
10. Newman, J. C., Jr. "A Crack-Closure Model for Predicting Fatigue-Crack Growth Under Aircraft Spectrum Loading," NASA TM-81941, January 1981.
11. Coffin, L. F., "A Note on Low Cycle Fatigue Laws," J. Mater., vol. 6, no. 2, 1971, pp-388-402.
12. Manson, S. S. and Hirschberg, M. H., "Fatigue Behavior in Strain Cycling in the Low and Intermediate Cycle Range," Fatigue: An Interdisciplinary Approach, Proceedings of the 10th Sagamore Army Materials Research Conference, J. J. Burke, et al., eds. Syracuse University Press, Sagamore, N.Y., 1964, pp. 133-178.
13. Abaqus User Manual.
14. Newman, J. A., Willard, S. A., Smith, S. W., and Piascik, R. S., "Replica-based Crack Inspection," Engineering Fracture Mechanics, Vol. 76, Issue 7, May 2009, pp. 898-910.

Appendices

A. Finite Element Modeling Approach
B. Phase 1 Fracture Surface Imaging
C. Phase 2 Fracture Surface Imaging

Appendix A. Finite Element Modeling Approach

Surface crack geometry was generated using commercial software FEACrack [1]. FEACrack takes in plate dimensions and surface crack parameters and outputs a finite element mesh. Finite element analysis was performed with Abaqus [2].

Material Model Calibration

The material model used in the finite element model was calibrated with data taken from cyclic tensile tests performed on specimens cut from the same sheet as the autofrettage simulation coupons. The Abaqus material model is composed of elastic and plastic properties. The elastic response is defined with two parameters, Young's modulus and Poisson's ratio. The Young's modulus was obtained by calculating the slope of the elastic portion of the first load cycle of the tensile data. The Poisson's ratio was set to 0.3, a typical value for Al alloys. The plasticity model used a combined kinematic/isotropic hardening model with a cyclic hardening option. Abaqus [1] has a number of options for defining the hardening response of the plastic material. The kinematic portion of the response was defined by providing half-cycle data from the tensile test. This data consists of the stress versus plastic strain data from the first loading cycle of the test data. This is obtained by converting the engineering stress and strain measured during the test and converting it to true stress and strain:

$$\varepsilon_{true} = \ln(1 + \varepsilon_{eng})$$
$$\sigma_{true} = \sigma_{eng} * e^{\varepsilon_{true}}$$

where σ_{true}, ε_{true}, σ_{eng}, ε_{eng} are true stress, true strain, engineering stress, engineering strain. The plastic strain can then be found by subtracting the elastic strain from the total strain values. Additionally, the number of backstresses, N, of the model can be specified. The isotropic portion of the hardening model was defined with three parameters, equivalent stress, Q_∞, b. The equivalent stress was set to the initial yield stress of 36,000 psi. The parameters N, Q_∞, and b were calibrated through an iterative process as:

1. Set initial values of N, Q_∞, and b
2. Use the resulting model to simulate the cyclic tensile test
3. Calculate engineering stress/strain response from simulation and compare with test results
4. Adjust values of N, Q_∞, and b
5. Repeat steps 2 – 4 until the model is a sufficient match to the test data

The Abaqus input listing of the final material model is provided in Figure A-1. A comparison of the simulated engineering stress/strain response to the test data is shown in Figure A-2. Good agreement between the simulation and test was observed for the derived material model.

```
*Material, name=Al6061
*Elastic
**Elastic modulus, Poisson's ratio
 9.94959e+06, 0.3
*Plastic, hardening=COMBINED, number backstresses=2
**Stress, Plastic Strain
 36000.0, 0.000000000
 36896.7, 0.000248181
 37715.0, 0.000491417
 38634.9, 0.000750292
 39448.2, 0.001122130
 39959.1, 0.001444820
 40541.7, 0.001887100
 40899.9, 0.002353090
 41227.8, 0.002879440
 41867.1, 0.004012270
 42127.0, 0.004627400
 42316.0, 0.005205360
 42427.6, 0.005697290
 42542.5, 0.006225000
 43385.4, 0.010112100
 43432.4, 0.010660100
 43479.1, 0.011290400
*Cyclic Hardening, parameters
**Equiv Stress, Q-infinity, Hardening Param b
36000.0,-8000.0, 1000.0
```

Figure A-1. Material input for Abaqus analysis.

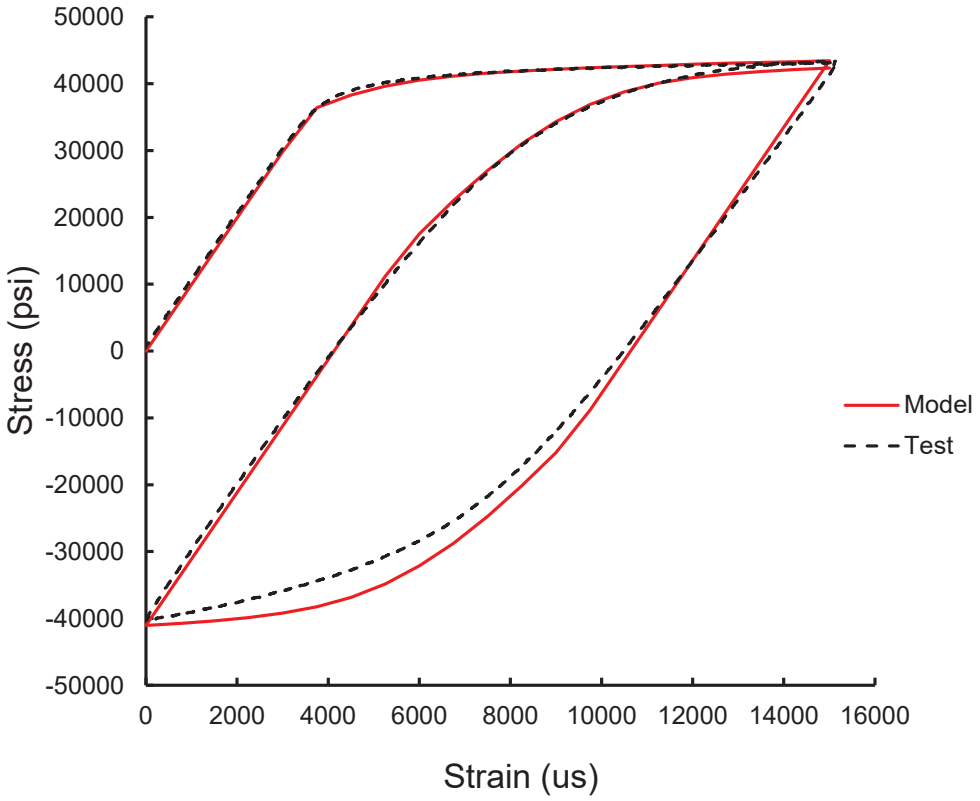

Figure A-2. Test measurements and FEA simulation of the cyclic tensile test.

Surface Crack Model

A half-symmetric model of a surface crack of size a = c = 0.025 inch was modeled using FEACrack and analyzed in Abaqus. Contact was enforced between crack surfaces to allow for crack closure during loading with negative stress ratios. The crack mesh with symmetry plane is shown in Figure A-3. Figure A-4 is a detailed view of the mesh around the crack front. Elements form 10 rings that are used to calculate contour integrals during the analysis for the computation of J-integrals and stress intensity factors. A small keyhole is included along the crack front. This artificial hole allows for a smooth radius at the crack tip that improves numerical stability during crack blunting at autofrettage strains. The CTOD and strain data approaching the crack tip was extracted along the red line in the depth, or a-direction shown in Figures A-3 and A-4.

Figure A-5 is a schematic of the loading boundary conditions. The model was fixed at the bottom and loaded axially. Loading was done in three steps. First, prescribed displacements were used to achieve autofrettage strain levels. Second, the 0 psi unloaded state of the COPV was achieved with a compressive traction boundary condition. Finally, the MDP cycle was simulated with a tensile traction boundary condition. For all simulations, the autofrettage strain was 1.5%, and MDP max was 30 ksi. The minimum load was varied to create load ratios, R, between -1.3 and 0.5. The model was validated by comparing CMOD for various test conditions. The model CMOD measurements matched test observations to within 10% as shown in Figure A-6.

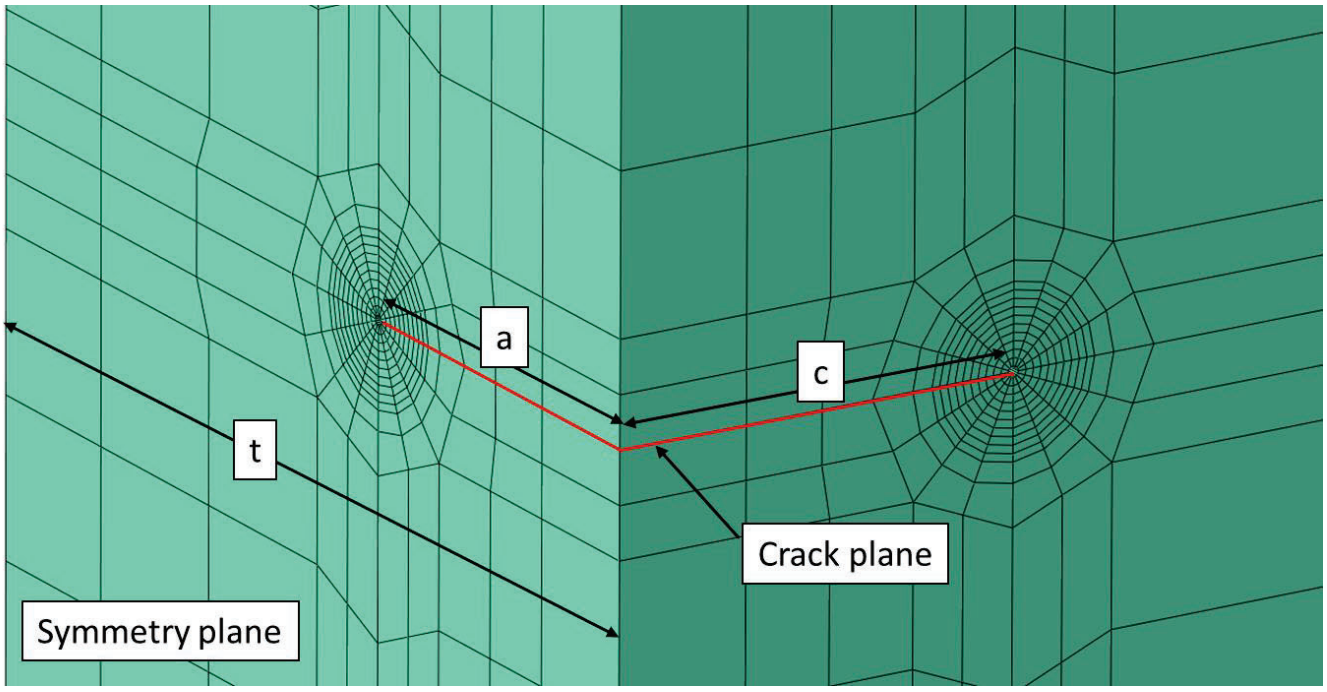

Figure A-3. Surface crack mesh.

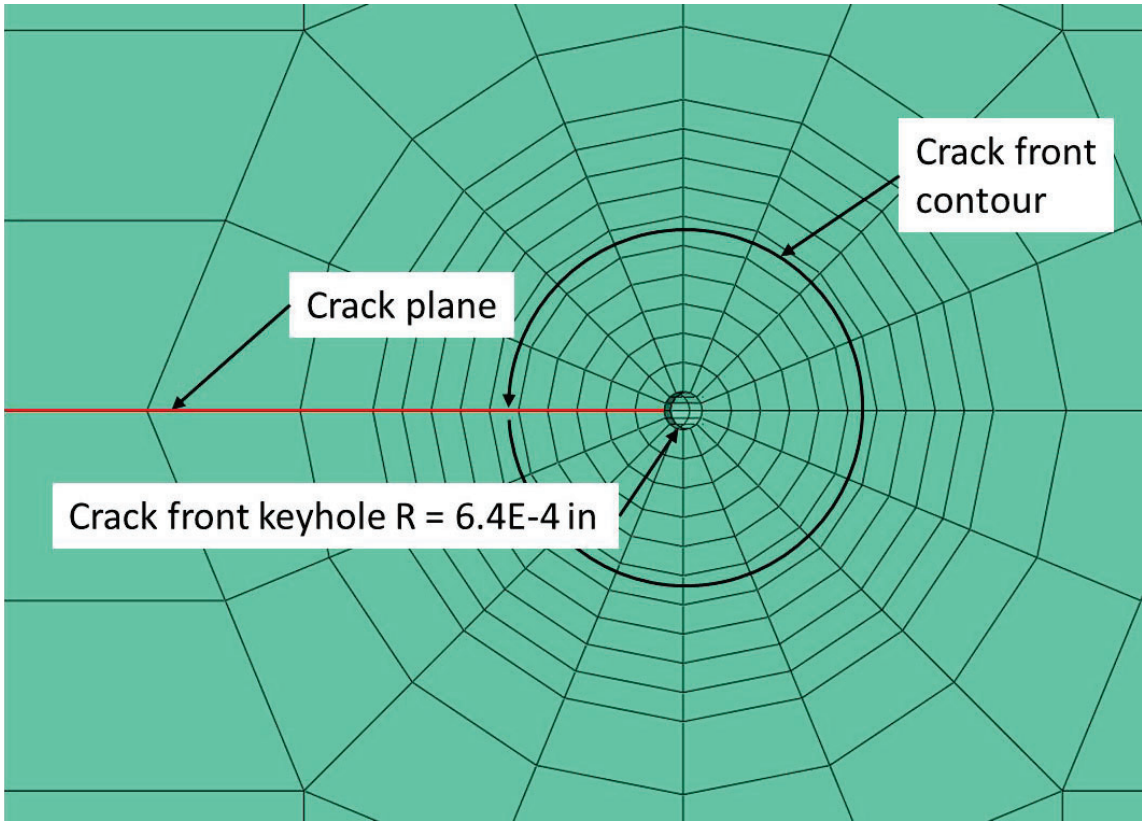

Figure A-4. Crack front mesh.
Crack front features 10 rings of elements for use in contour integral calculations for J-integral and stress intensity factors. Additionally there is a small keyhole along the crack front that increases numerical stability during blunting.

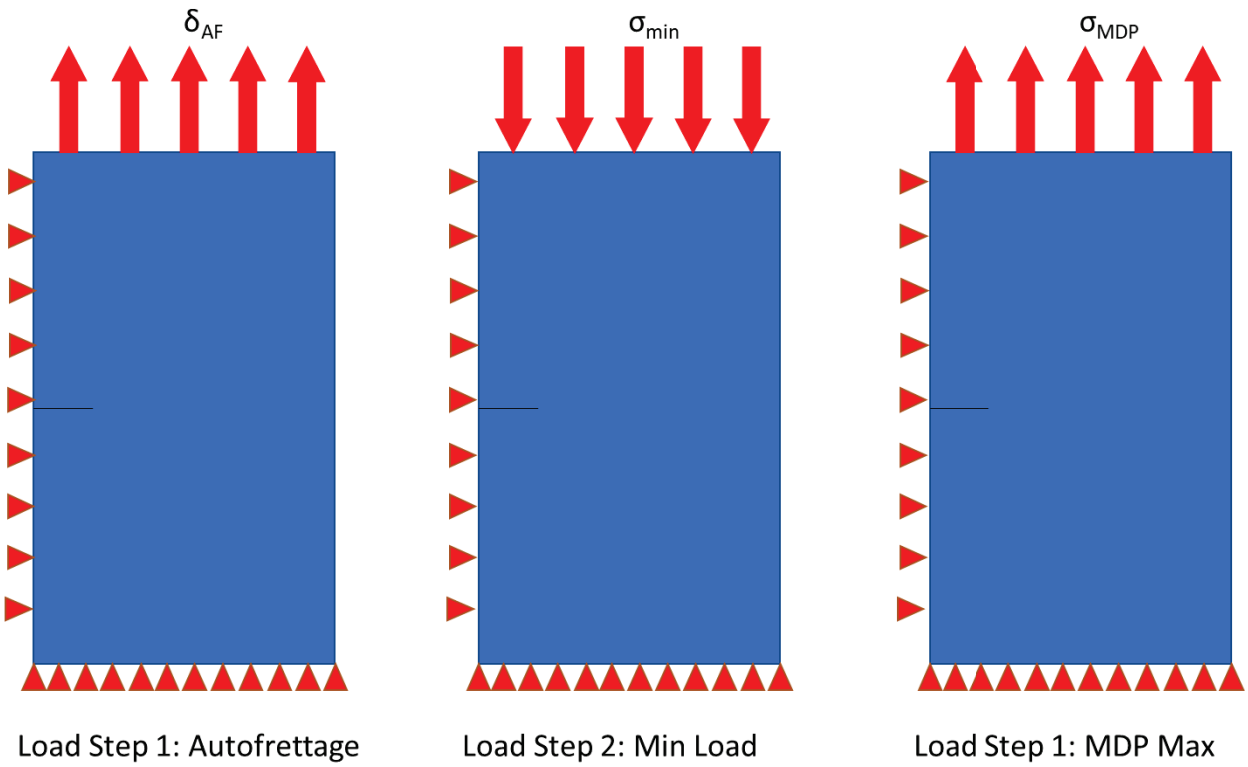

Figure A-5. Load step boundary conditions for FEA.

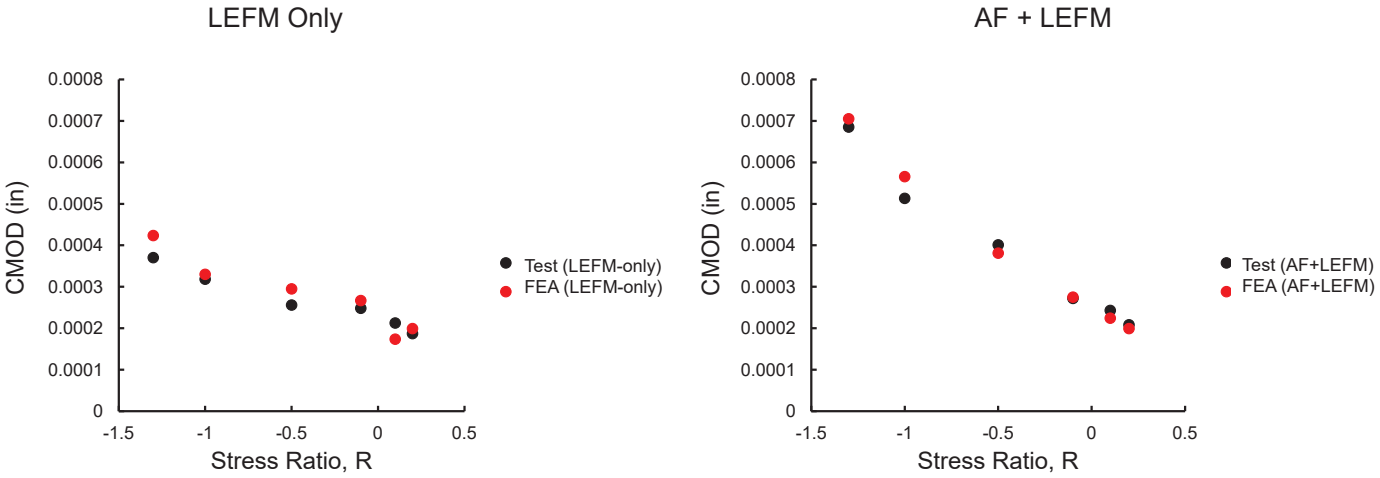

Figure A-6. CMOD extracted at the peak stress of the first LEFM cycle from the DIC data and the FEA simulations.

References

1. Abaqus FEA, Dassault Systems, https://www.3ds.com/products-services/simulia/
2. FEACrack, Quest Integrity Group, https://www.questintegrity.com/software-products/feacrack

Appendix B. Phase 1 Fracture Surface Imaging

The following figures contain the DIC CMOD measurements and fracture surfaces for all of the Phase 1 tests. All of the autofrettage cycles had a peak strain of 1.25%.

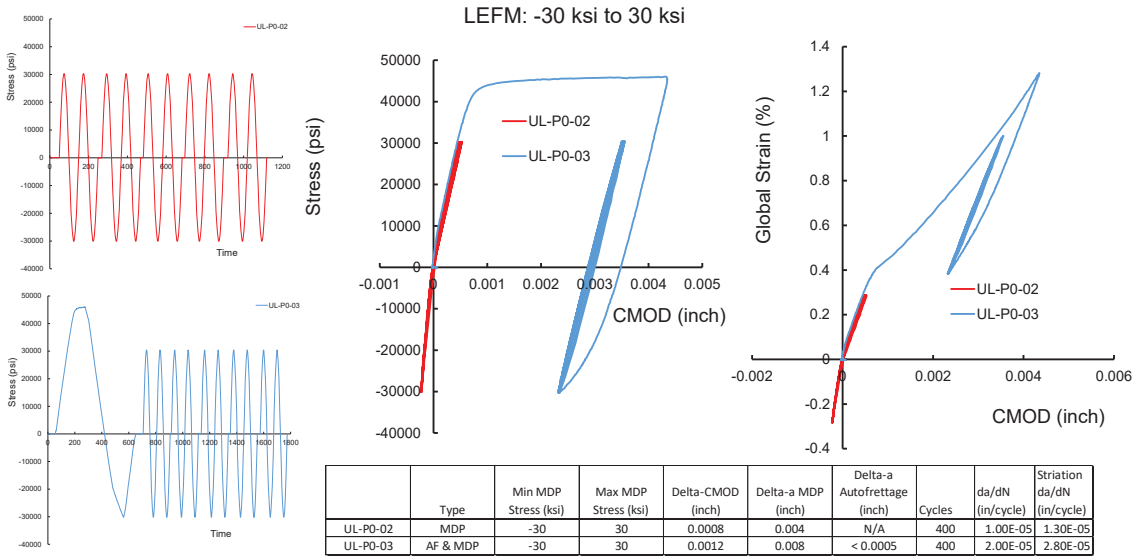

	Type	Min MDP Stress (ksi)	Max MDP Stress (ksi)	Delta-CMOD (inch)	Delta-a MDP (inch)	Delta-a Autofrettage (inch)	Cycles	da/dN (in/cycle)	Striation da/dN (in/cycle)
UL-P0-02	MDP	-30	30	0.0008	0.004	N/A	400	1.00E-05	1.30E-05
UL-P0-03	AF & MDP	-30	30	0.0012	0.008	< 0.0005	400	2.00E-05	2.80E-05

Figure B-1. DIC CMOD measurements for AF+LEFM and LEFM-only tests with LEFM cycles with a maximum stress of 30,000 psi and a minimum stress of -30,000 psi.

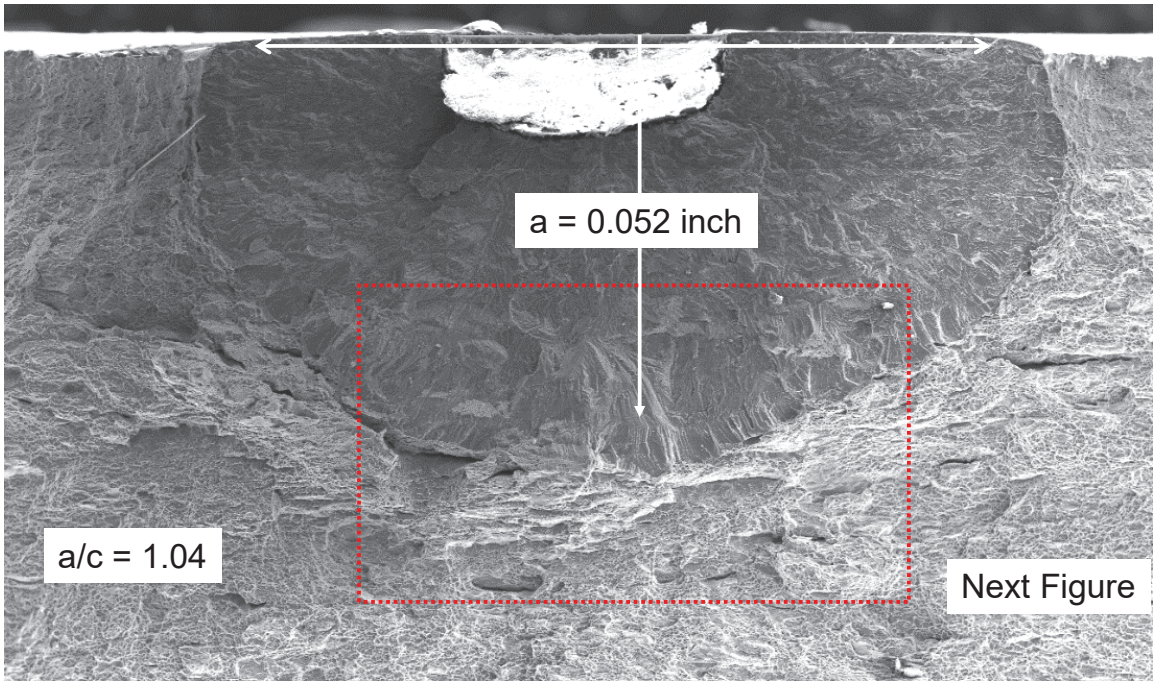

Figure B-2. Fracture surface of the LEFM-only test UL-P0-02 (LEFM: -30,000 psi to 30,000 psi).

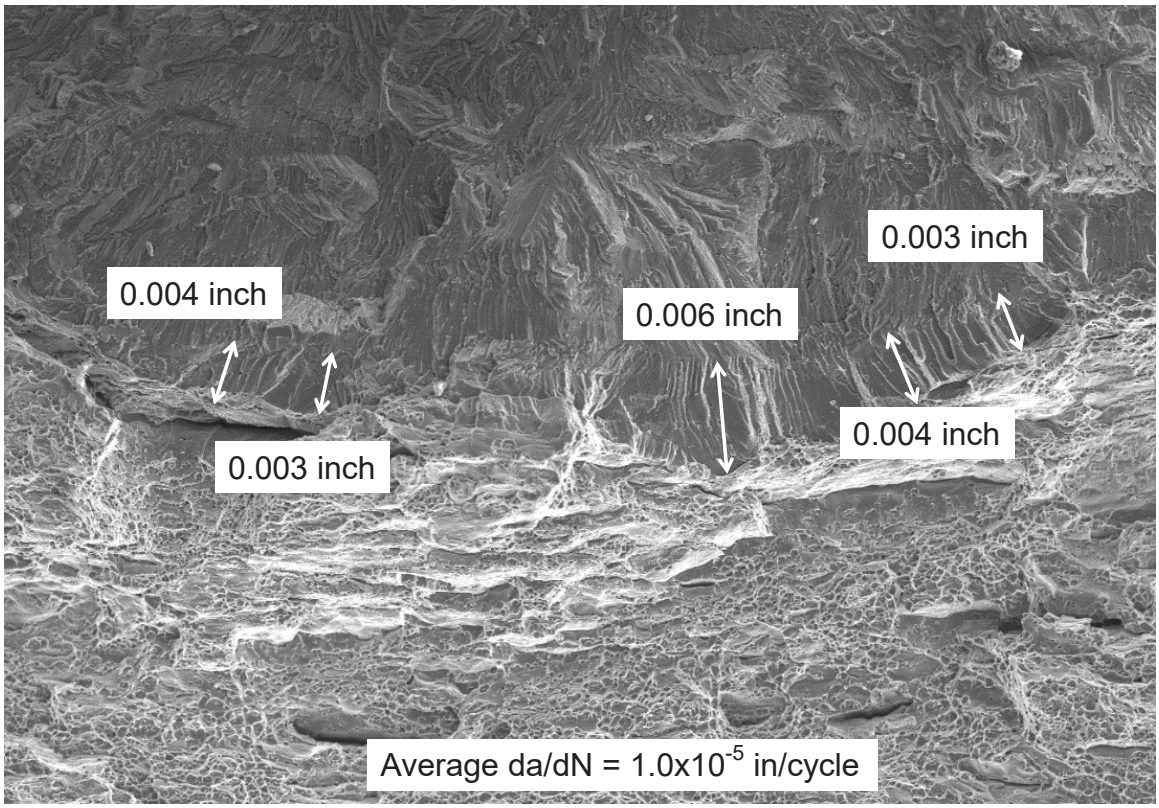

Figure B-3. Fracture surface at the maximum depth location for the LEFM-only test UL-P0-02 (LEFM: -30,000 psi to 30,000 psi).

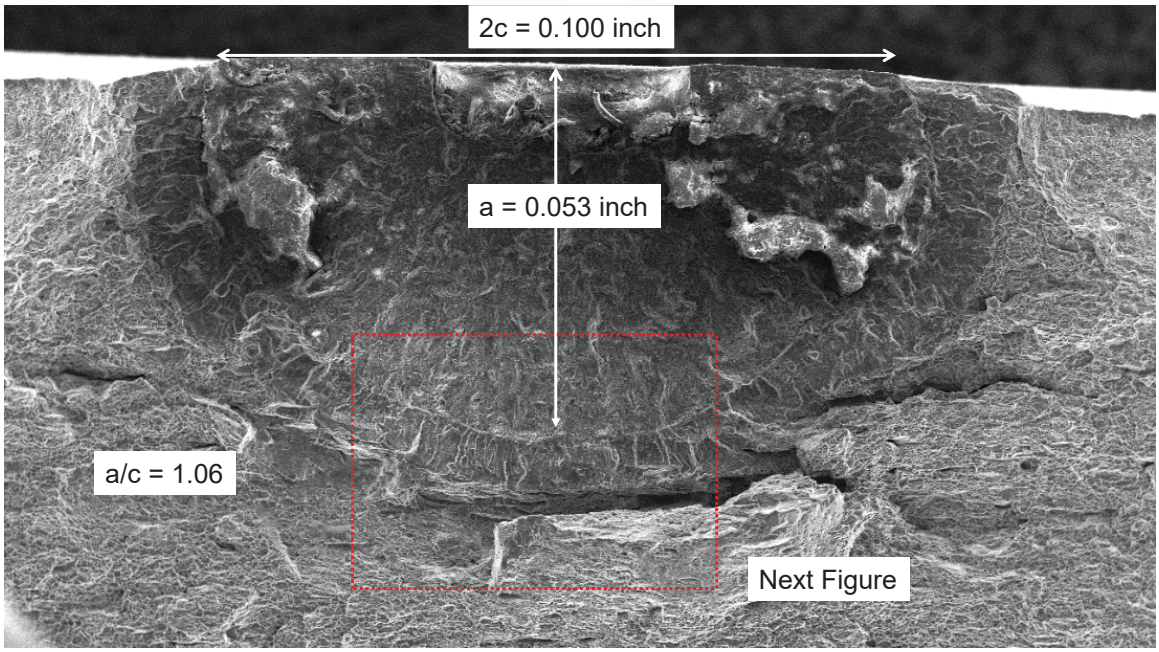

Figure B-4. Fracture surface of the AF+LEFM test UL-P0-03 (LEFM: -30,000 psi to 30,000 psi).

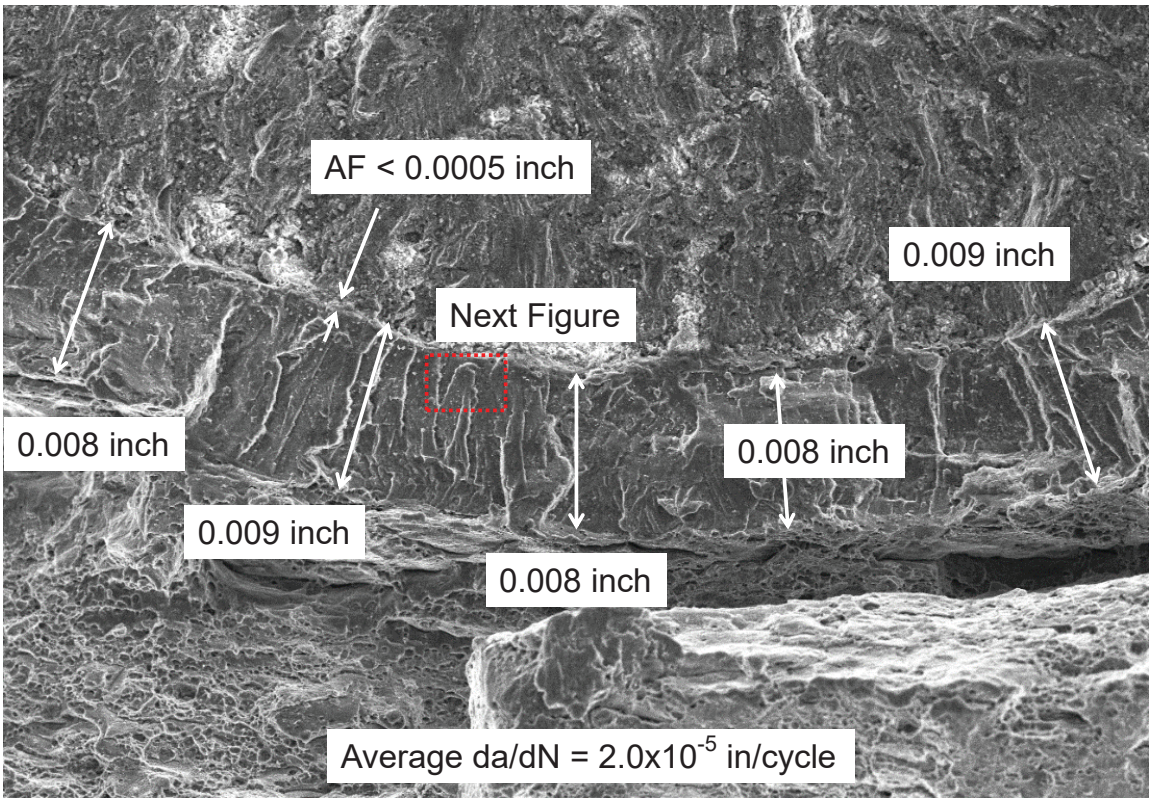

Figure B-5. Fracture surface at the maximum depth location for the AF+LEFM test UL-P0-03 (LEFM: -30,000 psi to 30,000 psi).

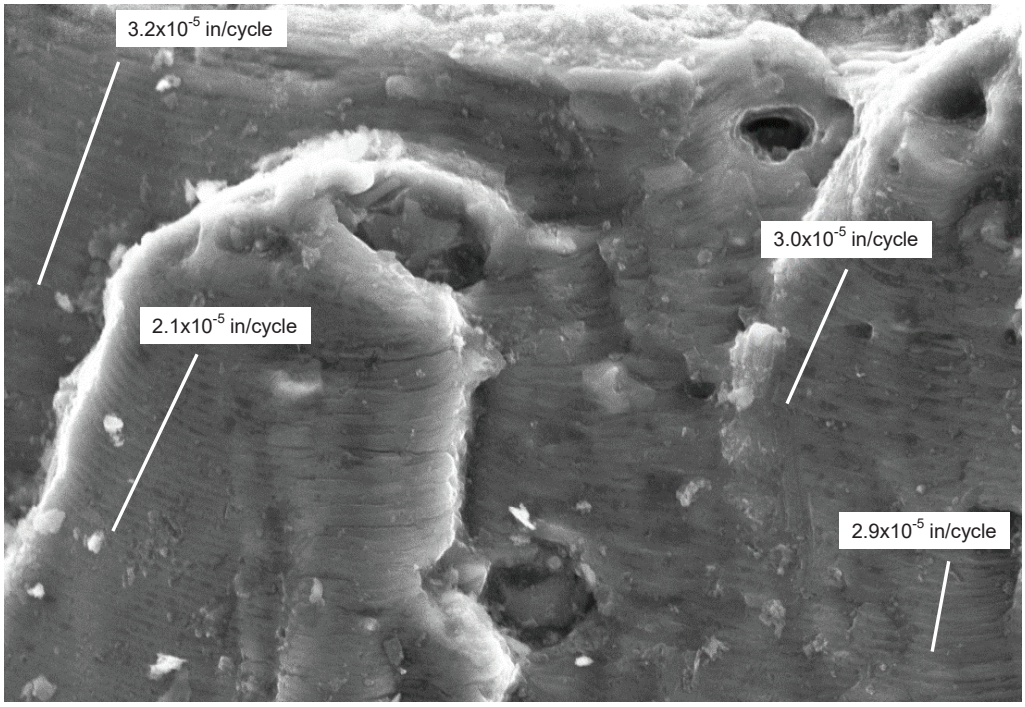

Figure B-6. Fracture striations near the maximum depth location for the AF+LEFM test UL-P0-03 (LEFM: -30,000 psi to 30,000 psi).

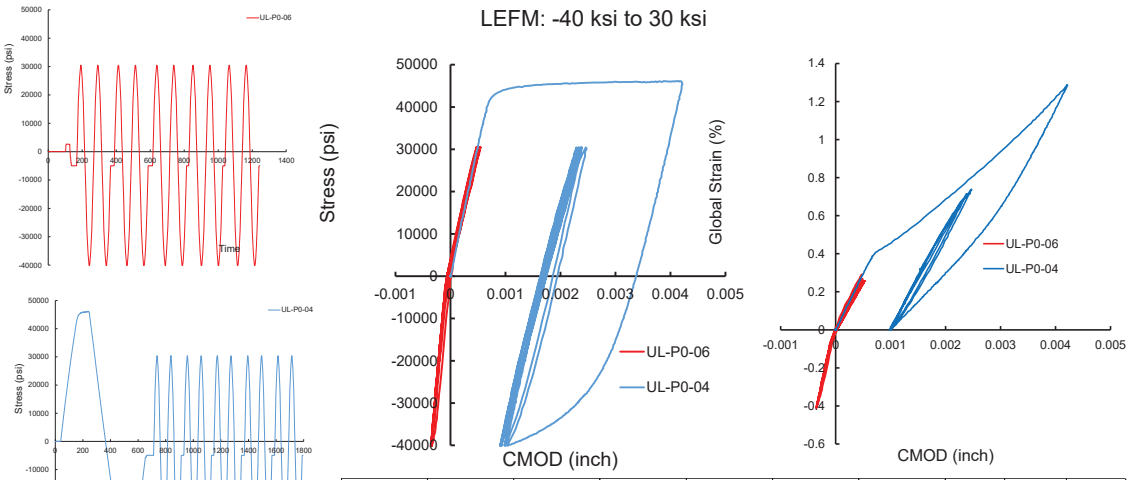

	Type	Min MDP Stress (ksi)	Max MDP Stress (ksi)	Delta-CMOD (inch)	Delta-a MDP (inch)	Delta-a Autofrettage (inch)	Cycles	da/dN (in/cycle)	Striation da/dN (in/cycle)
UL-P0-04	AF & MDP	-40	30	0.0014	0.012	< 0.0005	400	3.00E-05	7.70E-05
UL-P0-06	MDP	-40	30	0.0008	0.005	N/A	400	1.30E-05	1.50E-05

Figure B-7. DIC CMOD measurements for AF+LEFM and LEFM-only tests with LEFM cycles with a maximum stress of 30,000 psi and a minimum stress of -40,000 psi.

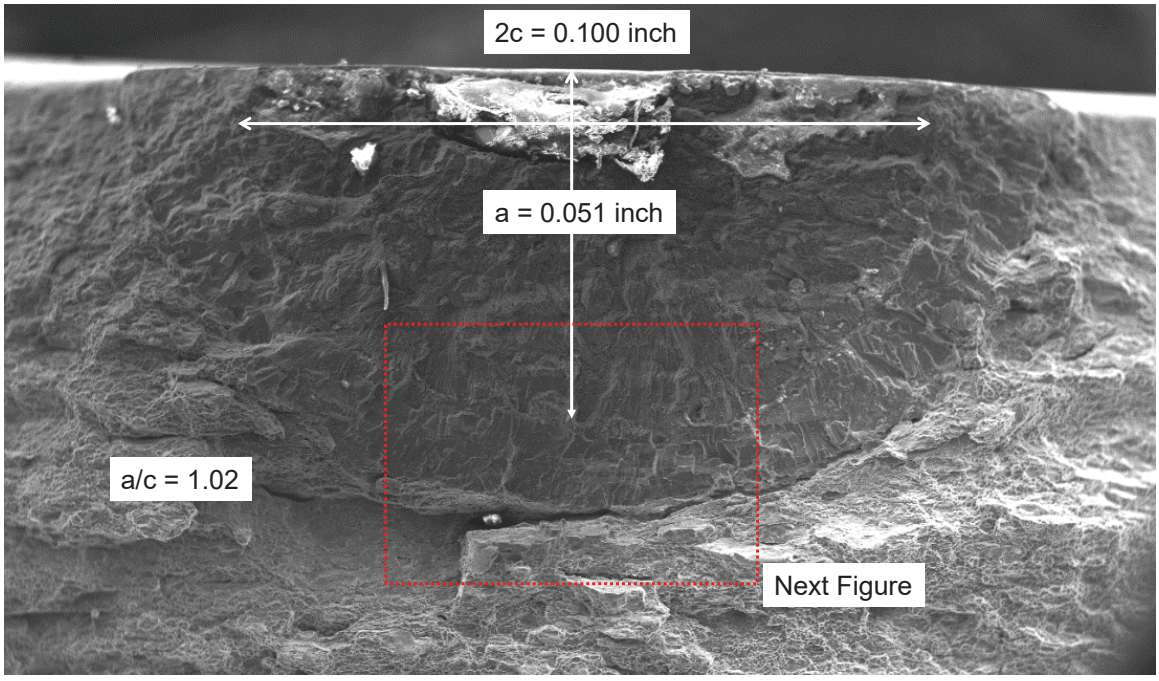

Figure B-8. Fracture surface of the AF+LEFM test UL-P0-04 (LEFM: -40,000 psi to 30,000 psi).

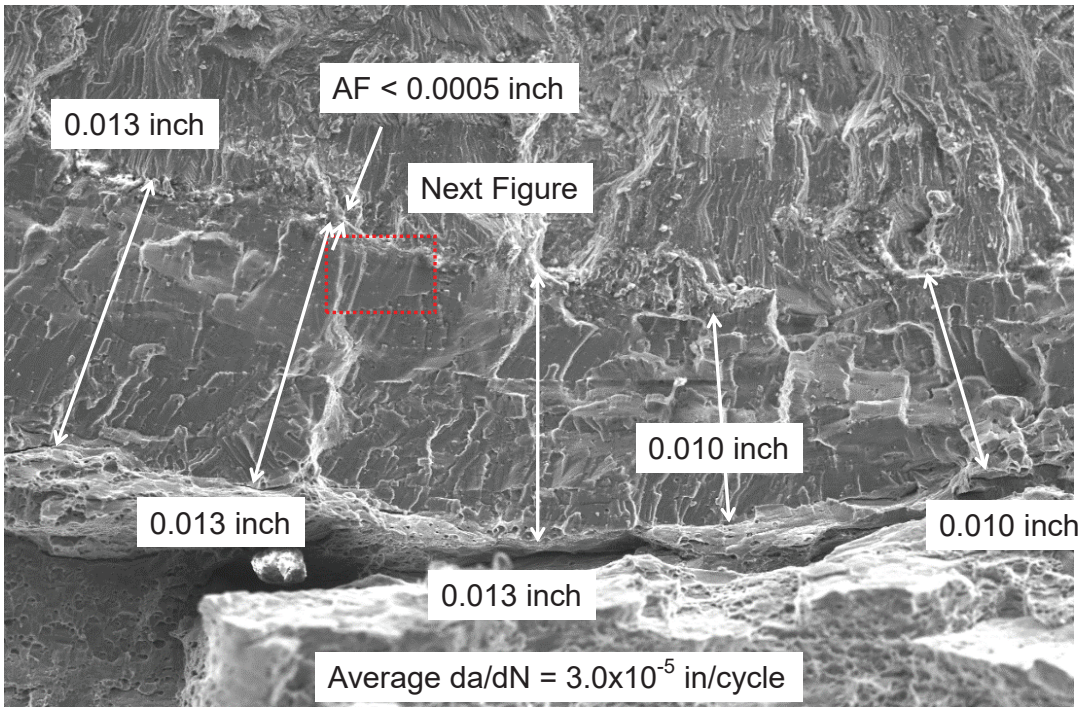

Figure B-9. Fracture surface at the maximum depth location for the AF+LEFM test UL-P0-04 (LEFM: -40,000 psi to 30,000 psi).

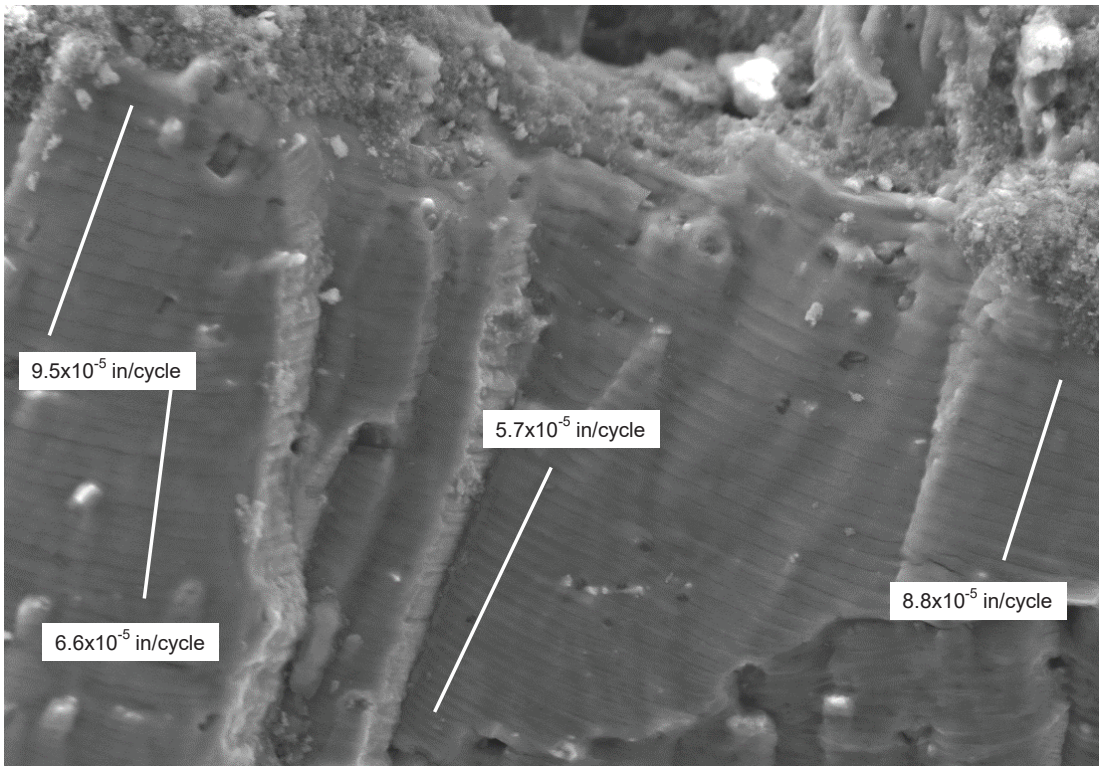

Figure B-10. Fracture striations near the maximum depth location for the AF+LEFM test UL-P0-04 (LEFM: -40,000 psi to 30,000 psi).

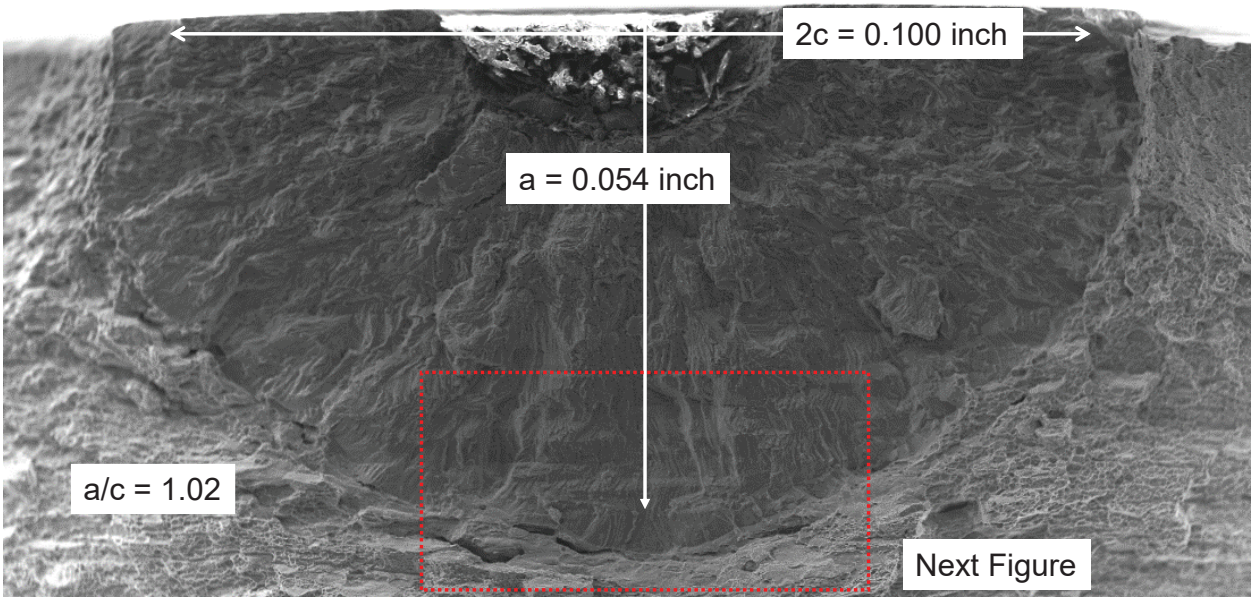

Figure B-11. Fracture surface of the LEFM-only test UL-P0-06 (LEFM: -40,000 psi to 30,000 psi).

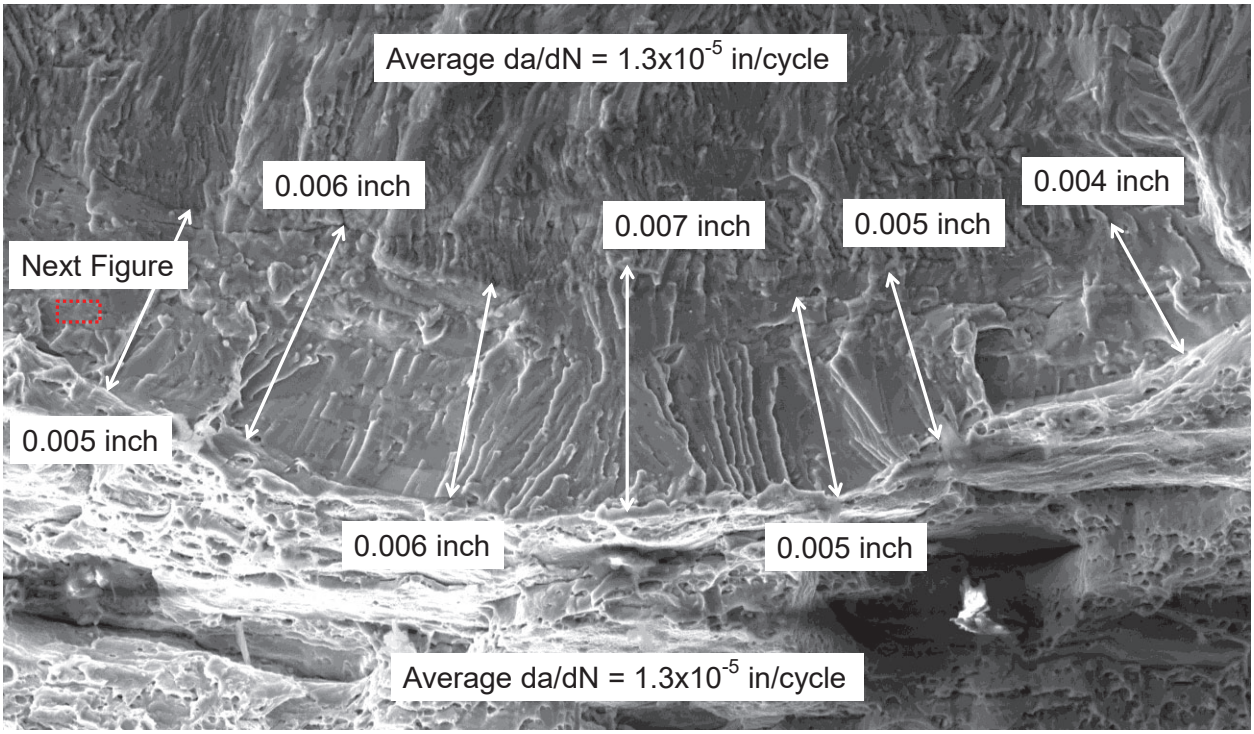

Figure B-12. Fracture surface at the maximum depth location for the LEFM-only test UL-P0-06 (LEFM: -40,000 psi to 30,000 psi).

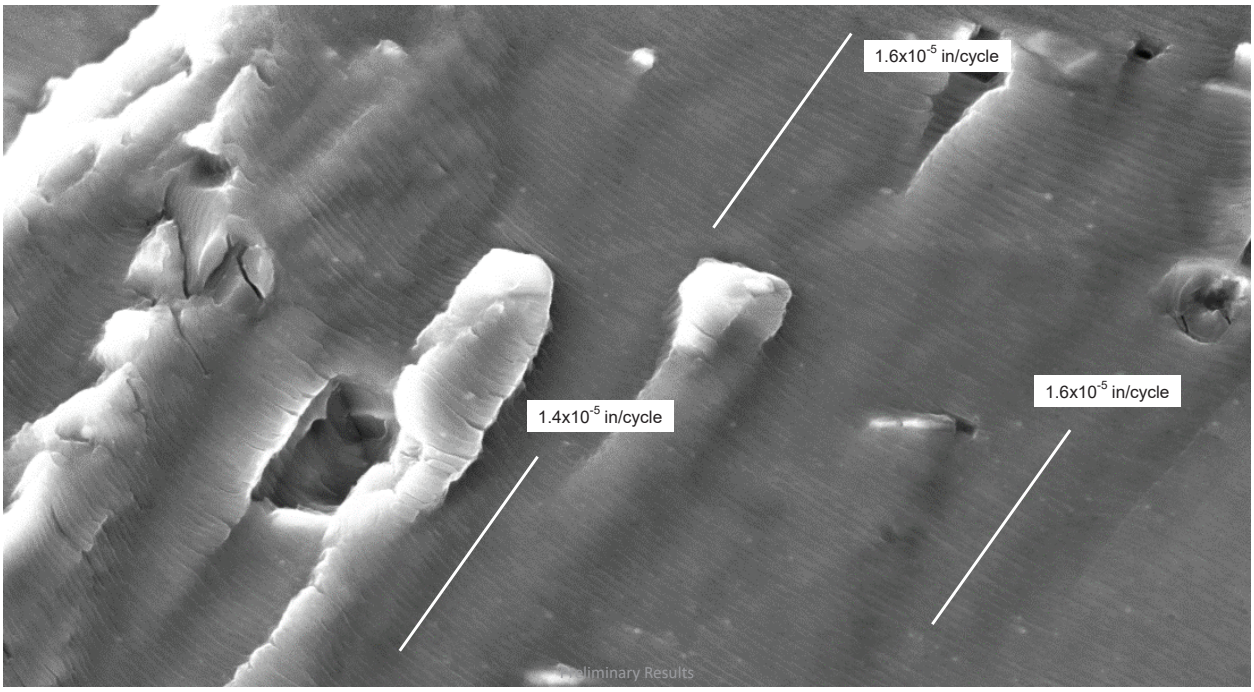

Figure B-13. Fracture striations near the maximum depth location for the LEFM-only test UL-P0-06 (LEFM: -40,000 psi to 30,000 psi).

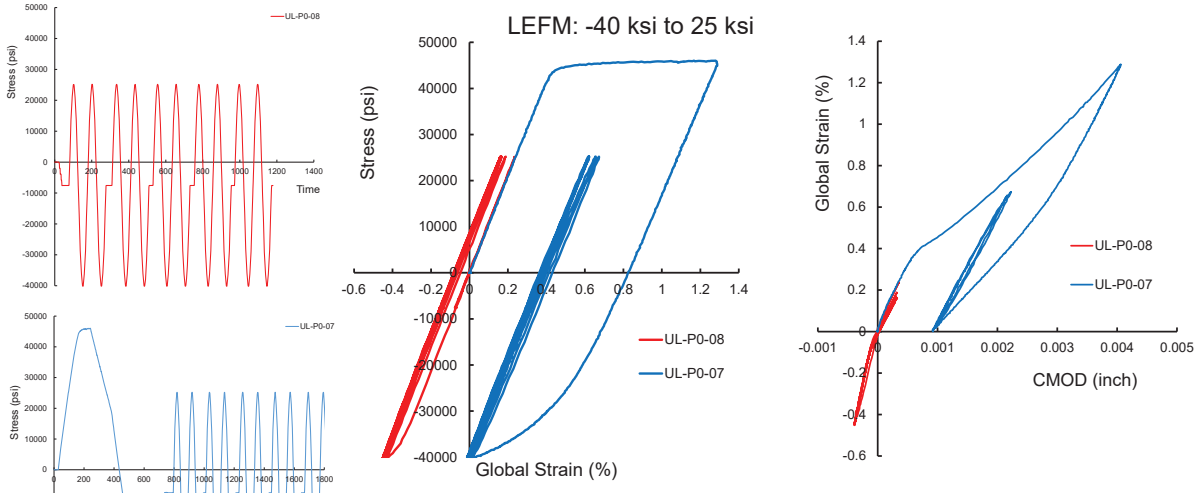

	Type	Min MDP Stress (ksi)	Max MDP Stress (ksi)	Delta-CMOD (inch)	Delta-a MDP (inch)	Delta-a Autofrettage (inch)	Cycles	da/dN (in/cycle)	Striation da/dN (in/cycle)
UL-P0-07	AF & MDP	-40	25	0.0012	0.007	0.0005	400	1.80E-05	1.50E-05
UL-P0-08	MDP	-40	25	0.0007	0.002	< 0.0005	400	5.00E-06	--

Figure B-14. DIC CMOD measurements for AF+LEFM and LEFM-only tests with LEFM cycles with a maximum stress of 25,000 psi and a minimum stress of -40,000 psi.

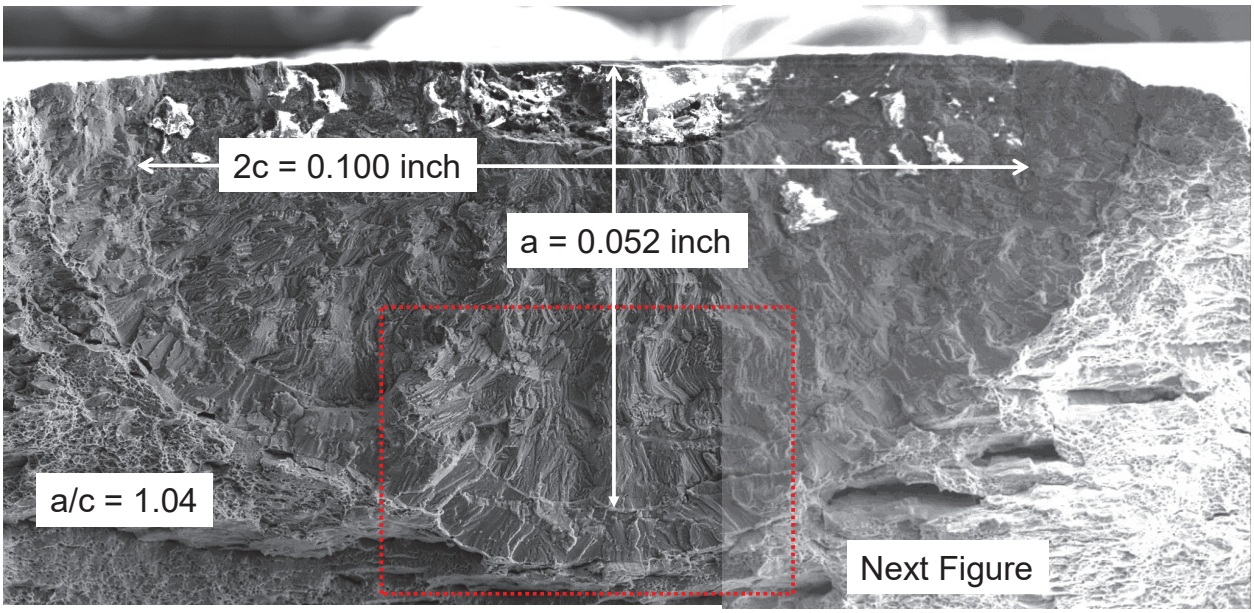

Figure B-15. Fracture surface of the AF+LEFM test UL-P0-07 (LEFM: -40,000 psi to 25,000 psi).

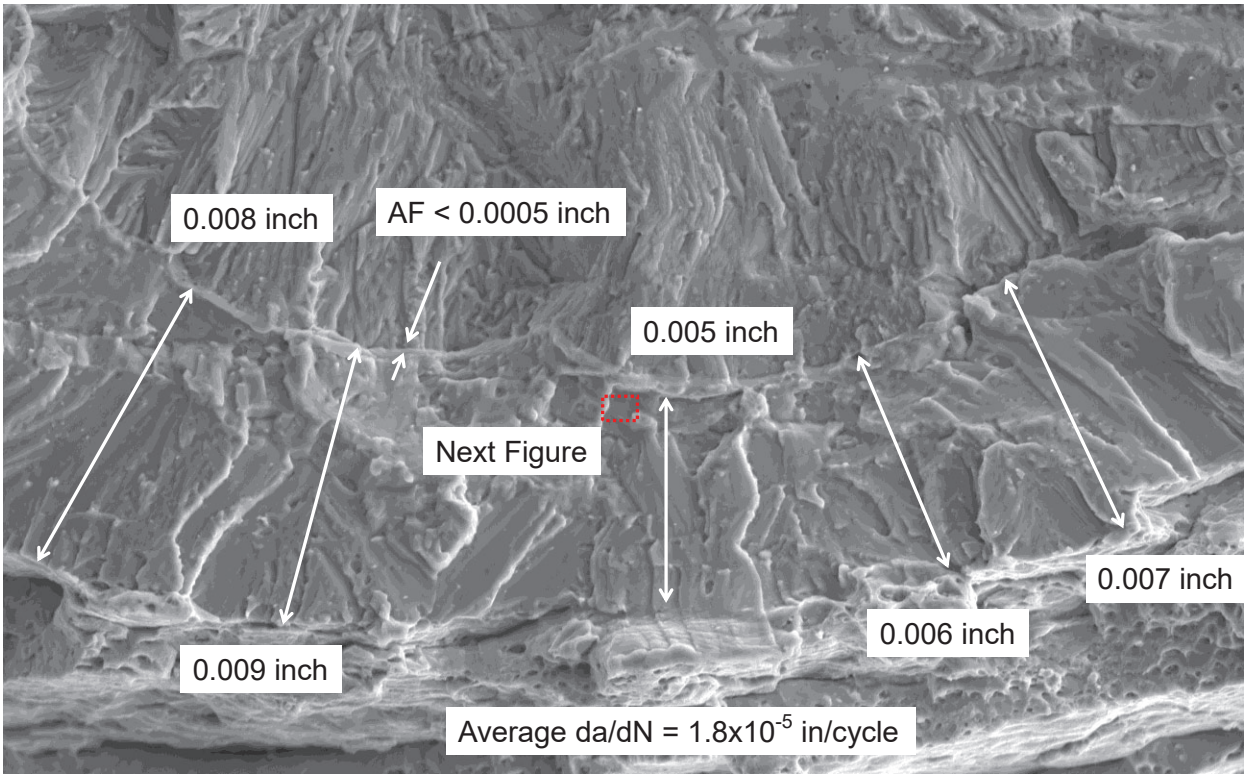

Figure B-16. Fracture surface at the maximum depth location for the AF+LEFM test UL-P0-07 (LEFM: -40,000 psi to 25,000 psi).

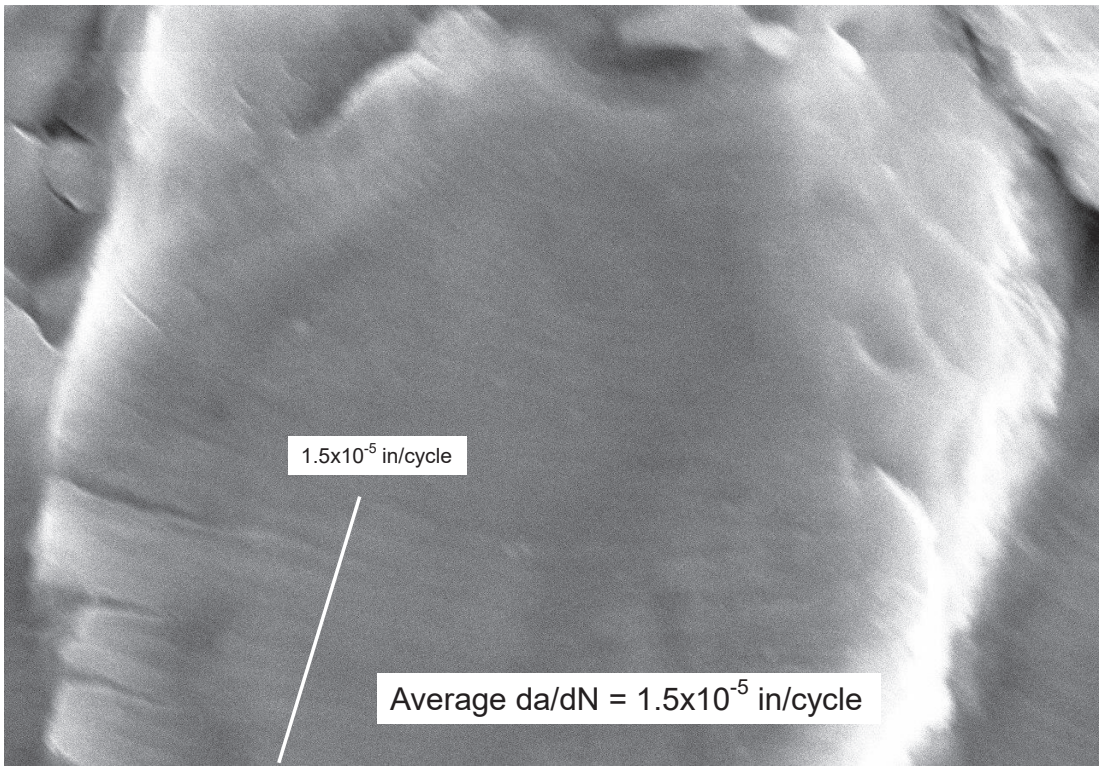

Figure B-17. Fracture striations near the maximum depth location for the AF+LEFM test UL-P0-07 (LEFM: -40,000 psi to 25,000 psi).

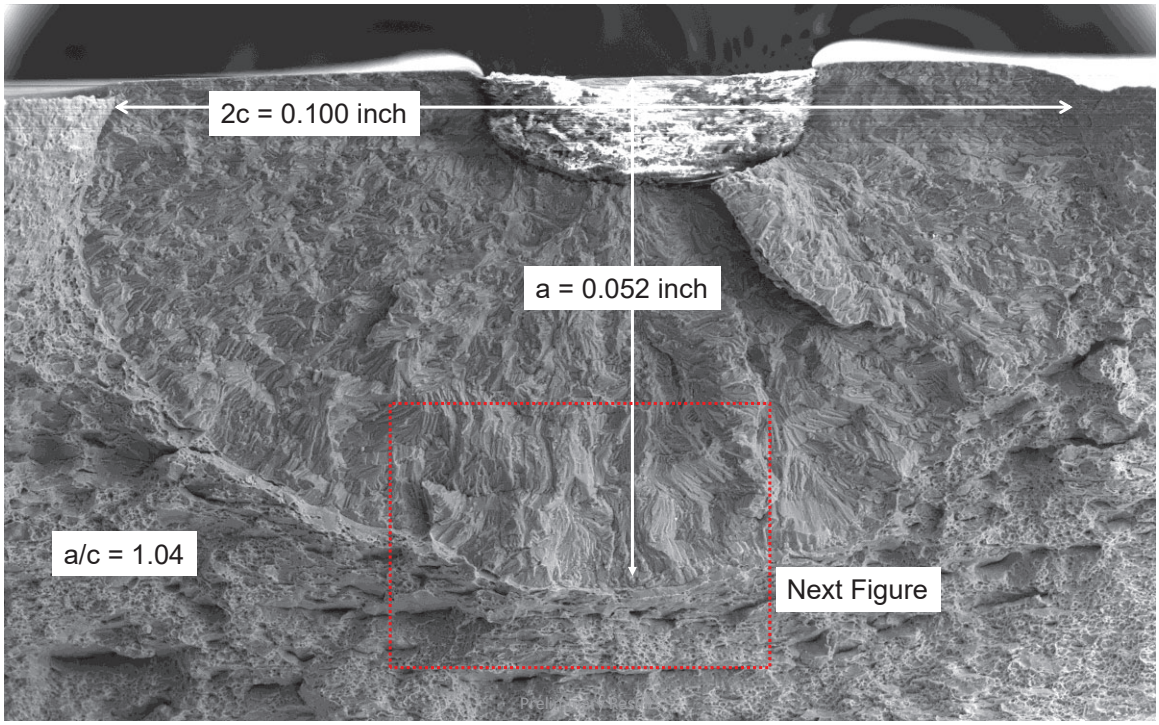

Figure B-18. Fracture surface of the LEFM-only test UL-P0-08 (LEFM: -40,000 psi to 25,000 psi).

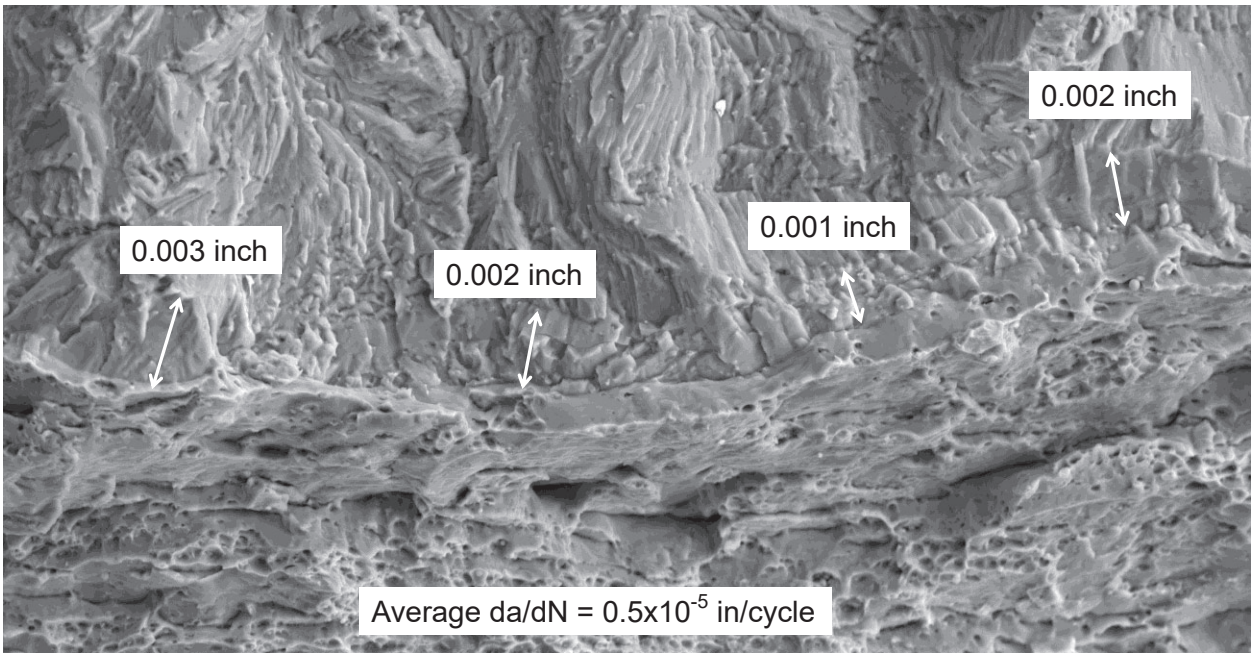

Figure B-19. Fracture surface at the maximum depth location for the LEFM-only test UL-P0-08 (LEFM: -40,000 psi to 25,000 psi).

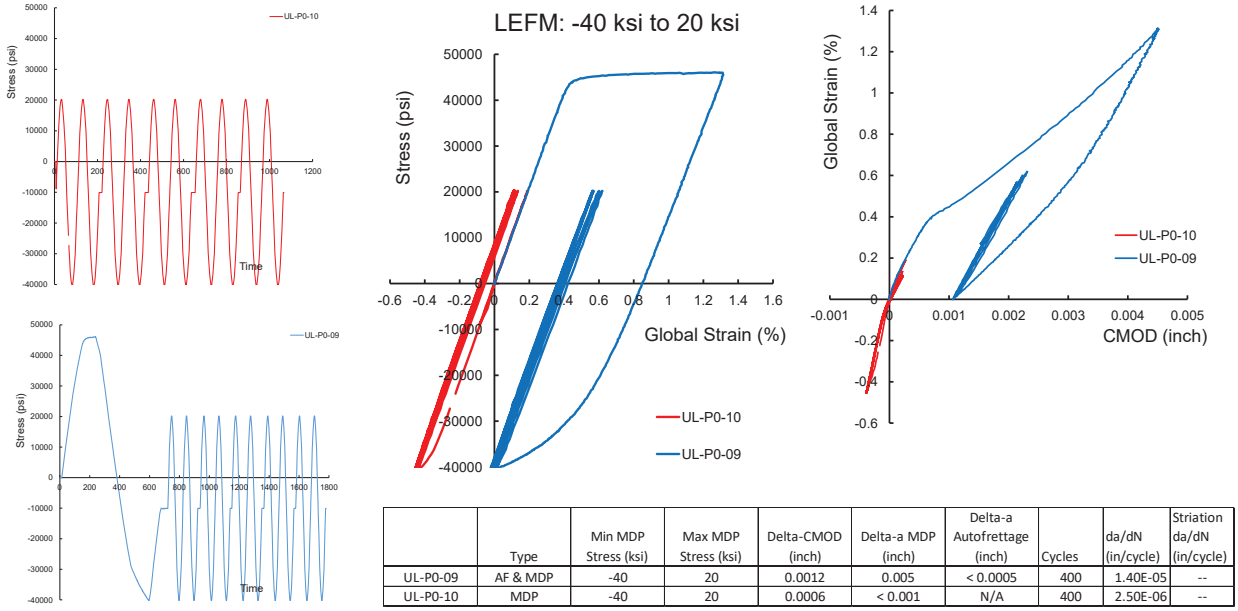

	Type	Min MDP Stress (ksi)	Max MDP Stress (ksi)	Delta-CMOD (inch)	Delta-a MDP (inch)	Delta-a Autofrettage (inch)	Cycles	da/dN (in/cycle)	Striation da/dN (in/cycle)
UL-P0-09	AF & MDP	-40	20	0.0012	0.005	< 0.0005	400	1.40E-05	--
UL-P0-10	MDP	-40	20	0.0006	< 0.001	N/A	400	2.50E-06	--

Figure B-20. DIC CMOD measurements for AF+LEFM and LEFM-only tests with LEFM cycles with a maximum stress of 20,000 psi and a minimum stress of -40,000 psi.

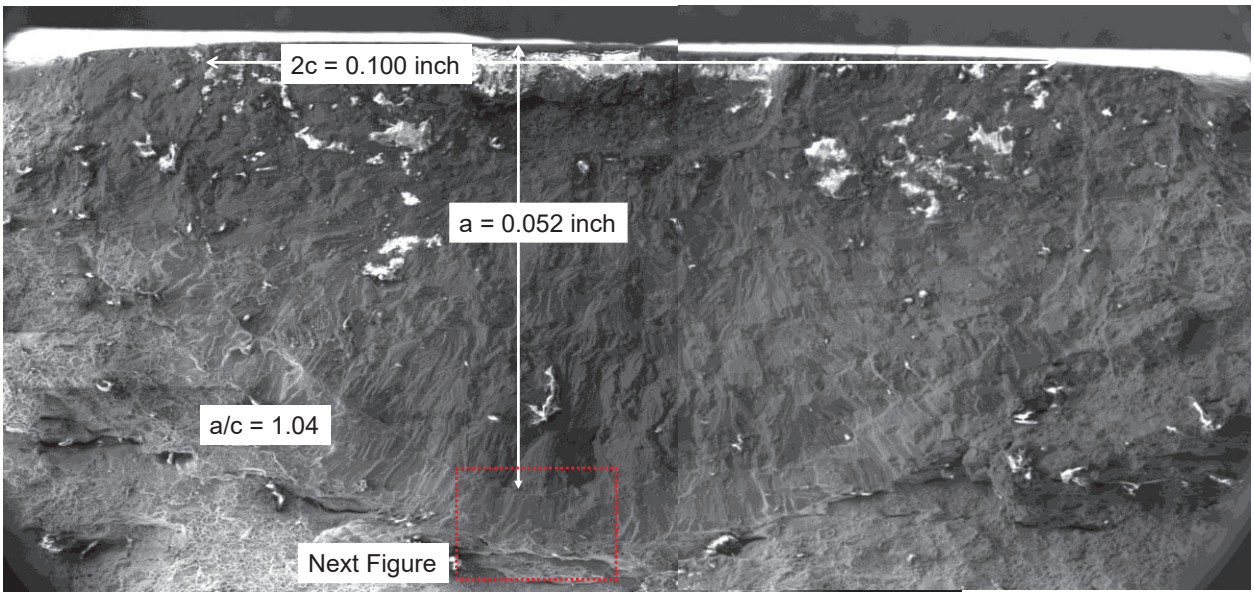

Figure B-21. Fracture surface of the AF+LEFM test UL-P0-09 (LEFM: -40,000 psi to 20,000 psi).

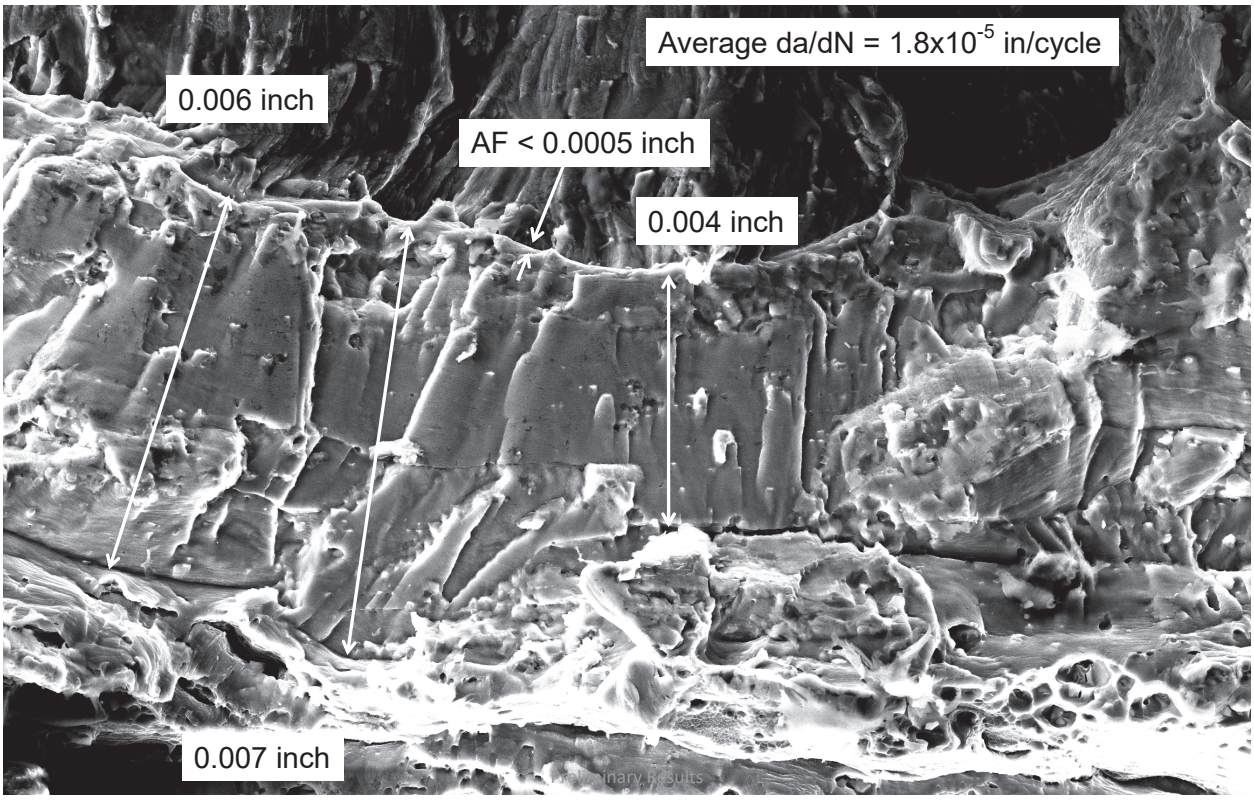

Figure B-22. Fracture surface at the maximum depth location for the AF+LEFM test UL-P0-09 (LEFM: -40,000 psi to 20,000 psi).

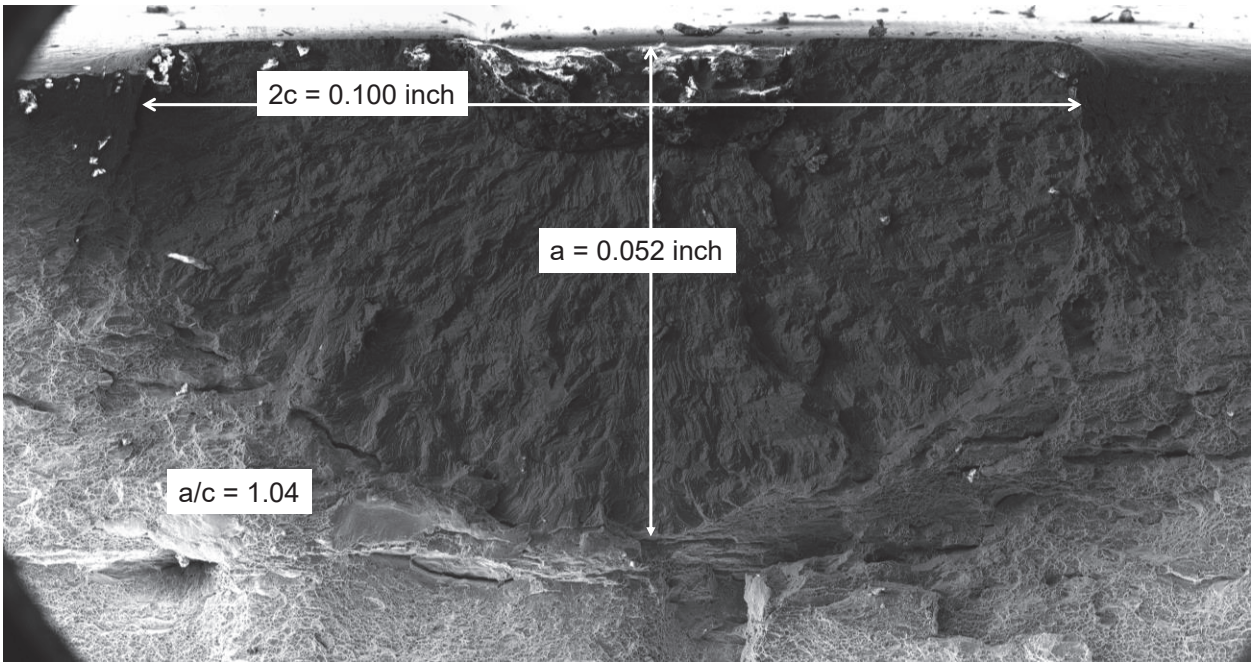

Figure B-23. Fracture surface of the LEFM-only test UL-P0-10 (LEFM: -40,000 psi to 20,000 psi).

Appendix C. Phase 2 Fracture Surfaces

The following figures contain the DIC CMOD measurements and fracture surfaces for all of the Phase 2 tests. All of the autofrettage cycles had a peak strain of 1.5%.

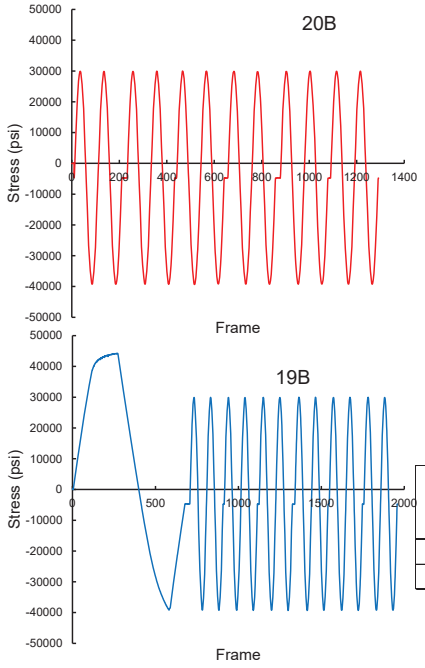

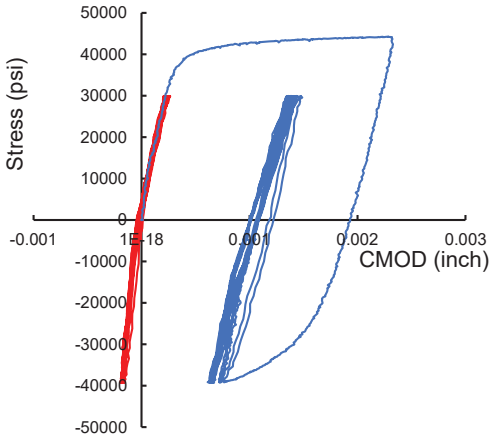

ID	LEFM Cycles	da (inch)	da/dN (in/cycle)	AF (% Strain)	Max Stress (psi)	Min Stress (psi)	R
19B	500	0.0077	1.5E-05	1.5	30000	-38500	-1.3
20B	500	0.0022	4.4E-06	None	30000	-38500	-1.3

Figure C-1. DIC CMOD measurements for AF+LEFM and LEFM-only tests with LEFM cycles with a maximum stress of 30,000 psi and a stress ratio of R = -1.3.

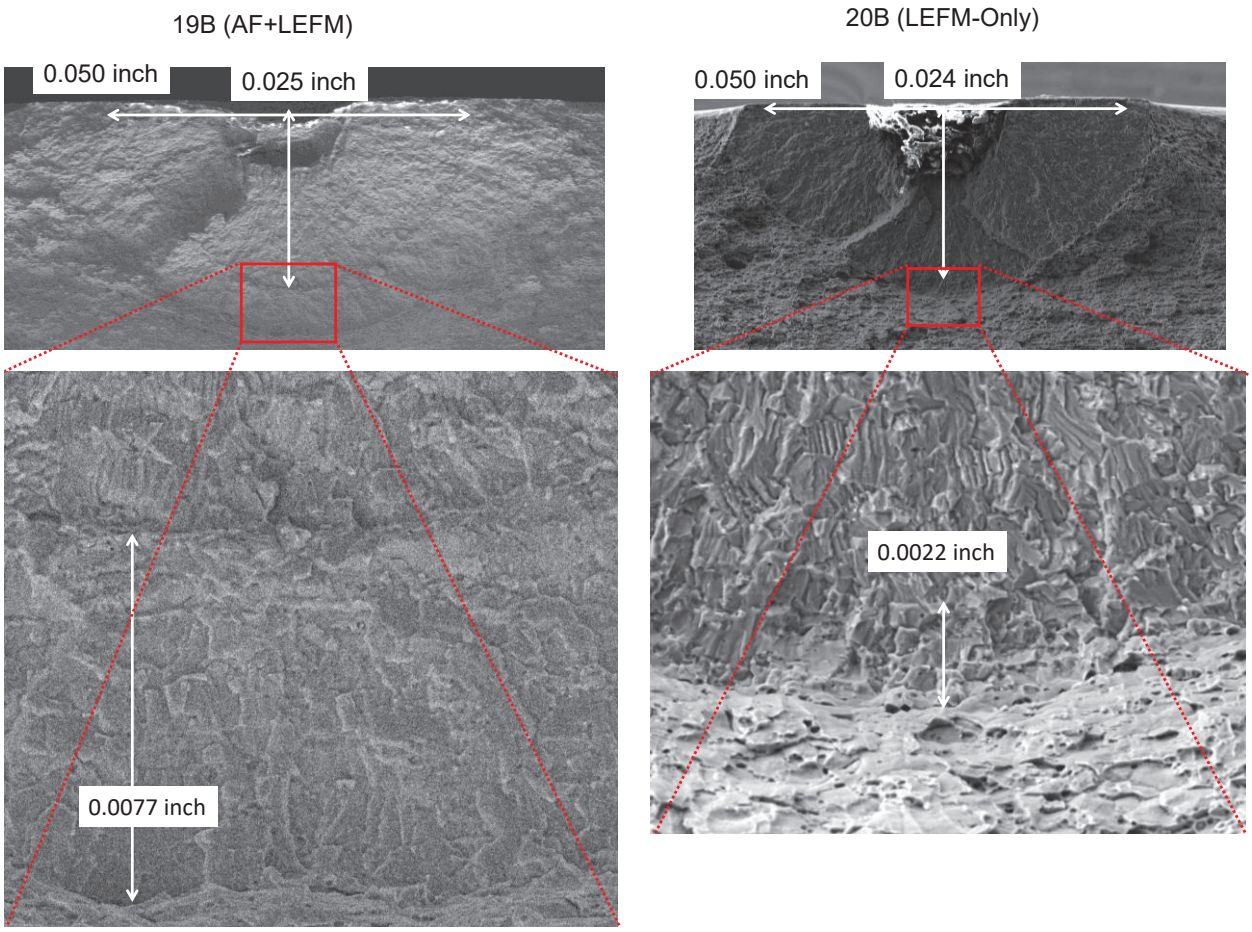

Figure C-2. Fracture surfaces for the 19B (AF+LEFM) and 20B (LEFM-only) tests with LEFM cycles with a maximum stress of 30,000 psi and a stress ratio of R = -1.3.

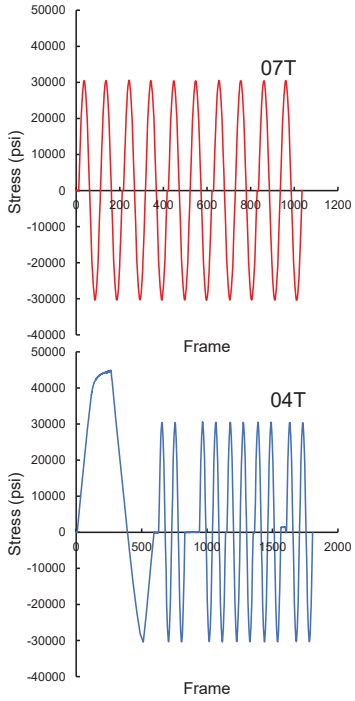

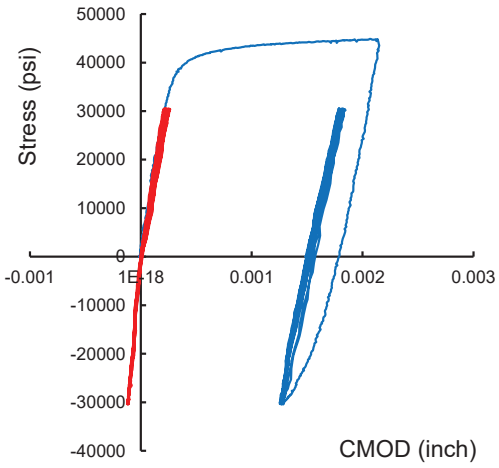

ID	LEFM Cycles	da (inch)	da/dN (in/cycle)	AF (% Strain)	Max Stress (psi)	Min Stress (psi)	R
04T	600	0.0046	7.7E-06	1.5	30000	-30000	-1.0
07T	600	0.0021	3.5E-06	None	30000	-30000	-1.0

Figure C-3. DIC CMOD measurements for AF+LEFM and LEFM-only tests with LEFM cycles with a maximum stress of 30,000 psi and a stress ratio of R = -1.0.

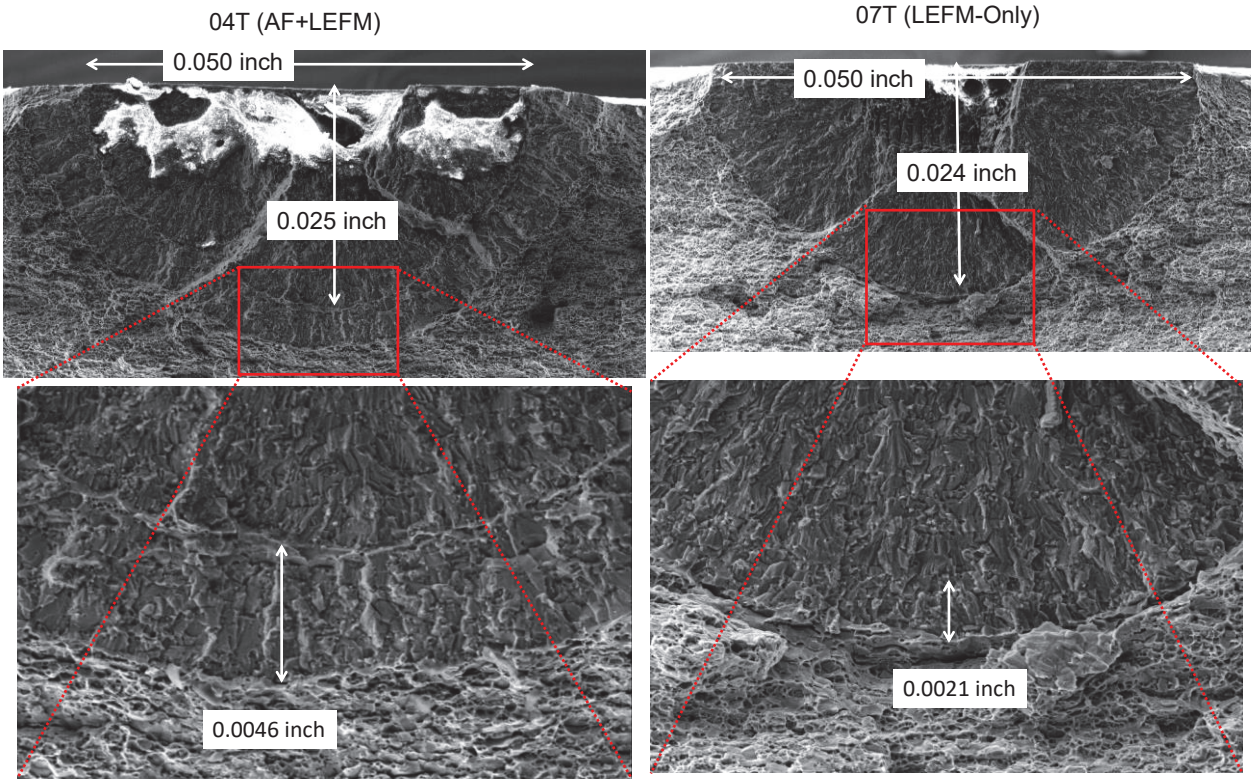

Figure C-4. Fracture surfaces for the 04T (AF+LEFM) and 07T (LEFM-only) tests with LEFM cycles with a maximum stress of 30,000 psi and a stress ratio of R = -1.0.

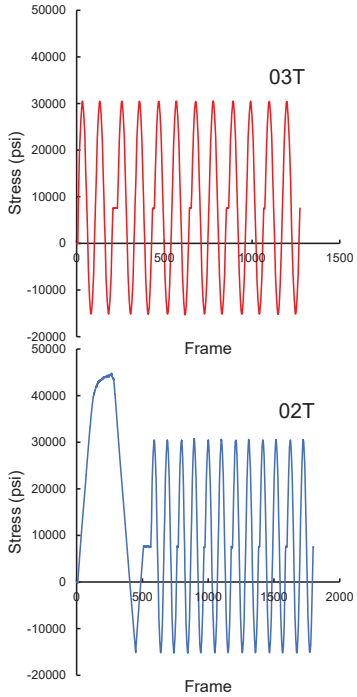

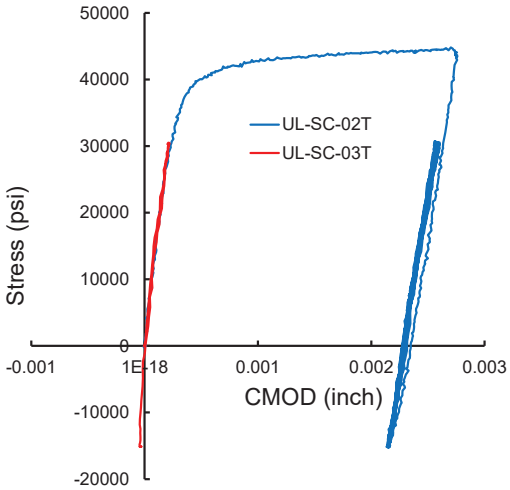

ID	LEFM Cycles	da (inch)	da/dN (in/cycle)	AF (% Strain)	Max Stress (psi)	Min Stress (psi)	R
02T	1000	0.0037	3.7E-06	1.5	30000	-15000	-0.5
03T	1000	0.0027	2.7E-06	None	30000	-15000	-0.5

Figure C-5. DIC CMOD measurements for AF+LEFM and LEFM-only tests with LEFM cycles with a maximum stress of 30,000 psi and a stress ratio of R = -0.5.

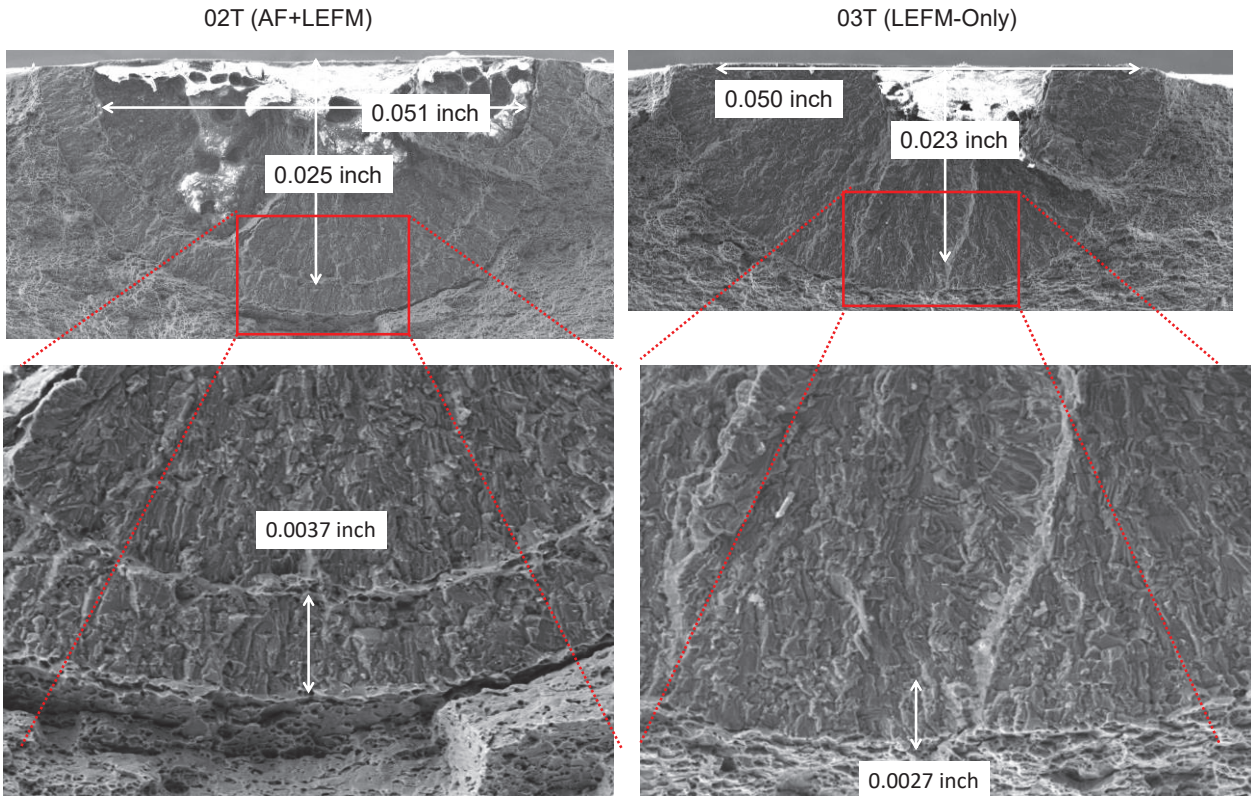

Figure C-6. Fracture surfaces for the 02T (AF+LEFM) and 03T (LEFM-only) tests with LEFM cycles with a maximum stress of 30,000 psi and a stress ratio of R = -0.5.

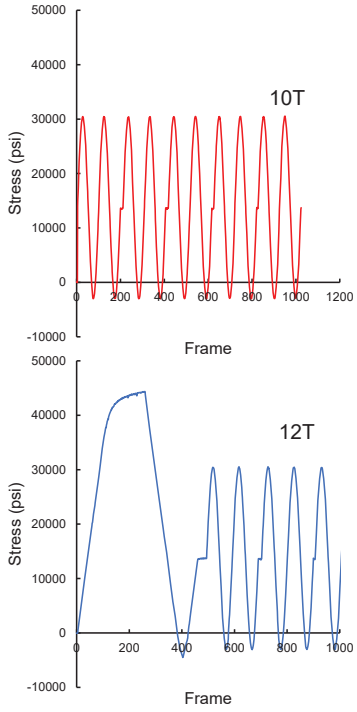

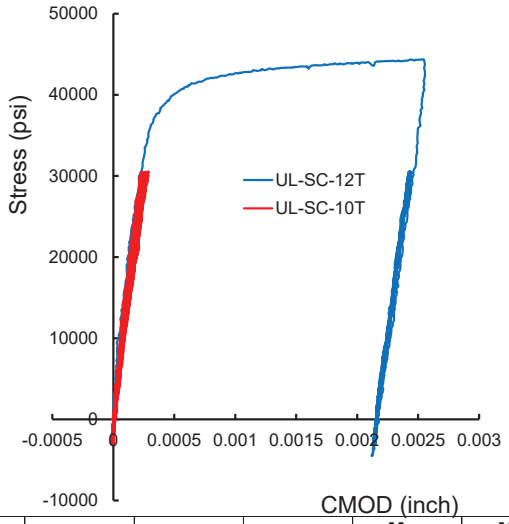

ID	LEFM Cycles	da (inch)	da/dN (in/cycle)	AF (% Strain)	Max Stress (psi)	Min Stress (psi)	R
12T	2000	0.0018	9.0E-07	1.5	30000	-3000	-0.1
10T	2000	0.0032	1.6E-06	None	30000	-3000	-0.1

Figure C-7. DIC CMOD measurements for AF+LEFM and LEFM-only tests with LEFM cycles with a maximum stress of 30,000 psi and a stress ratio of R = -0.1.

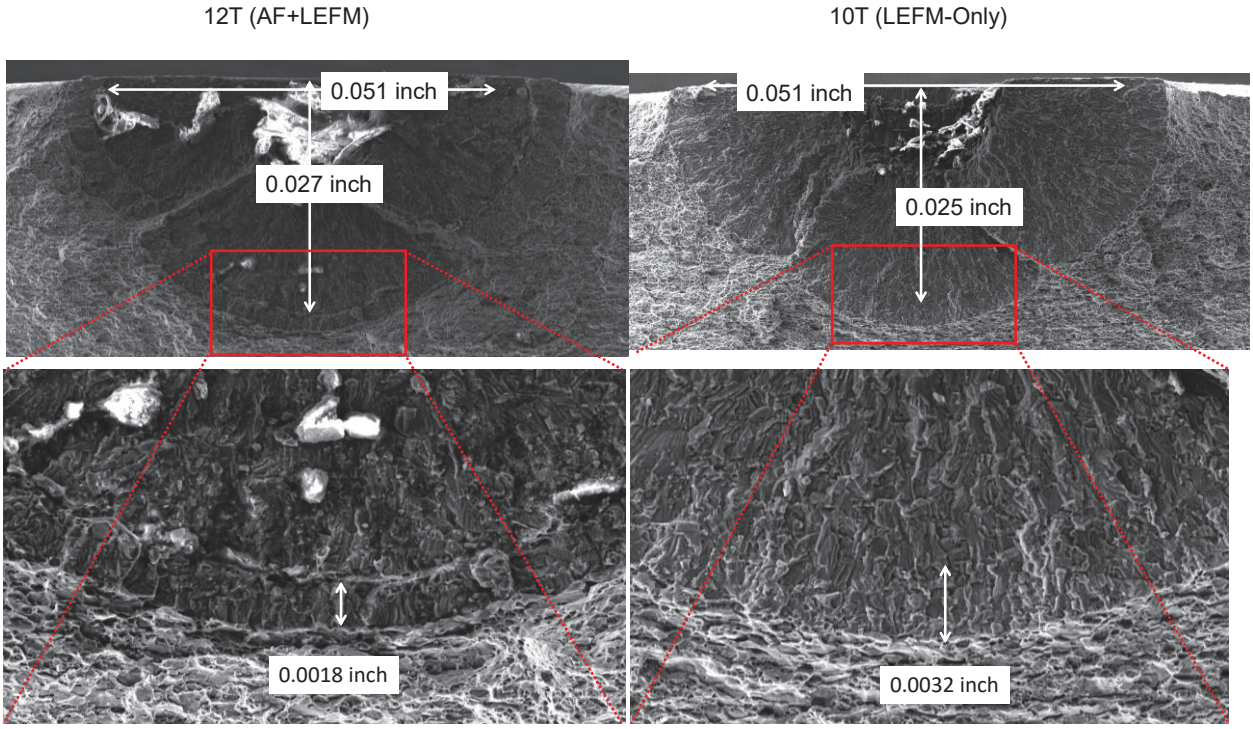

Figure C-8. Fracture surfaces for the 12T (AF+LEFM) and 10T (LEFM-only) tests with LEFM cycles with a maximum stress of 30,000 psi and a stress ratio of R = -0.1.

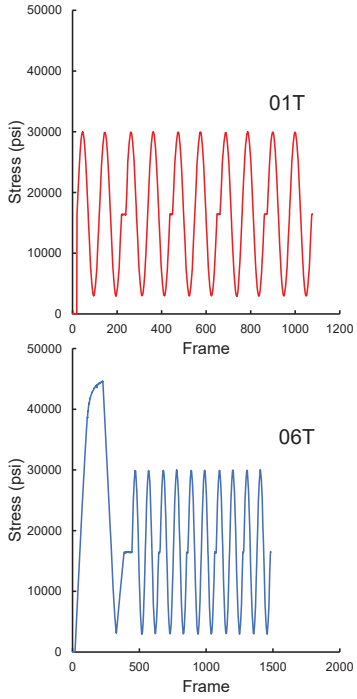

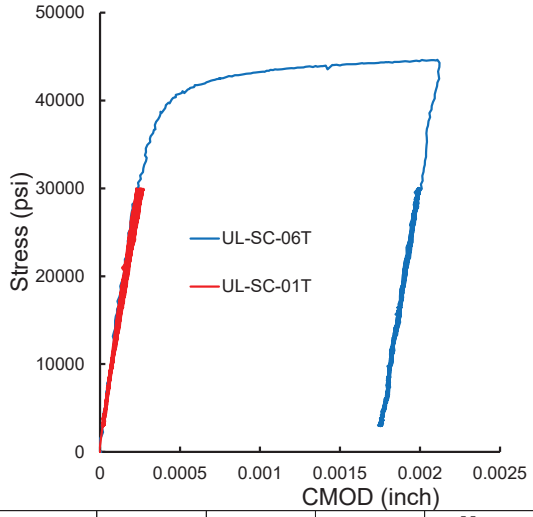

ID	LEFM Cycles	da (inch)	da/dN (in/cycle)	AF (% Strain)	Max Stress (psi)	Min Stress (psi)	R
06T	4000	0.0014	3.5E-07	1.5	30000	3000	0.1
01T	4000	0.0040	1.0E-06	None	30000	3000	0.1

Figure C-9. DIC CMOD measurements for AF+LEFM and LEFM-only tests with LEFM cycles with a maximum stress of 30,000 psi and a stress ratio of R = 0.1.

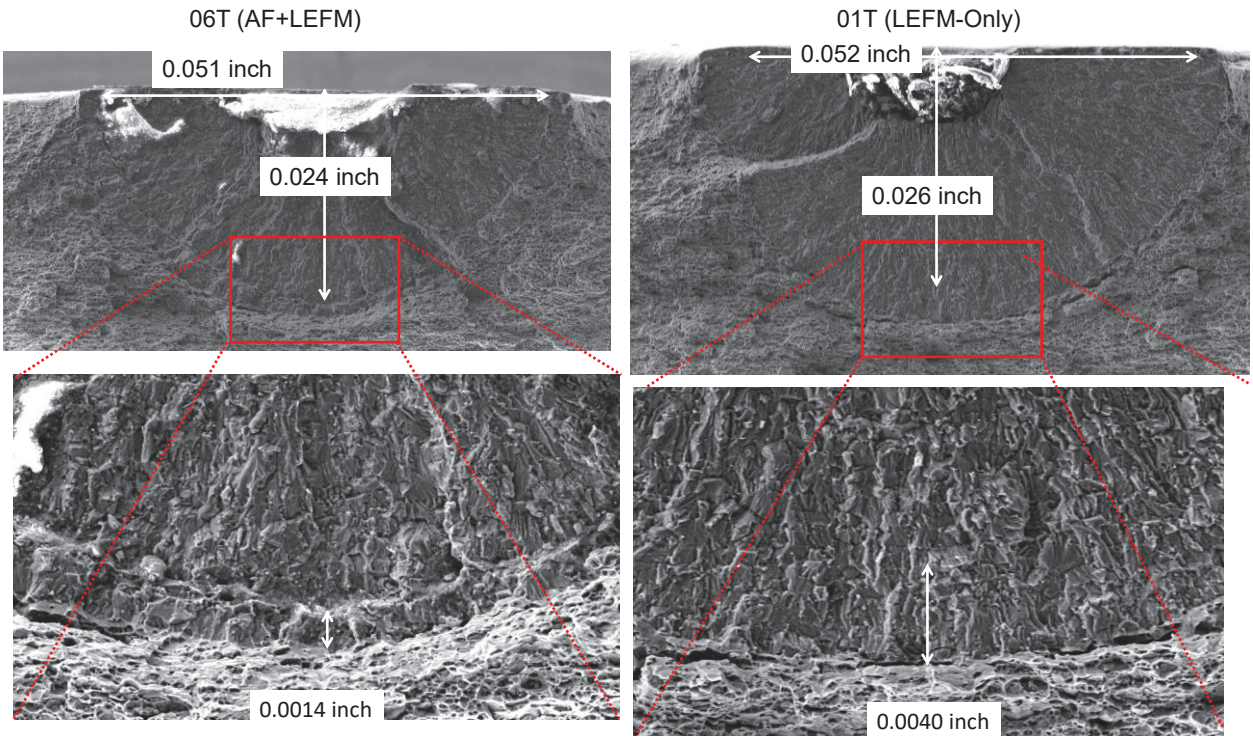

Figure C-10. Fracture surfaces for the 06T (AF+LEFM) and 01T (LEFM-only) tests with LEFM cycles with a maximum stress of 30,000 psi and a stress ratio of R = 0.1.

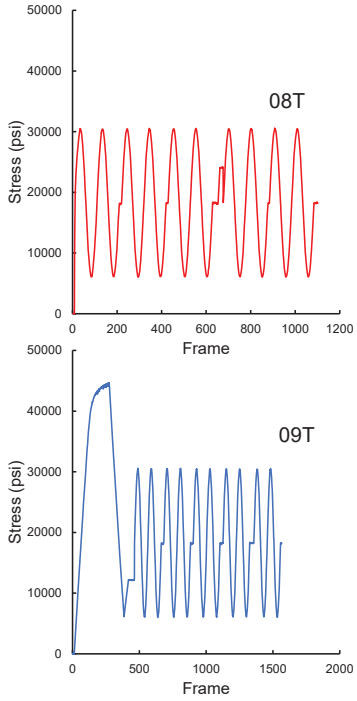

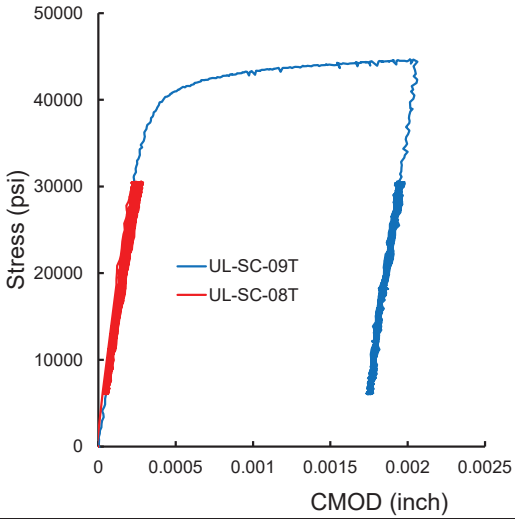

ID	LEFM Cycles	da (inch)	da/dN (in/cycle)	AF (% Strain)	Max Stress (psi)	Min Stress (psi)	R
09T	6000	0.0014	2.3E-07	1.5	30000	6000	0.2
08T	6000	0.0044	7.3E-07	None	30000	6000	0.2

Figure C-11. DIC CMOD measurements for AF+LEFM and LEFM-only tests with LEFM cycles with a maximum stress of 30,000 psi and a stress ratio of R = 0.2.

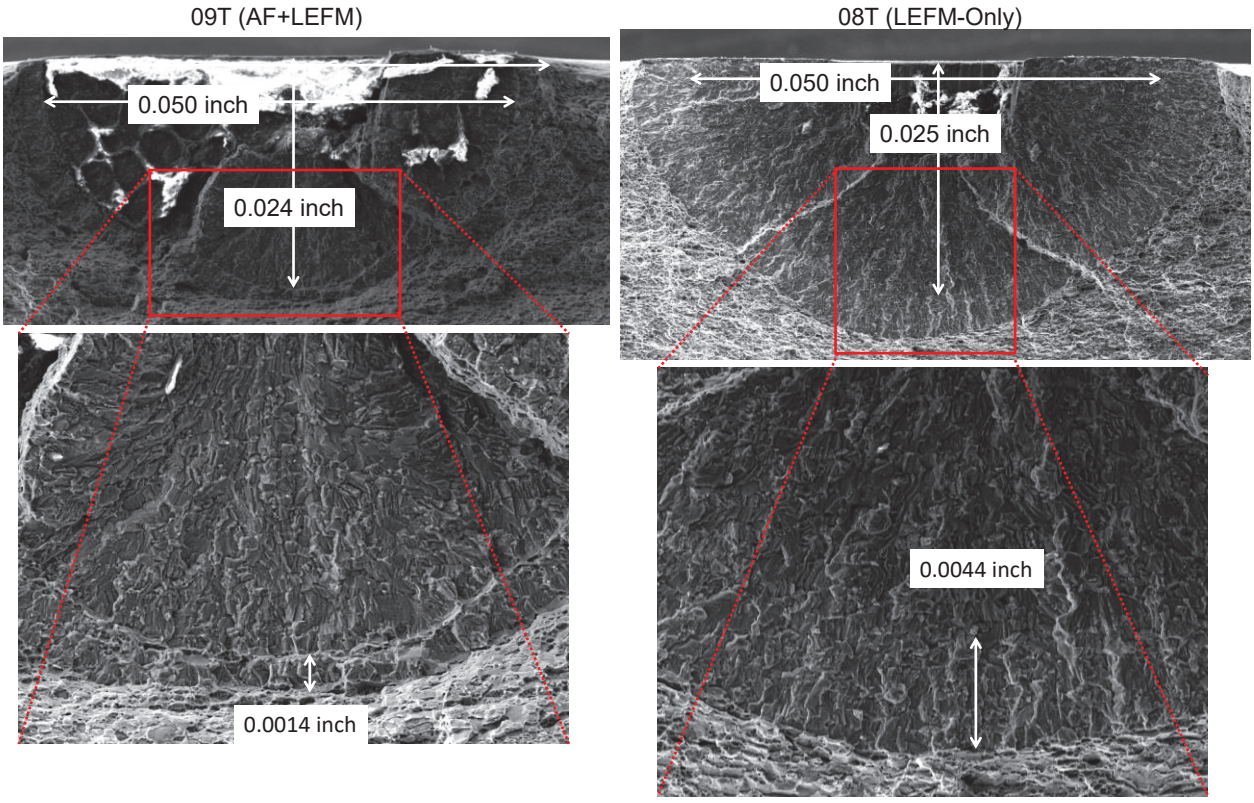

Figure C-12. Fracture surfaces for the 09T (AF+LEFM) and 08T (LEFM-only) tests with LEFM cycles with a maximum stress of 30,000 psi and a stress ratio of R = 0.2.

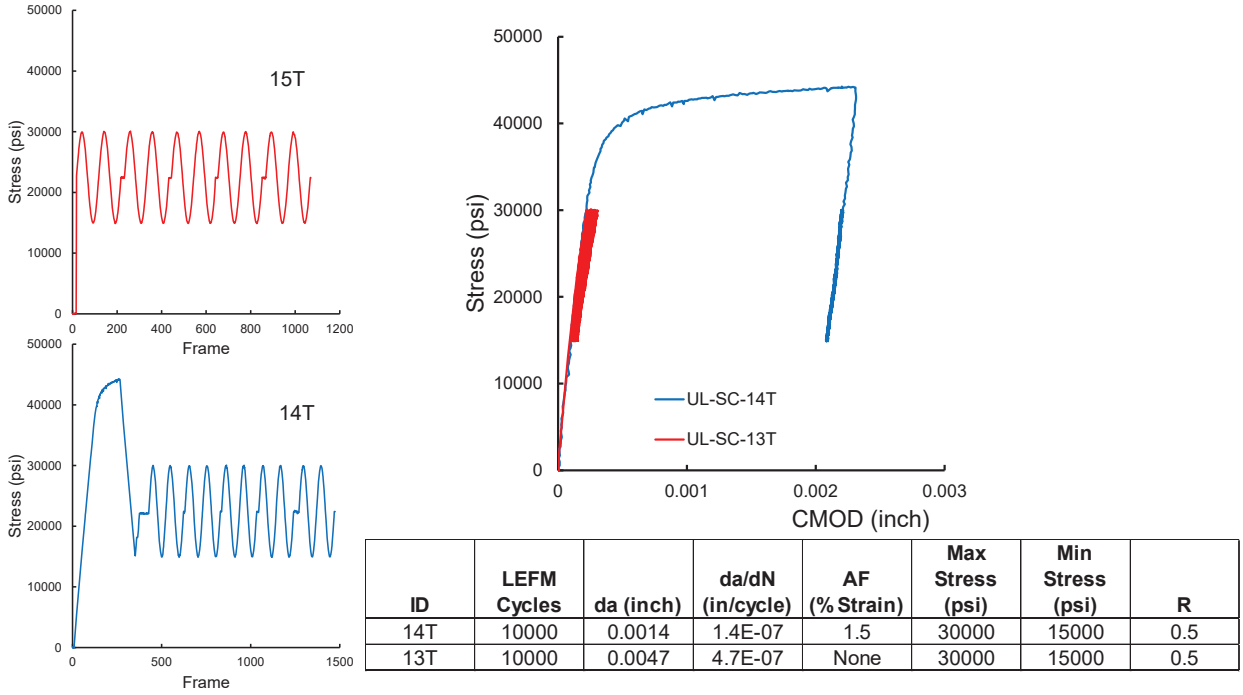

ID	LEFM Cycles	da (inch)	da/dN (in/cycle)	AF (% Strain)	Max Stress (psi)	Min Stress (psi)	R
14T	10000	0.0014	1.4E-07	1.5	30000	15000	0.5
13T	10000	0.0047	4.7E-07	None	30000	15000	0.5

Figure C-13. DIC CMOD measurements for AF+LEFM and LEFM-only tests with LEFM cycles with a maximum stress of 30,000 psi and a stress ratio of R = 0.5.

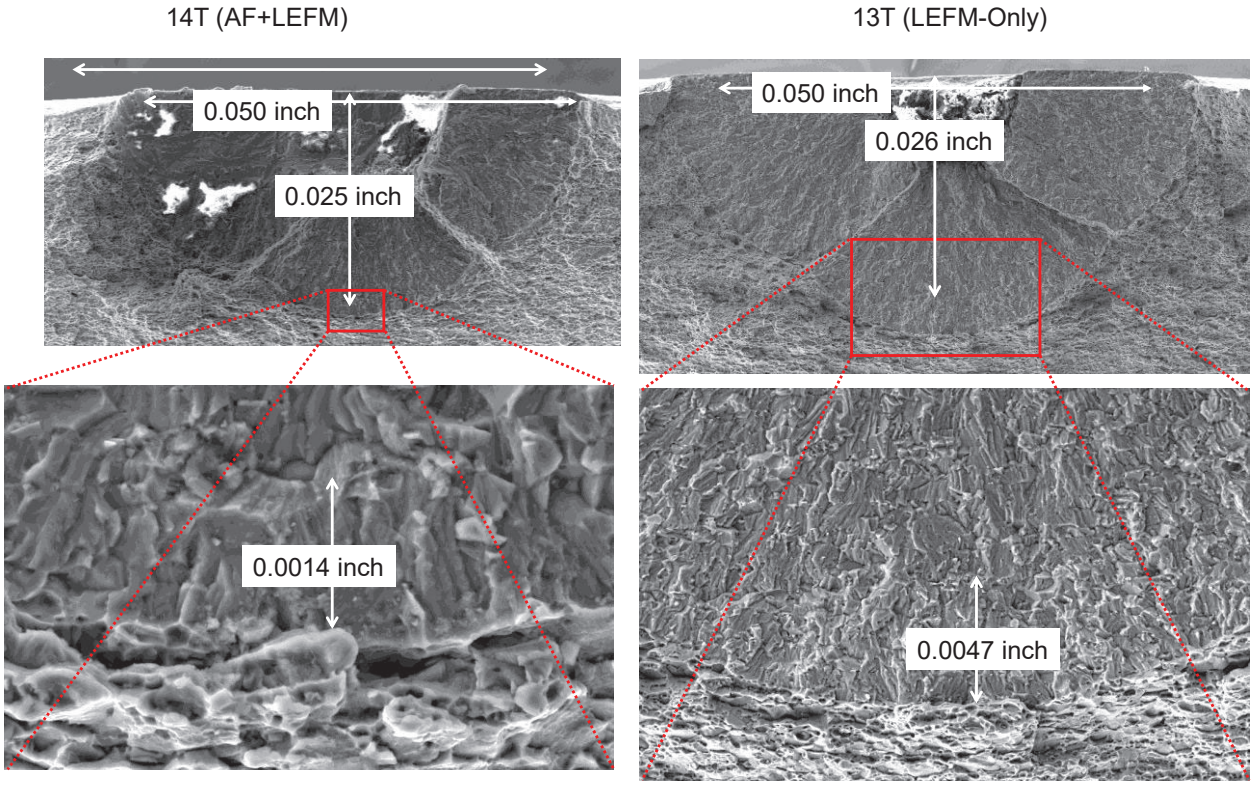

Figure C-12. Fracture surfaces for the 14T (AF+LEFM) and 13T (LEFM-only) tests with LEFM cycles with a maximum stress of 30,000 psi and a stress ratio of R = 0.5.

REPORT DOCUMENTATION PAGE

Form Approved
OMB No. 0704-0188

1. REPORT DATE *(DD-MM-YYYY)*	2. REPORT TYPE	3. DATES COVERED *(From - To)*
09/13/2023	Technical Memorandum	

4. TITLE AND SUBTITLE
Unconservatism of Linear-Elastic Fracture Mechanics (LEFM) Analysis Post Autofrettage

5a. CONTRACT NUMBER

5b. GRANT NUMBER

5c. PROGRAM ELEMENT NUMBER

6. AUTHOR(S)
Hickman, Heather K.; Dawicke, David S.; Leser, William P.

5d. PROJECT NUMBER

5e. TASK NUMBER

5f. WORK UNIT NUMBER
869021.01.23.01.01

7. PERFORMING ORGANIZATION NAME(S) AND ADDRESS(ES)
NASA Langley Research Center
Hampton, VA 23681-2199

8. PERFORMING ORGANIZATION REPORT NUMBER
NESC-RP-20-01567

9. SPONSORING/MONITORING AGENCY NAME(S) AND ADDRESS(ES)
National Aeronautics and Space Administration
Washington, DC 20546-0001

10. SPONSOR/MONITOR'S ACRONYM(S)
NASA

11. SPONSOR/MONITOR'S REPORT NUMBER(S)
NASA/TM-20230013348

12. DISTRIBUTION/AVAILABILITY STATEMENT
Unclassified - Unlimited
Subject Category Space Transportation and Safety
Availability: NASA STI Program (757) 864-9658

13. SUPPLEMENTARY NOTES

14. ABSTRACT
The scope of the NASA Engineering and Safety Center (NESC) Unconservatism of Linear-Elastic Fracture Mechanics (LEFM) Analysis Post Autofrettage assessment was to evaluate the influence of the elastic-plastic autofrettage cycle on elastic cycles post autofrettage and generate data to support damage tolerance life analysis verification approach. The decision to include an elastic-plastic autofrettage cycle is informed by other factors beyond damage tolerance, including manufacturing and fatigue crack initiation. The results of the NESC assessment are contained in this report.

15. SUBJECT TERMS
Linear-Elastic Fracture Mechanics; NASA Engineering and Safety Center; Autofrettage Cycle; Composite Overwrapped Pressure Vessel

16. SECURITY CLASSIFICATION OF:			17. LIMITATION OF ABSTRACT	18. NUMBER OF PAGES	19a. NAME OF RESPONSIBLE PERSON
a. REPORT	b. ABSTRACT	c. THIS PAGE			STI Help Desk (email: help@sti.nasa.gov)
					19b. TELEPHONE NUMBER *(Include area code)*
U	U	U	UU	84	(443) 757-5802